

ACOUSTIC TRANSMISSION IN THE RESPIRATORY SYSTEM

by

George Robert Wodicka

B.E.S., The Johns Hopkins University
(1982)

S.M., Massachusetts Institute of Technology
(1985)

SUBMITTED TO THE HARVARD/MIT
DIVISION OF HEALTH SCIENCES AND TECHNOLOGY

IN PARTIAL FULFILLMENT OF THE
REQUIREMENTS FOR THE DEGREE OF

DOCTOR OF PHILOSOPHY

at the

MASSACHUSETTS INSTITUTE OF TECHNOLOGY

June 1989

© George Robert Wodicka, 1989. All rights reserved.

The author hereby grants to MIT permission to reproduce and to
distribute copies of this thesis document in whole or in part.

Signature of Author _____
Division of Health Sciences and Technology
May 5, 1989

Certified by _____
Daniel C. Shannon
Thesis Supervisor

Certified by _____
Kenneth N. Stevens
Thesis Supervisor

Accepted by _____
Roger G. Mark
Chairman, Graduate Committee

ACOUSTIC TRANSMISSION IN THE RESPIRATORY SYSTEM

by

George Robert Wodicka

Submitted to the Harvard/MIT
Division of Health Sciences and Technology
on May 5, 1989 in partial fulfillment
of the requirements for the degree of
Doctor of Philosophy in Medical Engineering

ABSTRACT

The changes in lung structure which occur in disease affect the transmission of sound from within the large airways to the chest wall. Clinicians routinely listen on the chest wall to transmitted voice sounds or sounds generated by fluid flow in the airways as an index of regional lung function. This non-invasive information frequently augments the structural information obtained from radiographic techniques. However, there are limitations of these acoustical techniques which stem primarily from an inadequate knowledge of the basic mechanisms of sound transmission and their relation to respiratory function.

A theoretical model of sound transmission from within the respiratory tract to the chest wall due to the motion of the walls of the large airways was developed. The vocal tract, trachea, and the first five bronchial generations are represented over the frequency range from 100 to 600 Hz by an equivalent acoustic circuit. This circuit allows the estimation of the magnitude of airway wall motion in response to an acoustic perturbation at the mouth. The propagation of sound through the surrounding lung parenchyma is represented as a cylindrical wave in a homogeneous mixture of air bubbles in water. The effect of thermal losses associated with the polytropic compressions and expansions of these bubbles by the acoustic wave is included and the chest wall is represented as a massive boundary to the wave propagation. The model estimates the magnitude of acceleration over the extrathoracic trachea and at three locations on the right posterior chest wall in the same vertical plane.

The amplitude of sound transmission from the mouth to a site overlying the extrathoracic trachea and two sites on the

right posterior chest wall over the 100 to 600 Hz frequency range was measured in 8 healthy adult subjects. An acoustic driver and a rigid tube were employed to introduce sound into the mouths of the subjects and the transmission measurements were performed at resting lung volume using light-weight accelerometers. Similar spectral characteristics of acceleration were observed in all of the subjects showing peaks in the transmission. These characteristics included two regions of increased transmission over the frequency range of the measurements, a decrease in the magnitude of acceleration of the chest wall as compared to the tracheal site of roughly 20 dB at lower frequencies, and a strong trend of decreasing acceleration of the chest wall with increasing frequency.

After the incorporation of the acoustical characteristics of the sound source and the transducers into the model of the acoustical properties of the respiratory system, the theoretical predictions agree favorably with these experimental observations. The model suggests that the resonance peaks depicted in the spectra of transmission are a strong function of the geometry and wall properties of the respiratory tract and that the decreased amplitude of transmission to the chest wall at higher frequencies can be largely attributed to the absorption of sound in the surrounding lung parenchyma. The model provides a theoretical framework for further investigation into the effects of structural changes on sound transmission in both health and disease.

Thesis Supervisors: Daniel C. Shannon, M.D.
Associate Professor of Pediatrics
Harvard Medical School

Kenneth N. Stevens, Sc.D.
Professor of Electrical Engineering
MIT

Thesis Committee: Ernest G. Cravalho, Ph.D.
Professor of Mechanical Engineering
MIT

Howard L. Golub, Ph.D., M.D.
Executive Vice President
Pediatric Diagnostic Service, Inc.

ACKNOWLEDGEMENTS

I am deeply indebted to Dr. Daniel C. Shannon for providing me with the academic freedom and financial support to pursue this thesis research. His enthusiasm, concern, and guidance have made this a truly rewarding educational experience. I sincerely hope that our friendship and collaborative ties will remain strong in the years to come.

Professor Kenneth N. Stevens provided me with valuable advice concerning the technical aspects of the research. Our many discussions built the framework for the theoretical model and helped me to comprehend many of the experimental findings. I hope, someday, to be as fine an engineering professor as he is.

I extend my thanks to Professor Ernest G. Cravalho for providing a home for this research in the Department of Biomedical Engineering at the Massachusetts General Hospital. My friends in the Department provided me with invaluable technical support and encouragement on many occasions and made the project a team effort. I am particularly grateful to Andres Aguirre for his continued friendship and assistance.

Dr. Howard L. Golub helped to secure the link between the members of this interdisciplinary research team. I extend my thanks to him for his dedication to, and his guidance of, many aspects of the project.

I am sincerely grateful to all of my friends for providing the humor necessary to keep it all in perspective.

I offer my deepest gratitude to my wife, MaryJo, and my son, James, for their unfailing love. Their support and patience has been indispensable. I extend my thanks to our entire families for their continued concern.

This thesis document is dedicated to my grandfather, James McIntosh.

BIOGRAPHICAL NOTE

George R. Wodicka was born in Malverne, New York on June 11, 1960. He received the B.E.S. degree in Biomedical Engineering from The Johns Hopkins University, Baltimore, Maryland, in 1982, and the S.M. degree in Electrical Engineering and Computer Science from the Massachusetts Institute of Technology, Cambridge, Massachusetts, in 1985.

Dr. Wodicka's research interests include the application of acoustic technologies, electronic instrumentation, and signal processing techniques toward the solution of problems in clinical medicine. From 1982 to 1985, he was the recipient of the Raytheon Company Fellowship in Medical Engineering. Since 1985, he has been associated with the Department of Biomedical Engineering and the Pediatric Pulmonary Unit of the Massachusetts General Hospital. From 1987 to 1989, he held the position of Graduate Instructor in the Harvard-MIT Division of Health Sciences and Technology. He currently is Assistant Professor of Electrical Engineering, Purdue University, West Lafayette, Indiana.

TABLE OF CONTENTS

| | | |
|-------|---|----|
| 1. | INTRODUCTION | 11 |
| 1.1 | Introduction and Goals | 11 |
| 1.2 | Literature Review | 12 |
| 1.2.1 | Acoustic circuit models of the airways | 12 |
| 1.2.2 | Acoustic models of the lung parenchyma | 15 |
| 1.2.3 | Absorption in a liquid with air bubbles | 17 |
| 1.2.4 | Measurements of sound transmission in the respiratory system | 18 |
| 1.2.5 | Effects of lung pathology | 24 |
| 1.2.6 | Summary | 25 |
| 2. | A THEORETICAL MODEL OF SOUND TRANSMISSION | 28 |
| 2.1 | Introduction and Goals | 28 |
| 2.2 | An Acoustic Circuit Model of the Respiratory Tract | 30 |
| 2.2.1 | A circuit analogy of a non-rigid tube | 30 |
| 2.2.2 | A circuit model of the vocal tract | 33 |
| 2.2.3 | A circuit model of the subglottal airways | 35 |
| 2.2.4 | A complete circuit model of the respiratory tract at frequencies below 600 Hz | 37 |
| 2.3 | Propagation of Sound Within the Parenchyma | 38 |
| 2.3.1 | The parenchyma as a homogeneous mixtur | 39 |
| 2.3.2 | Cylindrical wave propagation due to large airway wall motion | 40 |
| 2.3.3 | Estimation of the radiation impedance of the surrounding parenchyma | 45 |
| 2.3.4 | The chest wall as a lumped mechanical mass | 49 |
| 2.4 | Absorption of Sound in the Parenchyma | 50 |
| 2.4.1 | The parenchyma as spherical air bubbles in water | 50 |
| 2.4.2 | An alveolus and the effective mass of the surrounding tissue as a locally reacting oscillator | 51 |
| 2.4.3 | Estimation of the magnitude of the thermal loss associated with wave propagation | 53 |
| 2.4.4 | Estimation of the attenuation of a pressure wave | 56 |
| 2.5 | Model Predictions | 58 |
| 2.5.1 | Transfer function between the chest wall and the mouth | 58 |
| 2.5.2 | Spectral characteristics of transmis- | |

| | |
|---|-----|
| sion | 59 |
| 2.5.3 Sensitivity to changes in parenchymal structure | 61 |
| 2.5.4 Sensitivity to changes in bronchial structure | 62 |
| 2.6 Discussion of the Theoretical Approach | 64 |
| 2.7 Summary | 69 |
| 3. MEASUREMENTS OF SOUND TRANSMISSION IN ADULT SUBJECTS | 71 |
| 3.1 Introduction and Goals | 71 |
| 3.2 Apparatus | 73 |
| 3.2.1 Hardware | 73 |
| 3.2.2 Experimental protocol | 76 |
| 3.2.3 Signal analysis | 77 |
| 3.3 Observed Frequency Characteristics | 78 |
| 3.3.1 Coherence spectra | 79 |
| 3.3.2 Spectral estimates of sound pressure at the mouth | 79 |
| 3.3.3 Spectral estimates of acceleration | 80 |
| 3.3.4 Effects of lung volume | 81 |
| 4. COMPARISON BETWEEN MODEL PREDICTIONS AND EXPERIMENTAL OBSERVATIONS | 85 |
| 4.1 Introduction and Goals | 85 |
| 4.2 The Sound Source and the Rigid Tube as Equivalent Circuits | 85 |
| 4.3 The Accelerometer as a Lumped Mechanical Mass | 89 |
| 4.4 Predicted Spectral Characteristics of Acceleration | 91 |
| 4.5 Direct Comparison Between Predictions and Observations | 92 |
| 4.5.1 Resonance peak locations of the tracheal spectra | 92 |
| 4.5.2 Magnitude of the acceleration of the chest wall | 93 |
| 4.6 Discussion | 94 |
| 4.6.1 The experimental model | 94 |
| 4.6.2 Inter-subject variability | 96 |
| 4.6.3 Experimental and theoretical comparison | 98 |
| 4.7 Summary | 101 |
| 5. CONCLUSIONS | 103 |
| 5.1 Theoretical | 103 |
| 5.1.1 Strengths and weaknesses of the approach | 103 |
| 5.1.2 Recommendations for future research | 106 |
| 5.2 Experimental | 109 |
| 5.2.1 Thoughts on the experimental protocol | 109 |
| 5.2.2 Recommendations for future research | 110 |

| | |
|------------|-----|
| TABLES | 113 |
| FIGURES | 119 |
| REFERENCES | 161 |

LIST OF TABLES

| | | |
|------|---|-----|
| I. | Dimensions of the model airway segments. | 113 |
| II. | Values of the thermal damping parameters. | 114 |
| III. | Spectral peak locations and quality factors. | 115 |
| IV. | Technical specifications of the sound source. | 116 |
| V. | Amplitude of the equalizer voltage gain. | 117 |
| VI. | Dimensions of the model rigid tube segments. | 118 |

LIST OF FIGURES

| | | |
|-----|---|-----|
| 1. | Diagram of the model respiratory system. | 119 |
| 2. | T equivalent circuit of an airway segment. | 120 |
| 3. | Block diagram of the equivalent acoustic circuit. | 121 |
| 4. | Magnitude of the vocal tract input impedance. | 122 |
| 5. | Phase of the vocal tract input impedance. | 123 |
| 6. | Cross-sectional area of the branching airways. | 124 |
| 7. | Magnitude of the subglottal input impedance. | 125 |
| 8. | Phase of the subglottal input impedance. | 126 |
| 9. | Magnitude of the respiratory tract input impedance. | 127 |
| 10. | Phase of the respiratory tract input impedance. | 128 |
| 11. | Time delay of adjacent segmental wall oscillations. | 129 |
| 12. | Amplitude of Bessel and Neumann functions. | 130 |
| 13. | Real part of the radiation impedance. | 131 |
| 14. | Imaginary part of the radiation impedance. | 132 |
| 15. | Attenuation of the pressure wave. | 133 |
| 16. | Transfer function of the model acceleration. | 134 |
| 17. | Effects of the volumetric proportion of tissue. | 135 |
| 18. | Effects of the bronchial cross-sectional area. | 136 |
| 19. | Block diagram of the experimental apparatus. | 137 |
| 20. | Circuit diagram of the amplification scheme. | 138 |
| 21. | A coherence spectrum. | 139 |
| 22. | A power spectrum of the pressure in the tube. | 140 |
| 23. | Average power spectra of acceleration, subject 1. | 141 |
| 24. | Average power spectra of acceleration, subject 2. | 142 |
| 25. | Average power spectra of acceleration, subject 3. | 143 |
| 26. | Average power spectra of acceleration, subject 4. | 144 |
| 27. | Average power spectra of acceleration, subject 5. | 145 |
| 28. | Average power spectra of acceleration, subject 6. | 146 |
| 29. | Average power spectra of acceleration, subject 7. | 147 |
| 30. | Average power spectra of acceleration, subject 8. | 148 |
| 31. | Average power spectra of acceleration at FRC. | 149 |
| 32. | Average power spectra of acceleration at TLC. | 150 |
| 33. | Effects of lung volume on acceleration. | 151 |
| 34. | Effects of lung volume on acceleration. | 152 |
| 35. | Electro-mechanical circuit of the sound source. | 153 |
| 36. | Norton equivalent circuit of the sound source. | 154 |
| 37. | Diagram of the rigid tube. | 155 |
| 38. | Block diagram of the sound source circuit. | 156 |
| 39. | Estimated volume velocity of the sound source. | 157 |
| 40. | Power spectra of acceleration with sound source. | 158 |
| 41. | Comparison between predictions and measurements. | 159 |
| 42. | Comparison between predictions and measurements. | 160 |

1. INTRODUCTION

1.1 Introduction and Goals

The changes in lung structure which occur in disease affect the transmission of sound from within the large airways to the chest wall at frequencies below approximately 1000 Hz. Since the invention of the stethoscope by Rene Laennec in 1819, clinicians routinely listen on the chest wall to transmitted voice sounds or sounds generated by fluid flow in the airways to obtain an index of regional lung function. These non-invasive, and largely empirical, techniques provide crucial diagnostic information in patients with illnesses as different as asthma and pulmonary edema. The information which is derived frequently augments the structural information obtained from radiographic techniques. However, there are significant limitations of these acoustical techniques which stem primarily from an inadequate knowledge of the basic mechanisms of sound transmission and their relation to respiratory function.

The primary goal of this thesis research was to begin to understand the relationship between the structure and the acoustical properties of the respiratory system. A theoretical

model of sound transmission from within the respiratory tract to the chest wall of the healthy adult male was developed. An experimental model was constructed to accurately assess the spectral characteristics of sound transmission in human subjects in vivo and to allow a direct comparison to be made with the theoretical predictions. Through this comparison, the strengths and weaknesses of the theoretical approach were identified and the key structural elements which affect transmission elucidated. This research provides a theoretical framework to comprehend many of the clinical observations regarding sound transmission in disease and to identify important acoustical parameters to measure as an index of the degree of lung dysfunction.

1.2 Literature Review

1.2.1 Acoustic circuit models of the airways

The first representation of the airways below the glottis as an equivalent circuit was proposed by van den Berg (1960). The model was based upon a mathematical representation of the complex branching structure of the airways developed by Rohrer (1915). An airway segment was represented by an equivalent T or π network, including the compliance of the airway walls (see Flanagan 1972). The model predictions were qualitatively com-

pared to input impedance (Z_{in}) measurements performed on cadavers over the 3 to 2000 Hz frequency range, and model parameters were altered to provide the closest agreement between the two. The lowest frequency peak of Z_{in} was measured to be approximately 10 cgs acoustic ohms at a frequency of 300 Hz - an observation which would later be shown to be an inaccurate representation of the intact subglottal system. However, these investigations provided the theoretical framework for more complicated and accurate circuit models of the subglottal airways.

Ishizaka, Matsudaira and Kaneko (1976) measured Z_{in} between 100 and 3000 Hz through a tracheostomy tube in laryngectomized subjects. Well-defined resonance peaks were observed at 640, 1400 and 2100 Hz, with impedance values of approximately 50 cgs acoustic ohms. In an approach similar to that of van den Berg, a distributed model of the system was developed based upon a complex branching structure of the airways proposed by Weibel (1963). In this model, the wall impedances were represented by series mass-resistance-compliance combinations, in contrast to only a compliance in van den Berg's model. Values of the wall compliances were estimated from previous physiological measurements, while mass and resistance values were chosen to fit the model prediction of Z_{in} to the experimental observations. The estimated values of the masses and resistances appeared to be reasonable from a structural perspective, and the resulting

model suggested that the location of the first resonance peak was largely dependent upon the dimensions and wall impedances of the trachea and primary bronchi. The estimated minimum values of the magnitude of the wall impedances of the trachea and the primary bronchi occurred at frequencies of approximately 100 and 600 Hz, respectively. The locations of these impedance minima suggest that significant wall motion of the large airways occurs in response to intra-airway oscillations between approximately 50 and 1000 Hz. Since the total cross-sectional area of the airways increases exponentially after the first few generations, the model also suggests that the subglottal airways may be represented over this frequency range by a single non-rigid tube terminated with the extremely large compliance of the gas contained within the small airways and the alveoli. Gupta (1973) had previously proposed a single tube model which only included the compliant properties of the airway walls. The predicted lowest resonance peak of this model occurred at approximately 300 Hz, a result similar to that found by van den Berg.

Fredberg (1980) expanded upon the distributed model proposed by Ishizaka et al. by including the effects of the asymmetry of small airway branching. Theoretically, these asymmetries affect Z_{in} only at frequencies greater than approximately 2000 Hz. This result is consistent with the strong

predicted dependence of Z_{in} on the large, relatively symmetric airways at lower frequencies.

A number of investigators have represented the vocal tract as an equivalent acoustic circuit (see Flanagan 1972). In these models, vocal tract segments were also represented by T or π circuits, which simulate one-dimensional acoustic wave propagation at low frequencies. The wall impedance of the vocal tract of adult subjects was estimated over the 20 to 140 Hz frequency range by Ishizaka, French, and Flanagan (1975), based on measurements performed on the neck and the cheek, the latter in both tensed and relaxed states. Results indicated that the minimum magnitudes of the wall impedances occur at frequencies which range from approximately 32 Hz for the relaxed cheek to approximately 72 Hz for the neck. The characteristics of each of the wall impedances were well-described by a series mass-resistance-compliance combination, and values for these elements were estimated from the data. The magnitude of these values suggest that the wall properties are important in the determination of the overall acoustic properties of the vocal tract, especially at low frequencies where wall motion may be significant.

1.2.2 Acoustic models of the lung parenchyma

The parenchyma, or gas-exchange region of the lung which surrounds the airways, consists of alveoli, small airways, capillaries, and supporting lung tissue. Rice (1983) proposed that from an acoustical perspective, the parenchyma acts as a homogeneous mixture of tissue and gas at frequencies below approximately 10,000 Hz. In this frequency range, the wavelengths of sound in the parenchyma are significantly greater than the alveolar radius, which has an average value in adult humans of approximately 0.015 cm. Butler, Lehr, and Drazen (1987) reported that it is likely that a significant amount of air moves between adjacent alveoli due to wave motion at frequencies associated with high-frequency ventilation (1-30 Hz). At higher frequencies, Rice assumes in his model that the forces required to move air between adjacent alveoli are large and therefore no gas exchange occurs due to the acoustic wave propagation.

The composite density and volumetric compliance of the mixture was estimated based upon the relative proportions of tissue (composed primarily of water) and gas (air) in the mixture under adiabatic conditions. The predicted speed of sound was in the 2000 to 7000 cm/s range, and these values compared well with in vitro experimental observations which will be discussed later. This model of the parenchyma suggests that the speed of

sound at low frequencies is not significantly affected by structural inhomogeneity on a microscopic level. However, the characteristics of transmission are a strong function of the relative proportions of tissue and gas - two factors which are altered in various diseases of the lung. The modeling approach by Rice did not include the effects of absorptive mechanisms on wave propagation in the parenchyma. Since the alveoli are roughly spherical in shape and the lung tissues are predominantly comprised of water, one could hypothesize that the mixture acts as air bubbles in water at frequencies where the wavelength is significantly greater than the bubble size.

1.2.3 Absorption in a liquid with air bubbles

The losses associated with sound propagation in a fluid which contains air bubbles has been investigated by Prosperetti (1977). This work was a more mathematically rigorous extension of the theory which was first proposed by Devin (1959). At frequencies where the wavelength of sound is significantly greater than the bubble radius, the thermal losses are predicted to dominate those due to either scattering or viscous effects. These thermal losses arise since the bubble compressions and expansions are polytropic; they are more adiabatic at the center of the bubble and isothermal where the air and liquid are in contact. Thus, the work performed on the bubble by

the acoustic wave during compression is greater than the work performed by the air during expansion, resulting in a net flow of heat into the liquid. While a single bubble may exhibit a negligible effect on the wave propagation, the composite attenuation due to many bubbles per unit volume can be quite pronounced.

The magnitude of the thermal effects can be estimated by representing a bubble and its surrounding liquid as a locally reacting oscillator (see Kinsler, Frey, Coppens and Sanders, 1982). The compliance of the bubble system is determined by the air within the bubble, the mass is determined by the liquid surrounding the bubble, and the resistance is determined by the aforementioned thermal effects. For plane wave propagation, the absorption due to a given number of bubbles per unit volume may then be represented by an extinction cross section which, in turn, may be employed to determine the attenuation in sound pressure as a function of the distance which a wave has propagated in the mixture.

1.2.4 Measurements of sound transmission in the respiratory system

In an attempt to characterize the acoustic properties of the respiratory system, investigators have focused their

studies toward the measurement of sonic propagation times and the frequency characteristics of transmission. Both in vitro and in vivo studies have been performed over a wide range of frequencies and experimental conditions.

Rice (1980) measured the transit time of high-frequency (>10,000 Hz) pulses in the large airways of an in vitro preparation. A knowledge of the distance between the sound source and the measurement provided estimates of the sound speed which was approximately equal to that observed in a free field of air at room temperature, 34,400 cm/s. This observed speed was a strong function of gas composition and temperature, suggesting that the airways act as rigid conduits at these high frequencies and thus the wave propagation occurs solely within the gas-filled lumen. At lower frequencies, Winter (1978) observed significantly slower speeds in a similar preparation. Sound speeds of 2500 to 5000 cm/s at a frequency of 10 Hz and roughly 15,000 cm/s at 80 Hz were estimated from time domain measurements. These speeds suggest that the large airway walls are non-rigid at these relatively low frequencies. These observations are consistent with the acoustic models of the subglottal airways which were proposed by Ishizaka et al. and Fredberg and Hoenig, both of which predict a resonance of the tracheal wall around 100 Hz. Below this resonance, the wall impedances are dominated by the compliance term, which results in wave speeds

which are less than the free field speed. At higher frequencies, the impedance due to the wall mass dominates the overall wall impedance.

Sound speed in the parenchyma of the lung was estimated by Rice (1983) from measurements of sonic propagation times in an in vitro preparation. An impulsive sound source was employed which contained energy from 5 to 30,000 Hz. After traveling through the lung, the signal was observed to contain very little energy outside the 100 to 1000 Hz frequency range. Estimated speeds were approximately 2500 to 7500 cm/s - values which are significantly less than the free field speeds in either gas or tissue. These observations were consistent with the aforementioned model of Rice which represents the parenchyma as a mixture of tissue and gas. As suggested by the model, increased speeds were observed as ambient pressure was increased or lung volume was decreased. The effect of gas composition on sound speed in the parenchyma was significantly less than observed in the large airways - a finding which is qualitatively consistent with the model predictions, since the composite parenchymal density is dominated by the tissue density.

The effect of gas composition and measurement site on the propagation time of sound between a site over the extrathoracic

trachea and sites on the posterior chest wall of adult subjects was investigated by Kraman (1983a). Sound in the 125 to 500 Hz frequency range was introduced into the mouths of healthy subjects, and cross-correlation techniques were employed to estimate propagation times. The measured times ranged from approximately 2 ms on the upper chest to 5 ms on the lower chest. Assuming that sound travels the distance toward the site within the airway and then propagates through 10 cm of parenchyma, the estimated parenchymal sound speed ranges from approximately 2000 to 6000 cm/s. Changing the inhaled gas from air to a mixture of 80% helium and 20% oxygen resulted in less than a 10% decrease in the measured propagation times. The predicted increase of sound speed if the propagation were through the gas alone would be greater than 100%. This observation is consistent with the in vitro findings of Rice and suggests that low-frequency sound introduced at the mouth spends a majority of its propagation time within the parenchyma rather than within the airways. In concert with previous model predictions and experimental observations regarding the large airways, these observations further suggest that a significant proportion of the acoustic energy within the large airways is directly coupled to the surrounding parenchyma via wall motion.

The observation that propagation times increased as the measurement site moved caudally to lower lobe regions is con-

sistent with the direct coupling of sound energy through the airway walls since the lower lobe regions are farthest, on a straight line, from the source, yet are approximately equidistant on an airway path. One would expect times to be equal at measurement sites which are equidistant from the carina if the propagation was purely within the airways - an expectation which is inconsistent with these observations.

In contrast with Kraman's findings, Jacobs (1982) observed that propagation times between mouth and chest wall decreased approximately 25% on helium-oxygen breathing at frequencies between 500 and 25,000 Hz. These observations suggest that more significant transmission in the airway lumen occurs at higher frequencies due to the effects of the mass of the airway walls. However, the effect of measurement site on the observed propagation times was not reported and thus a direct comparison to the aforementioned findings at lower frequencies cannot be performed.

In an abstract, Rice (1986) reported measurements of the time of propagation of 251 Hz Gaussian pulses between a site overlying the extrathoracic trachea and the chest wall in healthy adult subjects. He hypothesized that alterations in gas composition would affect the sound speed within the large airways while changes in pressure would affect the speed in the

parenchyma. Propagation times were observed to decrease from a mean value of 3.5 ms to 2.6 ms when the subject breathed a helium-oxygen mixture and decreased to 2.6 ms under conditions of a four-fold increase in ambient pressure. These observations were qualitatively consistent with his previous in vitro findings in the trachea and parenchyma, respectively. A statistical model was employed in which the propagation time was dependent upon the sum of two terms, one term due to the free field speed in airways and the other term reflecting the predicted pressure^{-1/2} dependence of speed in the parenchyma. A quantitative comparison between the model predictions and the sound speed estimates was not reported, yet it was stated that this approach yielded a reasonably close agreement between the two.

The frequency characteristics of sound transmitted from mouth to chest wall were first investigated by Kraman (1983a). Noise in the 50 to 500 Hz frequency range was introduced via an uncharacterized sound source into the mouths of healthy adult subjects at resting lung volume. Measurements were performed using shielded microphones in the proximity of the chest wall at various locations. A decrease in transmitted power was observed over lower lobe regions with respect to upper regions and over the left lung with respect to the right. The latter observations suggests that preferential coupling of sound oc-

curs to the right lung due to the effects of the massive mediastinum (primarily the heart), which lies to the left of the major airways. More recently, Kraman (1986) measured the transfer function of sound transmission between the mouth and four sites on the chest wall in healthy subjects using a 25 Hz square wave input to the sound source. Thus, the frequency resolution of the estimate is approximately 50 Hz. In each case, the spectra contained one or more spectral peaks at frequencies between 50 and 175 Hz, with a variable roll-off and minimal power above approximately 400 Hz. The most interesting observation was that no significant change in the spectral characteristics of transmission was observed when the subjects breathed a helium-oxygen mixture. This result, despite the very poor resolution of the estimate, provides more evidence that transmission occurs not only within the airways, but also directly through the parenchyma.

1.2.5 Effects of lung pathology

Many diseases of the lung alter the transmission of sound from within the airways to the chest wall. Clinicians use the altered characteristics of a transmitted sound routinely as a qualitative index of regional lung function (see Bates (1979)). However, it appears that only two formal studies have been undertaken to better understand this phenomenon. Donnerberg et

al. (1980) measured the intensity of sound transmitted from the trachea to the chest wall in dogs over the 50 to 2000 Hz frequency range as a function of the degree of cardiogenic pulmonary edema. Intensity was compared to post mortem wet-to-dry lung ratios and a reasonably linear relationship was observed over a wide range of edema. This observation, that the increase in lung density and decrease in air volume with edema led to increased transmitted power is consistent with parenchymal transport at these frequencies. However, the frequency dependence of the increase was not measured in this study.

Ploysongsang (1981) measured the transmission of sound from mouth to chest wall in patients with emphysema and compared the results with measurements performed on healthy subjects. Regions of both increased and decreased transmission were observed in the patients with no consistent anatomical distribution. Given the complex and heterogeneous structural changes which occur in this pathology, these results are understandable, yet provide little insight into the relationship between structure and alterations in sound transmission.

1.2.6 Summary

Although there have been a number of investigations into the transmission of audible sound in the thorax, many issues

remain poorly understood. The lack of standardization and characterization of sound sources and transducers which were employed in the studies make direct comparisons between them difficult to perform. The frequency characteristics of sound transmission between the mouth and the chest wall have not been rigorously assessed or theoretically predicted. The relationships between the complex structures of the respiratory system and sound transmission have only begun to be elucidated.

The propagation time of sound between the airways and the chest wall is currently the most investigated and modeled parameter in the transmission studies. It has provided evidence that helps to delineate of the pathways taken by sound induced into the airways. At low frequencies, sound energy is directly coupled from within the large airways to the surrounding lung parenchyma via wall motion. At higher frequencies, the airways act more similar to rigid conduits and thus sound propagates primarily within the lumens of the complex branching airway network.

Prior to the undertaking of this thesis research, there existed no cohesive acoustic model of sound transmission within the respiratory system at frequencies below 1000 Hz. Detailed models of the airways have been proposed and successfully compared to input acoustic impedance measurements. A model of the

lung parenchyma has been hypothesized and its predictions of sound speed are in agreement with experimental findings in vitro. Heretofore, the theory concerning the effects of air bubbles in a liquid on an acoustic wave has largely been applied to the effects of wakes of ships on sound transmission in the sea. There is a need to bring these findings and models together to formulate a comprehensive model of sound transmission within the intact respiratory system.

In this thesis document, a detailed description of a theoretical model of sound transmission from within the large airways to the chest wall is provided in chapter 2. Chapter 3 overviews the development of an experimental model to accurately assess the frequency characteristics of sound transmission in healthy adult subjects. The spectral estimates obtained from measurements performed on eight subjects are presented. A direct comparison between the model predictions of the frequency characteristics of transmission and these experimental findings is detailed in chapter 4. Lastly, recommendations for future research endeavors are summarized in chapter 5.

2. A THEORETICAL MODEL OF SOUND TRANSMISSION

2.1 Introduction and Goals

In this chapter, a theoretical model of acoustic transmission in the intact human respiratory system in the 100 to 600 Hz frequency range is presented. This approach provides a theoretical framework for further investigation into the relationship between the structure and the acoustic properties of the lung in both health and disease. The model allows quantitative comparisons to be performed between experimental observations and theoretical predictions.

As described in chapter 1, the acoustic properties of the vocal tract and the airways below the glottis have been previously modeled as equivalent acoustic circuits. The estimated input impedances of these circuits are consistent with measurements performed on human subjects. These approaches suggest that a significant amount of wall motion of the large airways below the glottis occurs in response to intra-airway pressure oscillations in the frequency range between 100 and 600 Hz. This motion results in the direct coupling of acoustic energy from within these large airways to the surrounding lung parenchyma (gas-exchange region), thus bypassing the smaller airways.

The representation of the parenchyma as a homogeneous mixture of gas and fluid suggests that the sound wavelengths at frequencies less than 1000 Hz are significantly longer than the alveolar radius of an average adult of roughly 0.015 cm. However, these wavelengths are of the order of the distance between the large airway walls and the chest wall. This relationship between the wavelength and the distance in which a wave must travel to reach the chest wall indicates that the parenchyma must be modeled as a more distributed acoustical system than the airways in this frequency range.

The analysis regarding the attenuation of sound in a fluid which contains air bubbles suggests that the thermal losses are considerably larger in magnitude than those associated with viscous or scattering effects when the sound wavelength is significantly greater than the bubble radius. The resulting attenuation of the propagating wave can be significant when there is a large number of bubbles per unit volume.

The theoretical approach presented in this chapter is an extension and integration of previous investigations into the acoustic properties of the respiratory tract and the dynamics of bubbles in a fluid. Figure 1 is a diagram of the model representation of the respiratory system. An equivalent circuit

is employed to represent the vocal tract and the large airways below the glottis as a single effective tube. When simulated using a computer (Tatum Laboratories, Ann Arbor, MI, ECA software), this circuit allows the estimation of the magnitude of wall motion in response to an acoustic perturbation within the airways or at the mouth. Each airway segment is modeled as a cylinder which radiates sound uniformly through the parenchyma, represented as a homogeneous mixture of air bubbles in water, analogous to gas and tissue. The attenuation of sound in the parenchyma due to thermal effects is incorporated and the chest wall is represented as a massive boundary to the propagation of the outgoing cylindrical wave. The magnitude of acceleration over the extrathoracic trachea and at three locations on the posterior chest wall is estimated. The sensitivity of the model to changes in parenchymal and airway structure is investigated.

2.2 An Acoustic Circuit Model of the Respiratory Tract

2.2.1 A circuit analogy of a non-rigid tube

To estimate the magnitude of large airway wall motion in response to an acoustic perturbation, the vocal tract and the subglottal airways are modeled as an equivalent acoustic cir-

cuit. In this approach, a respiratory tract segment of uniform diameter, and length, l , is represented by a T network, as described in detail in Flanagan (1972) and depicted in figure 2. The circuit elements which relate pressure in dynes/cm² to volume velocity in cm³/s are: L , the acoustic inertance of the air mass in g/cm⁴, R , the viscous loss in dyne-s/cm⁵, C , the acoustic compliance of the air volume in cm⁵/dyne, and G , the heat conduction loss in cm⁵/dyne-s. These parameters are linearized and are estimated using the following equations:

$$L = \rho_g l / A$$

$$C = Al / \rho_g c_g^2$$

$$R = (Sl/A^2) \left[\omega \rho_g v / 2 \right]^{1/2}$$

$$G = \left\{ Sl(\gamma-1) / \rho_g c_g^2 \right\} \left[\omega \chi / 2 c_p \rho_g \right]^{1/2}$$

where l is the length of the segment, A is the cross-sectional area, S is the circumference, ρ_g is the density of air, c_g is the free field sound speed in air, v is the viscosity coefficient, χ is the coefficient of heat conduction, γ is the adiabatic constant for air, and c_p is the specific heat of air

at a constant pressure. Values employed in the equations are $\rho_g = 1.14 \times 10^{-3} \text{ g/cm}^3$, $c_g = 35,000 \text{ cm/s}$, $v = 1.86 \times 10^{-4} \text{ dyne-s/cm}^2$, $\chi = 0.055 \times 10^{-3} \text{ cal/cm-s-deg}$, $c = 0.24 \text{ cal/g-deg}$, and $\gamma = 1.4$.

This network accurately represents the acoustic behavior of a cylindrical tube under the constraint that l be significantly less than the shortest wavelength, λ , of interest. Since our model represents airway properties up to 600 Hz, we employed the constraint that l be less than roughly $\lambda/10$, where λ is approximately 58 cm in air at this frequency. Thus, each T network represents a segment of the airway less than or equal to 6 cm in length. Since the linearized approximations are of the form

$$\tanh(x) \cong x \quad \text{and} \quad \text{csch}(x) \cong 1/x$$

this T-network representation results in an error of approximately 3% in the approximation of the impedance by a linearized circuit parameter such as L at a frequency of 600 Hz.

The properties of the airway walls are represented by a series network of acoustic elements L_w , R_w , C_w which is, in turn, in series with the acoustic radiation impedance of the surround, Z_{rad} , as shown in Figure 2. Figure 3 depicts in block

form the interconnection of the T networks which comprise the complete equivalent acoustic circuit of the respiratory tract. Table I provides the dimensions of each segment and the values of the acoustic elements which represent the airway walls.

2.2.2 A circuit model of the vocal tract

For the vocal tract, values for the circuit elements in the three T networks are based upon the average anatomy of an adult male as specified in Stevens (1989), and previous measurements of the wall properties by Ishizaka, French and Flanagan (1975). The model represents a vocal tract which is 16.5 cm in length. The mechanical values employed to estimate the acoustic elements which represent the walls of the vocal tract (see Table I) are : $C_m = 2 \times 10^{-5} \text{ cm}^3/\text{dyne}$, $M_m = 1.5 \text{ g/cm}^2$, and $R_m = 1400 \text{ dyne-s/cm}^3$, with a total surface area of 140 cm^2 . The frequency at which the magnitude of the wall impedance is a minimum is roughly 30 Hz. Thus, the walls are primarily massive and resistive at frequencies above 100 Hz. The acoustic radiation impedance of the surrounding air, Z_{rad} , is small in magnitude when compared to that of the vocal-tract wall. The magnitude and the phase of the input acoustic impedance at the mouth of the model vocal tract with the glottis closed (in units of decibels referenced to 1 cgs acoustic ohm for the magnitude plot), are depicted in figures 4 and 5. The resonance

frequency is approximately 180 Hz and the quality factor is 3.2. In this frequency range, the losses associated with wall motion are dominant and largely determine the sharpness of the spectral peak.

The constriction presented by an open glottis is represented by the acoustic inertance of air within the vocal folds and the associated viscous loss, as described by Flanagan (1972). The values of these two parameters were calculated assuming a glottal cross-sectional area of 0.54 cm^2 and a length of 0.3 cm, representing the open glottis of an adult male during quiet breathing, as specified by Judson and Weaver (1942).

The anatomy of the neck below the glottis with respect to the extrathoracic tracheal wall is non-concentric; the wall is approximately 1 cm from the external surface of the skin anteriorly and more than 6 cm posteriorly. The effective loading of the neck tissues on the tracheal wall has not been quantitatively assessed. We incorporated the concentric effect of 1 cm of tissue mass surrounding the extrathoracic tracheal wall into the equivalent circuit model. This incorporation allows the acceleration of the anterior tissue which overlies the trachea to be estimated in response to an intra-airway perturbation, yet it may underestimate the loading effects of the more posterior structures.

2.2.3 A circuit model of the subglottal airways

The subglottal airways (intra- and extrathoracic trachea and bronchi) are represented as an equivalent circuit of a single tube whose cross-sectional area is equal to the total cross-sectional area of the branching airways, as first proposed by Gupta, Wilson and Beavers (1973). Values for the circuit elements in the four T networks are derived from the Weibel (1963) anatomical model of the airways. Since the total cross-sectional area of the airways increases rapidly after the first few airway bifurcations, as depicted in figure 6, the circuit model is terminated in a short circuit, corresponding to an open acoustic tube, after the sixth airway generation. This procedure resulted in an equivalent subglottal airway which is 22 cm in length.

In the circuit model, the overall wall properties of each segmental airway are represented by the wall acoustic elements in series with the radiation impedance of the surround, Z_{rad} . The procedure employed to estimate Z_{rad} for the subglottal airways is detailed in section 2.3.3. Values for the wall elements were estimated from previous complex branching models of the airways by Ishizaka, Matsudaira and Keneko (1976) and Fredberg and Hoenig (1978), in concert with a knowledge of the

value of Z_{rad} . Values derived for the wall acoustic elements result in wall motion which is roughly critically damped. The elements which represent the bronchial wall were estimated based upon the average wall properties of the first five bronchial generations and their respective surface areas, as detailed by Fredberg and Hoenig (1978). These values are the same for the two T networks which represent the bronchi. The bronchial walls are significantly less massive and more compliant than the tracheal walls. The frequency at which the wall impedance has a minimum value is less than 100 Hz for the trachea and slightly greater than 200 Hz for the bronchi.

The magnitude and the phase of the input acoustic impedance of the model subglottal airways are depicted in figures 7 and 8 (in units of decibels referenced to 1 cgs acoustic ohm for the magnitude plot). The impedance has a resonance frequency of approximately 510 Hz with a quality factor of roughly 2.5. The quality factor is largely determined by the losses associated with airway wall motion. The magnitude of the input acoustic impedance which was measured in Japanese subjects through a tracheostomy tube by Ishizaka, Matsudaira and Flanagan (1976) indicated a resonance frequency of approximately 640 Hz with a quality factor of roughly 3.0. A direct comparison between the model estimate and these measurements is difficult because of 1) the shorter airway length of the Japanese as compared to the

Western airways, 2) the lung volume of the subjects being significantly greater than resting lung volume during the procedure, and 3) the location of the tracheostomy tube approximately 2 cm below the glottis of the experimental subjects. It is likely that the first two of these factors contribute to an increase in the resonance frequencies, and thus quality factors, obtained from the experimental measurements while the location of the tube below the glottis affects the magnitude of the observed input impedance.

2.2.4 A complete circuit model of the respiratory tract at frequencies below 600 Hz

The acoustic circuit models of the vocal tract and the subglottal airways were connected in series to form a model of the entire respiratory tract at frequencies below 600 Hz (see Figure 3). This procedure resulted in an equivalent tract which is 38.5 cm in length - 16.5 cm for the vocal tract and 22 cm for the airways below the glottis. The magnitude and phase of the input acoustic impedance at the mouth is depicted in figures 9 and 10. The units of magnitude are decibels referenced to 1 cgs acoustic ohm. The resonance frequency, where the phase angle of the impedance is zero, is approximately 250 Hz with a quality factor of the magnitude peak of roughly 3.6. This frequency corresponds to the fundamental resonance of a

rigid pipe of length 35 cm which is filled with air and open at one end. As is the case for the vocal tract and the subglottal airways acting separately, the quality factor is largely determined by the losses associated with wall motion. The sensitivity of the magnitude of the motion to changes in the values of the circuit elements which represent the airway walls will be investigated later in this chapter.

Standing waves are produced in response to a sinusoidal perturbation within the airways due to the termination impedance of the model. Since the wavelengths of interest are greater than roughly 60 cm and the length of the model subglottal airways is 16 cm, the phase shift between the oscillations of adjacent wall segments is small. Figure 11 depicts the estimated time delay difference between the oscillations of adjacent model wall segments as a function of frequency. The largest delay occurs between the upper and lower tracheal segments, yet its magnitude is less than 0.15 ms. However, there exist significant differences in the amplitude of the motion - an observation which will be discussed in more detail at the end of this chapter with regard to the coupling of sound into the surrounding lung parenchyma.

2.3 Propagation of Sound Within the Parenchyma

2.3.1 The parenchyma as a homogeneous mixture

The lung parenchyma which surrounds the intrathoracic airways is represented as a homogeneous mixture of gas and tissue (see Rice, 1983) in the form of air bubbles in water. Under the constraint that the wavelength of sound in the parenchyma, λ_p , is much greater than the equilibrium radius, r_0 , of the bubbles which represent the alveoli, the composite density, ρ , in g/cm³ and volumetric compliance, K , in cm²/dyne of the mixture are given by:

$$\rho = (1-h)\rho_g + h\rho_t$$

$$K = (1-h)K_g + hK_t$$

where the subscripts g,t represent gas and tissue, respectively. The parameter h is the volumetric proportion of the tissue phase in the mixture and thus $(1-h)$ is the volumetric proportion of the gas phase. The volumetric gas compliance, K_g , is given by $1/(\kappa P)$, where κ is the polytropic constant representing the ratio of specific heats, and P is the gas pressure in dynes/cm². The determination of the values of κ used in this representation are discussed in detail in section 2.4.3.

Values employed in the equations are: $\rho_g = 1.14 \times 10^{-3}$ g/cm³, $\rho_t = 1.00$ g/cm³, $K_t = 4.35 \times 10^{-11}$ cm²/dyne and $P = 1.00 \times 10^6$ dyne/cm². This value of P represents an estimate of standard atmospheric pressure and results in a value of $K_g = 1.00 \times 10^{-6}$ cm²/dyne when $\kappa = 1.0$. Since $(1-h)K_g \gg hK_t$ for physiologic ranges of h , the composite compliance is dominated by the air compliance. In contrast, since $h\rho_t \gg (1-h)\rho_g$, the composite density is controlled by the tissue density.

The resulting sound speed in the parenchyma, c , in cm/s is:

$$c = \left[1/(\rho K) \right]^{1/2}$$

which has a value of approximately 2300 cm/s when $\kappa = 1.0$ and $h = 0.25$. This value of h approximately represents the average lung resting volume of air (2500 ml) and volume of tissue (900 ml) of an adult male, as estimated by Armstrong, et al. (1982). Thus, λ_p is approximately 4 cm at 600 Hz which satisfies the relation $\lambda_p \gg r_0$, the equilibrium radius of the bubbles.

2.3.2 Cylindrical wave propagation due to large airway wall motion

Since the large airways are roughly cylindrical in geometry, the vibrating walls of each airway segment are represented as a long cylinder which radiates sound uniformly through the parenchyma. One may then employ the wave equation in cylindrical coordinates to estimate the pressure at some distance from the airway due to this wall motion. In this application, the parenchyma is considered to be lossless, and the distance the wave travels is from the airway wall to the chest wall. The attenuation of the pressure wave due to thermal losses in the parenchyma are included in the model subsequently, and this procedure is detailed in section 2.4.

Morse and Ingard (1986) provide a detailed description of the solution to the general wave equation in cylindrical coordinates. If we assume that the waves generated by the airway segments are only a spatial function of the radial distance, r , from each airway wall and not a function of the angle, θ , or the position along the segment, z , then the general wave equation:

$$\partial^2 p / \partial t^2 = c^2 \nabla^2 p$$

where ∇^2 is the Laplacian operator in cylindrical coordinates:

$$\nabla^2 = \partial^2/\partial r^2 + \partial/r\partial r + \partial^2/r^2\partial\theta^2 + \partial^2/\partial z^2$$

reduces to:

$$\partial^2 p/\partial t^2 = c^2 \left[(\partial^2 p/\partial r^2) + (\partial p/r\partial r) \right]$$

The solution of this radial equation is a combination of Bessel (J_m) and Neumann (N_m) functions. For a wave spreading out uniformly from the cylindrical airway segment with a surface velocity amplitude of u_0 , the complex pressure $p(r)$ in dynes/cm² at a distance r from an airway segment of outer radius d is:

$$p(r) = A \left[J_0(2\pi f r/c) - j N_0(2\pi f r/c) \right]$$

where A is a constant, f is the frequency in Hz ($\omega = 2\pi f$) and J_0 , N_0 are Bessel and Neumann functions of the first kind, respectively. Figure 12 depicts $J_0(x)$, $N_0(x)$, and the magnitude of the radial dependence term (above in brackets), evaluated at a distance r of 10 cm from the airways where the abscissa $x = 2\pi f r/c$. This distance corresponds roughly to the extent of the parenchyma in which the wave must travel to reach

the posterior chest wall. Over the 100 to 600 Hz frequency range in this application, the abscissa x varies from approximately 2 to 12 while the magnitude of the radial dependence term in the equation for $p(r)$ ranges from roughly 0.5 to 0.2.

Given an airway wall velocity amplitude of u_0 , the constant A is chosen such that the velocity of air perpendicular to the cylindrical surface, u , is equal to u_0 at $r=d$, the outer radius of the segment:

$$u = (j\omega\rho) (\partial p(r)/\partial r) |_{r=d} = u_0$$

where ρ is the density of the propagation medium (the parenchyma). For a sinusoidal wall velocity ($u_0 e^{j\omega t}$), and when d is small when compared with the wavelength λ , substitution and differentiation yields:

$$A = \pi^2 f \rho d u_0$$

and thus the solution to the radial wave equation in cylindrical coordinates is:

$$p(r) = d\pi^2 f \rho u_0 \left[J_0(2\pi f r/c) - jN_0(2\pi f r/c) \right]$$

which at large distances from the cylinder ($r/\lambda > 1$) reduces to the more familiar:

$$p(r) = \pi \rho d u_0 \left[c f / r \right]^{1/2}$$

which depicts the $r^{-1/2}$ dependence of the pressure of a cylindrical wave.

As previously mentioned, the extent of parenchyma in which a wave generated by large airway wall motion must travel to reach the posterior chest wall is roughly 10 cm. This value is not significantly greater than the sound wavelengths in the parenchyma of approximately 23 cm to 4 cm over the 100 to 600 Hz frequency range. Thus, the approximate solution of the wave equation in which the radial dependence has an $r^{-1/2}$ dependence was not employed in our representation. Instead, the more exact solution which incorporates the Bessel and Neumann functions was used. The constraint that the radius of the airway is small when compared to the sound wavelength is satisfied well at low frequencies. However, since the radius of the largest airway, the trachea, is approximately 0.9 cm, the ratio of λ/d reduces to a value of roughly 5 at a frequency of 600 Hz. Thus, this more exact solution to the wave equation is a more accurate representation of the pressure in the parenchyma

at lower frequencies and for the smaller airways, where the ratio of λ/d is large.

2.3.3 Estimation of the radiation impedance of the surrounding parenchyma

The parameter, Z_{rad} , in the T equivalent network, which represents the acoustic radiation impedance imposed by the parenchyma on the intrathoracic airways, is estimated for each segment by evaluating the solution to the wave equation at the outer airway wall surface ($r=d$):

$$Z_{\text{rad}} = p(r)/Au_0 \cong (d\pi^2 f \rho / A) \left[J_0(2\pi f d / c) - jN_0(2\pi f d / c) \right]$$

where A is the external surface area of the intrathoracic airway segment in cm^2 . Figures 13 and 14 depict the predicted mechanical radiation resistance and reactance, in unit of cgs ohms, for the model parenchyma which represents resting lung volume ($h = 0.25$). To a first order, this impedance behaves like a lumped mechanical resistance, $R_m(f)$ which is frequency

dependent, compliance, C_m , and mass, M_m , series combination and is incorporated into the circuit model of the airways in the general form:

$$Z_{\text{rad}} = R_{\text{rad}}(f) + j \left[\omega L_{\text{rad}} - (1/\omega C_{\text{rad}}) \right]$$

where the subscript rad denotes the acoustic impedances, which are derived from the estimated mechanical impedances in concert with a knowledge of the outer surface area, A , of the airway walls. This form of Z_{rad} was chosen in order to allow direct comparisons to be made with the values of the wall acoustic elements. The frequency dependent values of the acoustic resistance $R_{\text{rad}}(f) = R_m(f)/A$ are estimated directly from $R_m(f)$ (figure 13).

The values of the acoustic inertance $L_{\text{rad}} = M_m/A$ and the acoustic compliance $C_{\text{rad}} = 1/K_{\text{rad}} = A/K_m$ are determined by a method employed by Ishizaka, French and Flanagan (1975). The imaginary part of the mechanical radiation impedance, $X(\omega)$, is assumed to be a series combination of a mechanical mass and compliance:

$$X(\omega) = \omega M_m - (K_m/\omega)$$

Thus, the resonance radian frequency of the wall mechanical impedance is:

$$\omega_0 = \left[K_m / M_m \right]^{1/2}$$

and substitution yields:

$$\begin{aligned} X(\omega) &= \left[M_m K_m \right]^{1/2} \left[(\omega / \omega_0) - (\omega_0 / \omega) \right] \\ &= \left[M_m K_m \right]^{1/2} \left[N_m - (1 / N_m) \right] \end{aligned}$$

where:

$$N_m = \omega / \omega_0$$

The radian frequency ω_0 is estimated directly from figure 14 since $X(\omega_0) = 0$. This procedure determines the quotient K_m / M_m . To estimate the $M_m K_m$ product, N_m is chosen equal to 0.5 and the value of $X(0.5\omega_0)$ is obtained from figure 14. The equations for ω_0 and $X(\omega)$ are solved simultaneously to determine M_m and C_m . L_{rad} and C_{rad} are then estimated directly from M_m and C_m , respectively, with a knowledge of the outer surface area, A , of the airway walls.

The estimated values which represent resting lung volume at 400 Hz are roughly: $R_{\text{rad}}(f) = 25 \text{ dyne-s/cm}^5$, $L_{\text{rad}} = 0.002 \text{ g/cm}^4$ and $C_{\text{rad}} = 0.000100 \text{ cm}^5/\text{dyne}$.

Upon comparing these values representing the radiation acoustic impedance to those estimated for the wall properties of the trachea and the bronchi (L_w , R_w , C_w in Table I), some interesting features become evident. For the trachea, the wall mass dominates the overall mass, the resistances are comparable, and the radiation compliance is roughly four times larger than the wall compliance. For the bronchi, the radiation mass is roughly seven times larger than the wall mass, the radiation resistance dominates the overall resistance, and the wall compliance dominates the overall compliance. These comparisons indicate that the effect of the surrounding parenchyma on airway wall motion is a strong function of the segmental wall properties over the 100 to 600 Hz frequency range. The magnitude of the loading effects of the radiation mass are estimated to increase as one moves further down the bronchial tree - a prediction which appears reasonable from a structural perspective. The magnitudes of the radiation resistances indicate that the surrounding parenchyma increases the losses associated with airway wall motion significantly in vivo.

The effect of the chest wall on Z_{rad} is assumed to be small when compared to that of the parenchyma. Incorporation of the

values of Z_{rad} into the circuit model allows the magnitude of the volume velocities, and thus linear velocities, of the airway walls to be estimated in response to a sinusoidal perturbation introduced into the large airways or the mouth. The solution to the wave equation, in concert with the terms associated with the absorption of sound in the parenchyma as described in section 2.4, is then employed to estimate the magnitude of the pressure in the parenchyma at a distance from the airway segment. Although the distance from the airway walls to the chest wall varies with location, the distance from the posterior tracheal wall to the inside of the posterior chest wall in the same vertical plane is roughly constant. It was estimated from chest radiographs of healthy adult males to be approximately 10 cm. This value was chosen as the extent of parenchyma through which the cylindrical wave propagates, noting that this concentric representation is an approximation of the elliptical cross section of the thorax.

2.3.4 The chest wall as a lumped mechanical mass.

The chest wall is represented as a massive boundary to the cylindrical wave propagation in the parenchyma. This representation is consistent with the measurements of the mechanical impedance of the chest wall by Takagi (1964), where the wall was observed to behave primarily as a lumped mechanical mass at

frequencies between 100 and 600 Hz. Due to the magnitude of sound attenuation which is estimated to occur in the parenchyma, only the effect of the outgoing wave is considered. The thickness of the posterior chest wall was estimated from chest radiographs to be 3 cm, and its density is assumed to be that of tissue, $\rho_t = 1 \text{ g/cm}^3$. The acceleration, a_{cw} , in cm/s^2 at three vertical locations on the posterior chest wall corresponding to the three underlying airway segments is estimated using the equation:

$$a_{cw} = p(r)/m_{cw}$$

evaluated at a value of r equal to 10 cm, where m_{cw} is the mass per unit area of the chest wall in g/cm^2 and the pressure, $p(r)$, is in units of dynes/cm^2 .

2.4 Absorption of Sound in the Parenchyma

2.4.1 The parenchyma as spherical air bubbles in water

As previously described in chapter 1, since the sound wavelengths λ_p , between 100 and 600 Hz are significantly longer than the average alveolar radius r_0 , the magnitude of the thermal losses are theoretically much larger than those associ-

ated with scattering or viscous effects. These thermal losses arise since the bubble compressions and expansions are polytropic; they are more adiabatic at the center of the bubble and isothermal where the air and the liquid are in contact. This section will describe the representation of the parenchyma as air bubbles in water to estimate the effect of these thermal losses on the acoustic wave.

2.4.2 An alveolus and the effective mass of the surrounding tissue as a locally reacting oscillator

Each bubble representing an alveolus is assumed to be driven into radial oscillations by an acoustic wave. In this chapter, the mechanical parameters which relate force to linear velocity at the bubble surface are denoted with italics. If the bubble is subject to a static compression which is small in amplitude, the effective mechanical compliance, \mathcal{C} , in cm/dyne of the bubble is provided in Kinsler, Frey, Coppens and Sanders (1982) as:

$$\mathcal{C} = 1/(12\pi r_0 \kappa P)$$

where κ is the polytropic constant which describes the compression. κ is a function of r_0 , λ_p and the thermal characteristics of the air and tissue. It reflects the depth of the thermal

penetration into the bubble due to the propagating wave. For an r_0 of 0.015 cm, κ ranges from approximately unity, indicating isothermal conditions, to approximately 1.03 over the 100 to 600 Hz frequency range (see Plesset and Prosperetti, 1977). Estimations of the values of κ are detailed in section 2.4.3. The resulting value of C for $\kappa = 1.0$ is approximately 1.77×10^{-6} cm/dyne.

When the bubble is in oscillation, it acts like a small pulsating sphere (simple source) and thus radiates sound uniformly in all directions. Although the bubbles are located at a distance from each other such that they act independently from a thermal perspective, as detailed in section 2.4.3, it is likely that the effect of neighboring bubbles on the effective mechanical mass of the tissue, M in grams, which surrounds the bubble is significant. This effect results in a magnitude of M which can be estimated to be approximately one-half of the magnitude of the radiation mass of a simple source in an infinite medium of tissue. Thus,:

$$M = 2\pi r_0^3 \rho_t$$

where ρ_t is the tissue density. For $r_0 = 0.015$ cm, the value of M is roughly 4.25×10^{-5} g. An alveolus-surround unit is defined as the combination of the bubble and this effective me-

chanical mass. Given the composite K of the parenchyma, for values of $h = 0.25$ and $r_0 = 0.015$ cm representing resting lung volume, the number of bubbles per unit volume, N , is approximately $5.3 \times 10^4/\text{cm}^3$.

2.4.3 Estimation of the magnitude of the thermal loss associated with wave propagation

Using a linear analysis, Prosperetti (1977) represented the thermal effects associated with the forced radial oscillations of bubbles in a liquid in terms of two dimensionless parameters, G_1 and G_2 . The parameter G_1 reflects the relationship between the depth of the thermal penetration into the bubble and the sound wavelength in air and G_2 includes the effects of the bubble size.

$$G_1 = D_g \omega / c_g^2$$

$$G_2 = r_0^2 \omega / D_g$$

The parameter D_g is the thermal diffusivity of air, which equals approximately $0.253 \text{ cm}^2/\text{s}$ at biological conditions of temperature and pressure. The angular frequency in radians is $\omega = 2\pi f$ and c_g is the sound speed in air in cm/s as determined by the density, ρ_g , in g/cm^3 and the compliance of air, K_g , in

cm²/dyne. G_2 is essentially the square of the ratio between the bubble radius and the thermal penetration depth, the latter which is of the order of $(D_g/\omega)^{1/2}$:

$$G_2 = \left[r_0 / (D_g/\omega)^{1/2} \right]^2$$

For values representing the parenchyma at resting lung volume over the frequency range from 100 to 600 Hz, G_1 ranges from approximately 1×10^{-7} to 1×10^{-6} and G_2 ranges from approximately 0.5 to 3.4. This range of G_2 indicates that the pressure-volume relationships of the compressions are roughly isothermal at 100 Hz ($G_2 < 1$) and deviate towards a more adiabatic state at higher frequencies ($G_2 > 1$).

Values for the polytropic constant κ and a dimensionless thermal damping constant B have been determined analytically for values of G_1 and G_2 . This information is provided in tabular form by Prosperetti (1977) and is adapted for this representation in table II. B is an extremely weak function of G_1 over the range of G_1 encountered in this representation of the parenchyma. The range of values estimated for the polytropic constant κ indicates the transition from the nearly isothermal towards more adiabatic conditions for the bubble compression. As this transition occurs with increasing frequency, the

thermal losses as estimated by B increase significantly. A quadratic was fit to the values of κ and B provided in Table II in order to estimate their values more precisely when G_2 ranges between 0.5 and 5.0. The resulting quadratic equations which represent the frequency dependence at resting lung volume are:

$$\kappa = 0.99908 + 1.45765 \times 10^{-5} f + 5.10660 \times 10^{-8} f^2$$

$$B = -1.23337 \times 10^{-3} + 1.66087 \times 10^{-4} f - 6.20364 \times 10^{-8} f^2$$

The effective mechanical resistance of each alveolus-surround unit, R , in dynes-s/cm can then be estimated as a function of frequency from the values of κ and B. This procedure, which completes the representation of the bubble as a locally reacting oscillator with resistance, mass and compliance, is detailed in Kinsler, Frey, Coppens and Sanders (1984). The resulting R is:

$$R = 2\pi r_o^2 \gamma B \left\{ 6P\rho_t / \kappa \right\}^{1/2}$$

where γ is the ratio of specific heats for air under adiabatic conditions. Estimated values of R are a strong function of

frequency and are approximately six-fold larger at 600 Hz than at 100 Hz.

The estimated thermal penetration depth into the tissue is of the order of $(D_1/\omega)^{1/2}$ and is less than roughly $r_0/10$ over the entire frequency range of interest. This maximum depth of roughly 0.0015 cm for an average alveolus indicates that although the thermal effects penetrate approximately into the center of each bubble, they only extend a small distance into the surrounding fluid. This distance dictates the spacing required between each bubble in order for each to act as individual absorptive units.

2.4.4 Estimation of the attenuation of a pressure wave

The extinction cross section, σ in cm^2 , for each unit may then be calculated using the estimated values of C , M and R (see Kinsler, Frey, Coppens and Sanders, 1982). Intuitively, σ is the area of a plane transverse to the incident sound beam that intercepts power equal to the power loss due to absorption:

$$\sigma = 16\pi^2 r_0^4 \rho_l c_l R / \left[R^2 + \left\{ \omega M - (1/(\omega C)) \right\}^2 \right]$$

where c_t is the sound speed in tissue in cm/s as determined by the density, ρ_t , in g/cm³ and the compliance of tissue, K_t , in cm²/dyne. The acoustic intensity at some distance r in the parenchyma, $I(r)$, due to an initial intensity I_0 for N bubbles per unit volume is given by:

$$I(r) = I_0 e^{-N\sigma r}$$

Since the intensity is proportional to the square of the pressure amplitude, the acoustic pressure in dynes/cm² for an initial pressure amplitude P_0 is:

$$p(r) = P_0 e^{-(N\sigma/2)r}$$

Thus, the attenuation coefficient, α , is:

$$\alpha = N\sigma/2 \quad \text{Nepers/cm}$$

$$\cong 4.35N\sigma \quad \text{dB/cm}$$

Figure 15 depicts the estimated attenuation, in dB, of a plane wave transmitted through 10 cm of model parenchyma in which the value of h is 0.25, representing resting lung volume, and equal to 0.35, representing excess fluid in the lung. For these two cases, the number of alveoli, N , is unchanged while

the radius of each alveolus, r_0 , is decreased from 0.0150 to 0.0143 cm to satisfy the increase in h . This increase in h represents the addition of roughly 300 ml of fluid uniformly into the lung. It has been estimated clinically that the addition of 600 ml results in a magnitude of gas-exchange dysfunction which can cause death. At resting lung volume, the magnitude of the absorption is negligible at 100 Hz and increases to approximately 30 dB at 600 Hz. The slope of the attenuation curve is a strong function of both r_0 and h , suggesting that losses in this frequency range are sensitive to changes in parenchymal structure. Increasing h to 0.35 decreases the predicted attenuation at 600 Hz by more than 12 dB.

In the model, the effect of this attenuation was incorporated into the characteristics of the wave propagation in the parenchyma. This incorporation assumes that the effect of the absorption on the cylindrical wave can be approximated by the effect on a plane wave traveling the same distance in the parenchyma. The plane wave approximation was employed primarily to decrease the computational complexity of the approach.

2.5 Model Predictions

2.5.1 Transfer function between the chest wall and the mouth

The integrated model predicts the magnitude of acceleration of the chest wall due to an acoustic perturbation at the mouth. Acceleration is the output variable since it is easily measured and is simply related to the acoustic pressure in the parenchyma, $p(r)$, for a primarily massive chest wall. The model estimates the acceleration at four approximate locations: over the extrathoracic trachea above the suprasternal notch, and on the right posterior chest wall, 5 cm lateral to the center of the spine, at the levels of the 3rd, 5th and 7th thoracic vertebrae (T_3 , T_5 , T_7 , respectively). These locations are accessible for measurement and the chest wall sites do not overlies the scapula.

2.5.2 Spectral characteristics of transmission

The magnitude of the transfer function of acceleration in cm/s^2 to volume velocity at the mouth in cm^3/s at frequencies between 100 and 600 Hz is depicted in figure 16. The location of the spectral peak at approximately 250 Hz in all four of the spectra is dictated by the dimensions of the model respiratory tract (38.5 cm in total length) and the mechanical properties of the airway walls. As noted previously, this frequency corresponds roughly to the fundamental resonance of a rigid pipe of length 35 cm which is filled with air and open at one end.

The decrease in the magnitude at the T_3 or T_5 chest wall sites relative to the tracheal site at lower frequencies is approximately 20 dB. This decrease is primarily due to two factors; the radial dependence of the cylindrical wave propagation through 10 cm of parenchyma and the effect of a more (approximately three times) massive chest wall relative to the tissue overlying the trachea. Each factor accounts for approximately one-half of the magnitude of the decrease (in dB) at lower frequencies. The additional decrease in the magnitude of acceleration of the chest wall at higher frequencies is primarily a function of the attenuation of sound in the parenchyma associated with thermal effects. The predicted acceleration at the T_5 site is slightly less than that of the T_3 site at lower frequencies yet greater than that of the T_3 site at frequencies above approximately 350 Hz. This difference occurs since the wall properties of the bronchi which underlie the T_5 site allow it to be a more efficient radiator of sound at higher frequencies than the trachea, which underlies the T_3 site. The decrease in the acceleration of the T_7 site with respect to the other chest wall sites largely depicts the effect of the zero pressure boundary condition (an open acoustic tube) of the underlying terminal airway segment.

2.5.3 Sensitivity to Changes in Parenchymal Structure

The effect of changes in the structure of the parenchyma on sound transmission may be estimated using this modeling approach. By altering the model parameters which represent the parenchyma, the effect of diseases of the parenchyma such as pulmonary edema may be investigated. Figure 17 depicts the predicted power spectrum of acceleration at the T_3 site for a value of the volumetric proportion of tissue, h , equal to 0.25 representing resting lung volume, and equal to 0.35, representing approximately 300 ml of excess fluid in the lung (refer to figure 15). The effects of the non-ideal sound source and the tube through which sound was introduced into the mouths of healthy subjects is included. These instrumentation effects are detailed in chapter 4.

The predicted increase in acceleration over the chest wall is significant at higher frequencies for this magnitude of increase in h . This prediction is consistent with previous clinical observations of increased transmission of voice sounds through the lung in pulmonary congestion, especially at higher frequencies (see Bates, 1979). It is also qualitatively consistent with the increased amplitude of transmission which was observed by Donnerberg et al. (1980) in dogs after the induction of pulmonary edema.

The magnitude of the absorption at higher frequencies is an extremely sensitive function of the values employed to represent the structure of the parenchyma. In this representation, average values based upon the anatomy of the adult male as determined by previous investigations were employed. The accuracy and variability of many of these values, for example the average alveolar radius, have never been quantitatively assessed, primarily due to experimental difficulties. Thus, a theoretical assessment of the accuracy of the magnitude of the absorption as a function of frequency cannot be attempted at this time.

2.5.4 Sensitivity to Changes in Bronchial Structure

The effect of changes in the size or wall properties of the bronchi may be estimated using the theoretical model. Two specific alterations in the model parameters were evaluated; a decrease in the effective cross sectional area of the bronchi and a decrease in the compliance of the bronchial walls. These two parameters qualitatively represent the changes in lung structure which occur in some forms of obstructive airways disease. A 40% decrease in these parameters was chosen in order to be consistent with the magnitude of the increase in the volumetric proportion of tissue employed in estimating the

parenchymal effects. In this manner, a qualitative comparison can be made concerning the theoretical importance of each of these structures in the determination of the frequency characteristics of transmission.

Figure 18 depicts the predicted power spectrum of acceleration at the T_5 site for a value of the effective cross-sectional area of the bronchi of 2.54 cm^2 , representing the normal lung at resting lung volume, and equal to 1.52 cm^2 , representing a 40% decrease in area. The predicted decrease in the quality factor of the spectral peak at low frequencies from roughly 3.5 to 2.5 stems primarily from the increased viscous resistance of the model bronchial segments. Each viscous and wall resistance in the circuit model representing the bronchi is increased by a factor of approximately 2.1 due to the 40% decrease in area. At higher frequencies, where the magnitude of the acceleration is determined largely by the structure of the parenchyma, the effect of the change in area is less significant. These model predictions suggest that the characteristics of the spectral peak at low frequencies may be indicative of the effective size or patency of the bronchial airways. Further experimental investigation is required to elicit the quantitative relationship between airway area and sound transmission.

The effect of changes in the compliance of the model bronchial walls on the spectrum of acceleration of the chest wall is negligible. This prediction is primarily due to the dominance of the combination of the bronchial wall and the radiation impedance by the latter. Thus, the model suggests that while the tracheal wall properties, especially the tracheal wall mass, are important in the determination of the total tracheal wall-radiation impedance, the bronchial wall properties are relatively less important. Even at low frequencies, where the bronchial walls are primarily compliant, significant changes in the magnitude of the compliance does not significantly affect the overall impedance. This prediction suggests that sound transmission to the chest wall may be relatively insensitive to bronchial airway wall properties in this frequency range.

2.6 Discussion of the Theoretical Approach

The complex acoustic properties of the respiratory system stem from its unique structure. The respiratory tract consists of the vocal tract, the trachea, and a network of branching airways. The intrathoracic airways are surrounded by lung parenchyma which is, in turn, encased by the chest wall and the diaphragm. Circuit models of these airways in concert with

measurements of the time of propagation of sound in the respiratory system of human subjects suggest that a significant amount of acoustic energy is coupled directly from within the large airways to the surrounding parenchyma via wall motion at frequencies between 100 and 600 Hz. This phenomenon is of interest since there is a wealth of clinical evidence which suggests that the characteristics of this transmission are sensitive to changes in lung structure which occur in disease. In this chapter, we have presented a theoretical model of sound transmission in the intact human respiratory system. This approach will allow quantitative comparisons to be made between experimental observations and model predictions. In this manner, the key parameters which affect sound transmission can be elucidated and a better understanding of the changes which occur with disease obtained.

The model is an integration and extension of previous theoretical and experimental investigations of the respiratory system and the dynamics of bubbles in a fluid. In our approach, a number of simplifications were employed due in part to the limited frequency range of interest and an attempt to limit the complexity of the representation. Acoustic circuit models of the airways, where the values of the intrathoracic wall properties were estimated from input impedance measurements, were modified to accurately represent the system over the 100

to 600 Hz frequency range. As depicted in chapter 4, this representation of the intrathoracic airways as a single effective tube estimates the input impedance of the subglottal system reasonably well. It simplifies the model from an intuitive and computational perspective. However, it does not include the possible spatial effects of the five branching levels included or the mediastinum, which lies primarily on the left side of the large airways. Thus the model predictions are likely to be more accurate at the measurement sites overlying the right lung rather than the left.

The representation of the parenchyma as a homogeneous mixture of tissue and gas by Rice (1983) was extended to incorporate the effect of thermal losses in the attenuation of the acoustic wave. The effects of local or regional heterogeneity of parenchymal structure are not included in the model. This representation assumes that only compression and expansion of the alveoli occurs and that there is no gas exchange between adjacent alveoli due to the wave propagation at frequencies greater than 100 Hz. Furthermore, it assumes that the losses associated with the propagation of the cylindrical wave can be estimated by the extinction coefficient of absorption for a plane wave. The validity of this approach increases as the distance from the airway wall, r , increases and the pressure of the cylindrical wave follows the more familiar $r^{-1/2}$ dependence.

The rapid increase in predicted absorption as a function of frequency qualitatively explains previous observations by Kraman (1983a) of poor sound transmission to the chest wall in human subjects at frequencies greater than approximately 400 Hz. Given the predicted magnitude of the absorption which occurs upon propagation through 10 cm of parenchyma, the consideration of only the outgoing wave is reasonable at higher frequencies. However, since the magnitude of the acoustic impedance of the chest wall is significantly greater than that of the parenchyma, neglecting reflections at the parenchyma-chest wall interface could result in the underestimation of the acceleration of the chest wall by as much as 6 dB. Also, since the magnitude of the absorption is small at frequencies below approximately 200 Hz, resonances of the thoracic cavity may be important in this range.

The assumption that each airway segment radiates a cylindrical wave which is only a function of the radial distance from the segment ignores the possible interactions between the waves generated by different segments. This assumption appears to be reasonable since the sound wavelengths in the airway lumen are greater than approximately 58 cm at these frequencies and standing waves are produced in response to a sinusoidal perturbation due to the termination impedance of the

circuit model. These two facts indicate that only a small time delay exists between the oscillations of adjacent airway segment walls. However, since there exists significant differences in the amplitude of the oscillation of the tracheal and bronchial walls, as depicted in figure 16 by the differences in the predicted acceleration of the chest wall as a function of the measurement site, the radiation of sound from the trachea may not be purely cylindrical and thereby contribute to the measured acceleration over bronchial regions.

As previously mentioned, the structure of the parenchyma plays a major role in the determination of the acceleration of the chest wall at higher frequencies. The increased acceleration due to an increase in the volumetric proportion of tissue, h , is qualitatively consistent with the clinical observation of the increased transmission of voice sounds to the chest wall in the congested lung, especially at higher frequencies. It is also in agreement with the increased transmission of sound observed by Donnerberg et al. (1980) in dogs after the induction of pulmonary edema. However, the frequency dependence of the increase was not measured and thus a quantitative comparison between the measurements and the model predictions cannot be made. In the model, a decrease in the equilibrium radius, r_0 , due to an increase in h , results in conditions of bubble compressions which are more isothermal and results in a decrease in the magnitude of the absorption in the parenchyma.

These thermal losses also suggest a possible mechanism for the clinical observation of decreased transmission of voice sounds in patients with emphysema, where there exists enlargement and destruction of the alveolar walls. A quantitative comparison is difficult in this pathology since it exists as a heterogeneous pattern in the lung, as observed by Ploysongsang (1982). Also, for values of h much less than 0.25, the constraint that each alveolar-surround unit acts independently from a thermal perspective can no longer be insured since the distance between each alveolus becomes of the order of the thermal penetration depth into the tissue.

2.7 Summary

This chapter details the development of a theoretical model of sound transmission in the intact human respiratory system at low frequencies. An attempt was made to limit the complexity of the approach by constraining the frequency range of interest, representing the respiratory tract as a single effective tube and the parenchyma as a homogeneous mixture of gas and tissue. The model outputs were chosen to allow direct comparisons to be made with measurements performed on human subjects. This approach provides the first theoretical framework

for further investigation into the effects of structural changes on sound transmission in both health and disease.

The model suggests two key relationships between the structure of the respiratory system and the spectral characteristics of the transmission of sound from the mouth to the chest wall. The first is the determination of the location and sharpness of the spectral peaks by the geometry and wall properties of the airways. This relationship suggests that changes in the effective length or size of the airways may be monitored through changes in the characteristics of the spectral peaks of transmission. The second relationship is the significant effect of the thermal losses in the parenchyma on the magnitude of transmission at higher frequencies. The predicted sensitivity of the attenuation to changes in parenchymal structure suggests that diseases which affect the parenchyma may alter the magnitude of the acceleration significantly.

3. MEASUREMENTS OF SOUND TRANSMISSION IN ADULT SUBJECTS

3.1 Introduction and Goals

The alterations in the characteristics of sound transmission in the respiratory system at frequencies below approximately 1000 Hz which occur in some disease states are qualitatively indicative of underlying lung structure and function. Clinicians routinely listen on the chest wall to transmitted voice or lung sounds in order to obtain regional information which augments the anatomical information obtained from radiographic techniques. A theoretical model of sound transmission in the intact human respiratory system at low frequencies has been described in chapter 2, and provides insight into the relationship between the structure and the acoustical properties of the system.

The frequency characteristics of sound transmission from within the respiratory tract to the chest wall have never been accurately assessed in humans. Kraman (1983a) estimated the power spectrum of sound transmission from mouth to chest wall at low frequencies in 5 adult subjects. However, since the primary goal of that study was to measure the propagation time of sound in the respiratory system, the experiment employed the

following: a variable input power level over the 150 to 500 Hz range, a high pass filter with a cutoff frequency of 200 Hz and a 12 dB/octave roll-off, an uncharacterized sound source and tube through which sound was introduced into the mouths of the subjects, and microphones which were calibrated in free field and not in their measurement configuration in the proximity of the chest wall. While minimally affecting propagation time measurements, these factors affect the spectral characteristics of the experimental model and make a direct comparison between these spectra and any theoretical model of sound transmission difficult.

This study was designed to accurately assess the frequency characteristics of sound transmission from the mouth to the chest wall by circumventing the aforementioned technical limitations. In our experimental approach, a sound source which was characterized from an acoustical perspective was employed to introduce sound into the mouths of 8 healthy subjects. Acceleration measurements of the chest wall were performed at resting lung volume using calibrated contact transducers. Statistically rigorous spectral estimates were obtained for each subject using signal averaging and smoothing techniques. In this chapter, the observed frequency characteristics of transmission for each subject are presented and issues concerning the observed intra- and inter-subject variability are discussed.

3.2 Apparatus

3.2.1 Hardware

The experimental apparatus which was employed to perform the acoustic transmission measurements is depicted in figure 19. Electrical noise with equal energy at 4 Hz intervals over the 100 to 1124 Hz frequency range (Hewlett-Packard Co., Loveland, CO, model 3582A) was input to a frequency equalizer (Realistic, Tandy Corp., Fort Worth, TX, model 31-2010). The equalizer output was connected to a power amplifier (Vector Research Inc., Chatsworth, CA, model VA-1400) which applied a voltage to a loudspeaker (Peavey Electronics Corp., Meridian, MS, model 22A compression driver).

To determine the adjustment of the spectrum of the input noise to be performed by the equalizer, a sinusoidal voltage source was employed as the input to the system. The frequency of this source was swept over the complete range of interest and the equalizer settings were adjusted such that the output of the loudspeaker, as measured at a distance of 20 cm in a large room, was flat as a function of frequency to ± 2 dB. This adjustment compensated for any non-ideal characteristics

of the sound source. The sinusoidal voltage source was then replaced by the aforementioned electrical noise source prior to the experimentation. The root mean square (rms) voltage of this noise was roughly 1.5 V and thus the electrical power supplied to the loudspeaker, which has a nominal input impedance of 8Ω , was 0.3 W. A rigid tube of length 18 cm and diameter roughly 3 cm was attached directly to the output of the compression driver to allow the sound to be coupled into the mouths of the subjects. Chapter 4 provides a detailed description of the acoustical properties of the sound source and the tube.

Sound pressure measurements were performed within the rigid tube using a small electret microphone (Realistic, Tandy Corp., Fort Worth, TX, model 33-1063) mounted flush with the tube wall at a distance of 2 cm from the mouths of the subjects. Acceleration measurements were performed using accelerometers constructed by Vermarian and Vollenhoven (1984, model FYSPac2) at three measurement locations: over the extrathoracic trachea, 5 cm below the glottis and on the right posterior chest wall, 5 cm lateral to the center of the spine, at the levels of the 3rd and 6th thoracic vertebrae (T_3 , T_6). These accelerometers, which are lightweight (< 2 g) and have a flat frequency response to ± 1 dB over the 100 to 1000 Hz frequency range, were attached to the skin using double-sided tape.

The output signals from the accelerometers were amplified to a voltage suitable for digitization using custom-built electronic circuits. A diagram of one channel of this amplification scheme is shown in figure 20. The output sensitivity of the preamplifier stage is estimated by multiplying the accelerometer sensitivity and the feedback resistance:

$$\text{sensitivity} = 10 \text{ pA}/(\text{m/s}^3) \times 10\text{M}\Omega = 0.1 \text{ mV}/(\text{m/s}^3)$$

The magnitude of the subsequent voltage amplification (figure 20) is a factor of 10 for the accelerometer at the tracheal site and a factor of 100 for the accelerometers on the chest wall. The amplifier output signals, in concert with the output of the microphone within the tube, are connected to a set of four-pole Butterworth bandpass filters with cutoff frequencies of 75 and 1400 Hz. These filters reduce the effects of low-frequency heart sounds and the aliasing of higher frequency information upon digitization at 4096 samples/s. The analog to digital conversion circuit board (Data Translation, Marlboro, MA, model 2801A) also contains a set of voltage amplifiers, the gain of which is under software control (Compaq Inc., Houston, TX, model portable III). At the time of the experiment, this voltage gain was chosen to be a factor of 1, 2 or 4 in order to

employ as much of the $\pm 10V$ dynamic range of the analog to digital converter as possible.

3.2.2 Experimental protocol

Eight healthy, non-smoking males between the ages of 25 and 30 were studied. None of the subjects had a history of chronic respiratory disease.

While seated with his shoulders rolled forward to ensure that the accelerometers did not overly the scapula, a subject was instructed to place his mouth tightly around the tube and to breathe through his nose. The noise source was turned on and the subject was instructed to practice holding his breath with his glottis open at resting lung volume, as qualitatively monitored using inductance plethysmography (Respirace Corp., Artsley, NY, model CAL-261). The acceleration signal from the tracheal site was monitored on an oscilloscope to insure that the glottis was open. A small microphone was placed near the subject's nasal cavity and its output was monitored on an oscilloscope to insure that the velum was positioned to close off the nasal cavity from the pharynx. After a short training period, sound transmission measurements were performed with the subject in the aforementioned closed-velum, open-glottis position at resting lung volume. Eight consecutive epochs of 250

ms duration from each site were obtained during each measurement. The subject was instructed to breathe normally through his nose between the measurements and to signal the data acquisition to begin by pressing a button. This procedure was repeated 3 to 5 times for each subject.

3.2.3 Signal analysis

With a knowledge of the sensitivity of the transducers and the magnitude of the amplification which was employed, each digital epoch representing 250 ms of sound transmission data from each measurement site was converted into cgs units of pressure or acceleration. The epochs were subsequently windowed with a Hanning function and transformed to the frequency domain using a 1024-point fast Fourier transform algorithm. Average power spectra were estimated from the eight individual spectra at each measurement site and the resulting spectral estimates were smoothed via a sinusoidal running-average method with 7 degrees of freedom. The resulting effective bandwidth (resolution) in the frequency domain is roughly 10 Hz after windowing and smoothing is performed. The spectra were then converted to a decibel scale referenced to either 2×10^{-4} dynes/cm² for sound pressure (dB SPL) or 1 cm/s² for acceleration.

The coherence spectra $\alpha(f)$ between the chest wall sites and the tracheal site were also estimated using the equation:

$$\alpha(f) = |G_{yx}|^2 / G_{xx}G_{yy}$$

where G_{xx} , G_{yy} represent the average power spectra estimated at the tracheal and a chest wall site, respectively, and G_{yx} is the average cross power spectrum. In this context, the coherence is a measure, as a linear function of frequency, of the interdependence between the two signals. Any non-linearities in a system may convert some of an input signal into energy at other frequencies, yet the coherence treats this energy as noise in the system. Thus, the coherence is related to the signal to noise ratio, SNR, by:

$$SNR = \alpha(f) / [1 - \alpha(f)]$$

evaluated at each frequency, f , of interest. Coherence values near unity indicate a large SNR while deviations from this value can be used to indicate a low SNR and the need for averaging or other signal processing techniques to be employed.

3.3 Observed Frequency Characteristics

3.3.1 Coherence spectra

A representative coherence spectrum estimated from measurements of acceleration at the T_6 chest wall site and the tracheal site is depicted in figure 21. In all of the subjects, the value of the coherence function was observed to deviate significantly from unity at frequencies above approximately 650 Hz. This property of the coherence function indicated a decrease in the amplitude of transmission to the chest wall at the higher frequencies and a low signal-to-noise ratio at this site. Consequently, the power spectra of acceleration of the chest wall were estimated only over the frequency range from 100 to 600 Hz. However, spectra obtained from measurements within the rigid tube or over the extrathoracic trachea were estimated over the entire 100 to 1000 Hz frequency range.

3.3.2 Spectral estimates of sound pressure at the mouth

A representative spectrum of the sound pressure (in dB SPL) measured by the microphone within the tube with a subject performing the study is depicted in figure 22. All of the spectra which were estimated from the measurements at this site depicted 1) a well-defined peak at frequencies between approximately 140 and 180 Hz, 2) roughly a -12 dB/octave rolloff as

frequency increased and 3) a less well-defined region of increased pressure between 400 and 650 Hz.

3.3.3 Spectral estimates of acceleration

The power spectra of acceleration which were estimated from the measurements performed at the three sites on each subject are shown in figures 23-30. Each spectrum, which is plotted in dB referenced to 1 cm/s^2 , is an average of 3 to 5 spectral estimates, each of which was derived from 8 individual spectra.

The background noise in the quiet room where the measurements were performed was less than roughly -40 dB on this scale over the entire frequency range. Thus, the SNR on the chest wall is less than 20 dB at 600 Hz, as depicted in figure 31. The coherence spectrum (figure 21) indicates that the SNR decreases rapidly toward a value near to unity ($\alpha(f)=0.5$) at a frequency of roughly 800 Hz.

Although there was a significant amount of inter-subject variability, there exists a similar spectral pattern of acceleration in all of the subjects which were studied. All of the spectra exhibited a low-frequency region of increased transmission (see table III) which occurred at approximately the same frequency at all measurement sites for each subject.

For the group, this spectral peak occurred at 162.9 ± 17.2 Hz (mean \pm sd) with a quality factor of 3.7 ± 1.2 . The individual quality factors were estimated by dividing the peak frequency by its respective half-power bandwidth in the average tracheal spectrum for each subject. A second, somewhat more variable region of increased transmission to the tracheal site was observed. For the group, this spectral peak occurred at 610.5 ± 38.6 Hz with a quality factor of 6.8 ± 1.7 . The trend of decreasing acceleration of the chest wall with increasing frequency was also observed, especially at the T_6 site. The average power spectrum of acceleration for the entire group, which is shown in figure 31, depicts these general spectral characteristics. A detailed discussion of these characteristics in comparison to those predicted by the theoretical model are found in Chapter 4.

3.3.4 Effects of lung volume

The effect of lung volume on the transmission of sound from the mouth to the chest wall was qualitatively assessed by performing measurements with the subject's volume at total lung capacity (TLC). The average spectrum of acceleration for the entire group at TLC, in dB referenced to 1cm/s^2 , is depicted in figure 32. The observed spectral characteristics of the group were not statistically different than those which were

estimated at resting lung volume (functional residual capacity, FRC), at any measurement site on the chest wall ($p > 0.1$ at the T_3 site and $p > 0.5$ at the T_6 site). Figures 33 and 34 provide a direct comparison between the spectra estimated from measurements obtained at the two lung volumes.

The locations of the resonance peaks at low frequencies on the chest wall shifted to slightly higher frequencies with the increase in lung volume. This shift indicates a shorter effective length of the subglottal airways at TLC with respect to FRC i.e. the increase in the total cross-sectional area of the branching airways occurs more rapidly. However, since the increase in the locations is only 8 Hz at the T_3 site and 4 Hz at the T_6 site, the effect of the volume on the terminal boundary condition appears to be small. This conclusion appears reasonable since the lung volume at FRC is already quite large, roughly 4 liters, and indicates a fast transition to a zero pressure boundary condition without any additional increase in volume.

The increase in lung volume from FRC to TLC occurs largely due to an increase in alveolar size, but a small increase in airway size also occurs. From an acoustical perspective, the increase in airway size results in a decrease in the viscous loss associated with wave propagation within the airway lumen.

This decreased attenuation results in an increase in the amplitude of transmission to the chest wall and a change in the terminal impedance of the airways. In contrast, the model of the parenchyma qualitatively suggests that an increase in alveolar size results in an increase in the magnitude of the absorption in the parenchyma and thus a decrease in the amplitude of transmission to the chest wall. At a first glance, one would expect these parenchymal effects to dominate those associated with airway changes and result in decreased transmission at higher frequencies for measurements performed as TLC. However, the model constraint that each individual alveolus acts independently from a thermal perspective is violated for alveolar sizes much greater than those found at FRC.

An increase in volume is not incorporated homogeneously in the lung - it is primarily incorporated in the lower lung regions. Our measurement sites on the chest wall are overlying upper and middle lung regions, not overlying the areas with the maximal structural change. Another confounding factor is that as lung volume changes, the region of lung which underlies a particular measurement position on the chest wall changes. Thus, any inhomogeneities of the lung tissue would cause an increase in the variability of the measurements performed at a single chest wall site. These facts make the interpretation of the observations concerning the effects of lung volume on sound

transmission difficult to perform. Considerably more investigation is required in order to shed more light on this issue.

4. COMPARISON BETWEEN MODEL PREDICTIONS AND EXPERIMENTAL OBSERVATIONS

4.1 Introduction and Goals

The theoretical model which we have developed represents the transmission of sound from within the respiratory tract to the chest wall and accounts for the acoustic coupling through the walls of the large airways. The model output, in response to an acoustic perturbation at the mouth, is the acceleration of the tissue overlying the extrathoracic trachea and the chest wall at three posterior locations in the same vertical plane. These output variables were chosen in order to allow a direct comparison to be performed between the model predictions of the frequency characteristics of transmission and the measurements performed on healthy adult subjects. Through this comparison, the strengths and weaknesses of the approach can be estimated and further model refinements suggested.

4.2 The Sound Source and the Rigid Tube as Equivalent Circuits

In order to perform a direct comparison between the experimental observations and the model predictions, the acoustical

characteristics of the sound source and the rigid tube are incorporated into the circuit model. An electro-mechanical circuit representation of the compression driver was developed, as depicted in figure 35 and detailed in Beranek (1986). The physical interpretations of the circuit elements and their values, as supplied by the manufacturer, are provided in Table IV. The parameter e_g represents the input electrical voltage. After taking the dual of the mechanical side of the circuit (which is a mobility analog) and representing the electrical side (at low frequencies where the effects of L_e are small) as equivalent mechanical components, an equivalent Norton mechanical circuit is obtained as depicted in figure 36. This mechanical circuit is converted to an equivalent acoustic circuit, which relates pressure in dynes/cm² to volume velocity in cm³/s, given the average cross-sectional area of the driver of approximately 8.75 cm². The resulting values which are employed to represent the shunt impedance of the Norton acoustic circuit are: $R = 18.21 \text{ dyne-s/cm}^5$, $M = 9.77 \times 10^{-3} \text{ g/cm}^4$ and $C = 6.9 \times 10 \text{ cm}^5/\text{dyne}$.

An estimate of the volume velocity of the source, U , in cm³/s was determined from the aforementioned specifications and knowledge of the amplitude of the input electrical voltage generated by the noise source and adjusted as a function of frequency by the equalizer. As described in chapter 3, the elec-

trical power (rms) supplied to the loudspeaker was 0.3 W. The amplitude of this frequency dependent adjustment is provided in Table V and resulted in an estimate of U of 14 ± 3 dB, referenced to $1 \text{ cm}^3/\text{s}$, over the frequency range from 100 to 600 Hz. The magnitude of the resulting estimate of U is depicted in figure 39, in units of decibels referenced to $1 \text{ cm}^3/\text{s}$.

The acoustical characteristics of the tube of length 18 cm is included in the circuit model as three equivalent T networks, as detailed in Flanagan (1972). The dimensions of the cylindrical tube are depicted in figure 37. Due to the construction of the driver, the first 12.5 cm of the tube is slightly flanged - its diameter increase from 1.6 cm to 2.2 cm over the first 5 cm of its length and increases further to 3.0 cm over the remaining 7.5 cm of its length. The lengths of the segments which are represented by a single T network in the circuit model were chosen to be 5.0, 7.5 and 5.5 cm so that each network represented a tube segment with a constant degree of flange. The effects of this flange on the relatively long sound wavelengths of interest (> 58 cm) was represented by using the average value of the diameter of each segment represented by a single T network to determine the values of the circuit elements. The representation of a length of tube of 7.5 cm by a single T network results in an error of approximately 5% in the approximation of the impedance by a linearized

circuit element such as L at a frequency of 600 Hz. Table VI provides the dimensions of the rigid tube segments employed in the circuit representations. Figure 38 is a block diagram of the equivalent acoustic circuit which represents the sound source and the rigid tube.

To evaluate the accuracy of the equivalent circuit of the source, a sinusoidal voltage source was employed as the input to the system. The frequency of the voltage source was swept over the 100 to 600 Hz range and calibrated sound pressure measurements were performed with the loudspeaker radiating in a large room. The measured pressure at any input frequency was not only observed to be flat as a function of frequency to ± 2 dB at a distance of 20 cm from the driver (as described in chapter 3), but also was observed to be an extremely weak function of the measurement angle and to roughly follow a distance⁻¹ dependence. These observations indicate that the loudspeaker approximates a simple source in free space over this frequency range. Thus, incorporating the radiation impedance of air for a simple source in the form of a parallel combination of an acoustic resistance, R_{air} in dyne-s/cm⁵, and mass, M_{air} in g/cm⁴, into the circuit model of the source allows one to estimate the volume velocity of the source from the pressure measurements.

$$R_{air} = \rho_g c_g / 4\pi a_s^2$$

$$M_{air} = \rho_g / 4\pi a_s$$

where ρ_g is the density of air in g/cm³, c_g is the free field sound speed in air in cm/s, and a_s is the radius of the source in cm. Again, assuming that the radiation is spherical, the pressure in dynes/cm² at some distance r_s from the source is related to its volume velocity by:

$$p(r_s) = \rho_g fU / 2r_s$$

This procedure resulted in a theoretical estimate of the pressure at a distance of 20 cm from the source of roughly 47 +/- 3 dB SPL at any frequency within the 100 to 600 Hz range. The measured values using a sound level meter at this distance was 48.5 +/- 3 dB SPL, a difference of approximately 2 dB. The accuracy of the circuit model was determined to be adequate for our purposes in this study based upon the small value of the difference between the predicted and the measured values.

4.3 The Accelerometer as a Lumped Mechanical Mass

The mechanical effects of the accelerometers which were employed in our experimental model are incorporated into the

theoretical model. These transducers have a mass of 1.9 g and a contact diameter of 2 cm (see Vermarian and van Vollenhoven, 1984). Since the contact region is circular, the mass per unit area, m_a in g/cm² is:

$$m_a = 1.9 \text{ g} / \pi[(0.5)2 \text{ cm}]^2 \cong 0.6 \text{ g/cm}^2$$

For the measurement site overlying the extrathoracic trachea, the effect of the mass of the accelerometer is incorporated directly into the T network which represents the extrathoracic tracheal airway segment. For the chest wall measurements sites, the relationship between the pressure at the parenchyma-chest wall interface, $p(r)$ in dynes/cm² and the mass per unit area of the chest wall, m_{cw} in g/cm² is modified to include the additive mass per unit area of the accelerometer:

$$a_{cw} = p(r)/(m_{cw} + m_a)$$

again, evaluated at a value of r equal to 10 cm. Since m_{cw} is estimated to be 3 g/cm^2 , this additional mass represents an increase in the total mass of roughly 20%.

4.4 Predicted Spectral Characteristics of Acceleration

The predicted power spectra of acceleration at the tracheal and the three chest wall measurement sites (T_3 , T_5 , T_7), including the effects of the sound source, tube, and accelerometers, are depicted in figure 40. The tube acts to increase the effective length of the respiratory tract by 18 cm, thereby decreasing the location of the fundamental resonance from roughly 250 Hz, as seen in figure 16, to 168 Hz. The quality factor of this spectral peak is 3.2. This lower frequency corresponds roughly to the fundamental resonance of a rigid tube of length 52 cm which is filled with air and open at one end. The model respiratory tract and the tube have a total length of 56.5 cm when they are connected in series. The location of the lower frequency resonance is shifted upwards due to the massive properties of the airway walls. The first odd-harmonic resonance peak is also evident in this frequency range in the tracheal spectra, occurring at a frequency of roughly 510 Hz, with a quality factor of 4.9.

As expected, the relationships between the predicted accelerations of the four anatomical locations are not affected by the source, tube or the transducers. This observation is expected since identical transducers were employed at the four locations and the source and the tube both behave as linear acoustical elements.

4.5 Direct Comparison Between Predictions and Observations

4.5.1 Resonance peak locations of the tracheal spectra

In order to perform a direct comparison between the theoretical prediction and the measurement performed at the T_6 chest wall site, the average value of the model acceleration between the T_5 and T_7 sites was determined. The model parameters were not adjusted based upon the experimental data. Figure 41 depicts the model power spectra of acceleration and the average spectral estimates for the study group at the tracheal and the T_3 chest wall site. Figure 42 depicts, in a similar fashion, the model predictions and the average spectral estimates for the group obtained at the tracheal and the T_6 chest wall site. The dotted lines in the figures demarcate the 95% confidence intervals of the spectral estimates at a particular measurement site.

There exists a reasonable agreement between the model prediction and our experimental measurements at the tracheal site. The mean of the magnitude of the difference between prediction and observation (mean residual error) over the entire frequency range is 0.1 dB and is not statistically different from zero ($p > 0.5$). The first resonance peak in the model prediction, which occurs at 168 Hz and has a quality factor of 3.2, agrees favorably with the resonance frequencies of the group of 162.9 ± 17.2 Hz ($0.05 < p < 0.1$) and the quality factors of 3.7 ± 1.2 . However, the model prediction of the second resonance peak in the tracheal spectrum of 488 Hz with a quality factor of 4.9 is significantly different from the locations of 610.5 ± 38.6 Hz ($p > 0.5$) and the quality factors of 6.8 ± 1.7 which were observed.

4.5.2 Magnitude of the acceleration of the chest wall

The difference of roughly 20 dB between the magnitude of the measured acceleration over the tracheal and the chest wall sites at lower frequencies is predicted by the model. The trend of decreasing acceleration of the chest wall with increasing frequency is observed in both the model prediction and the experimental observations. The magnitude of the mean residual error over the entire frequency range is 5.1 dB at the

T_3 site, which is statistically different from zero ($p < 0.01$) and 4.9 dB at the T_6 site, which is not statistically different from zero ($p > 0.1$). Thus the agreement between the model prediction and the spectral estimates of the chest wall acceleration is more favorable at the T_6 site than the T_3 site from a statistical perspective. The largest differences occur between approximately 300 and 500 Hz, where the model significantly overestimates the magnitude of the measured acceleration.

4.6 Discussion

4.6.1 The experimental model

In this chapter, our experimental findings were directly compared to the predictions of a theoretical model of sound transmission in the respiratory system. Through this comparison, we hope to begin to identify the key structural elements which affect transmission, determine the strengths and limitations of our particular theoretical approach, and elicit the important acoustical parameters to measure as an index of pathology.

In the design of our experimental model, an attempt was made to insure that the effects of all of the acoustical com-

ponents in the system could be represented readily from a theoretical perspective. The sound source which was employed can be modeled as a Norton equivalent circuit given a knowledge of the input electrical voltage and the manufacturer's electro-mechanical specifications. This particular sound source was chosen primarily because of its small bore and output power capabilities over the frequency range of interest. The rigid tube through which sound was introduced into the mouths of the subjects has acoustical characteristics which can be described by an acoustic circuit analog in a straightforward manner.

The characteristics of the contact accelerometers (FYSPac 2) which were employed are detailed in the manuscript of Vermarian and Vollenhoven (1984). Their relatively small mass (< 2 g) as compared to that of the chest wall reduces significantly the loading effects exhibited by more massive transducers. The sensitivity-to-mass ratio of these accelerometers is roughly an order of magnitude greater than other commercially available devices. These facts, in concert with their flat frequency response over the range of interest in this study, make them well-suited for the detection of low-amplitude vibrations on the chest wall. Also, from a theoretical perspective, the dynamics of accelerometers on the highly massive chest wall are more easily described than the action of either a stethoscope-microphone arrangement or an air-coupled microphone

placed in a chamber (for ambient noise reduction) in the proximity of the chest wall. A detailed comparison between the characteristics of these and other transducers was performed in our laboratory and reported by Lara (1988).

Since a random noise source was employed as the acoustical input to the respiratory system, any spectrum which is obtained from a finite-time measurement is only an approximation of the true spectrum of the random process. Thus, signal averaging and smoothing techniques were employed to provide accurate estimates of the true spectral characteristics of sound transmission from a statistical perspective. The mean 95% confidence interval over the entire frequency range and all of the measurement sites was ± 2.1 dB, when evaluated for the subjects individually (figures 23-30). This value depicts the statistical rigor of the estimates in concert with the reproducibility of the measurements for each subject. When the spectra obtained from each subject were averaged to form three spectra representing the entire study group (figure 31), the mean 95% confidence interval increased to ± 6.3 dB. This increase indicates the variability which was observed in our measurements across all of the subjects.

4.6.2 Inter-subject variability

The observed inter-subject variability reflects the differences in the anatomy of the respiratory systems of the subjects. Our theoretical model is based upon the average anatomy of the adult male. The variability across the entire population of many of the parameter values in the model have not been measured, primarily due to experimental difficulties. Thus, the current form of the model cannot be employed to quantitatively explain the observed variability across the subjects. However, the model suggests that the magnitude of sound transmission to the chest wall is a function of structural parameters, the value of which are likely to vary considerably from individual to individual. For example, parameters such as the geometry of the large airways, the thorax, and the chest wall, and the mechanical properties of the lung parenchyma are predicted to significantly affect transmission. Also, in our experimental model, the inability to assess the exact configuration of the subject's vocal tract during the procedure is likely to increase the variability of the measurement, especially across subjects. Although the closed-velum, open-glottis position was insured, parameters such as the size of the opening of the vocal folds was not measured. By measuring some of these parameters in future studies, it may be possible to more quantitatively explain the magnitude of the observed variability.

4.6.3 Experimental and theoretical comparison

The location of the first resonance peak in the spectrum of transmission corresponds to the fundamental resonance of a rigid tube of length 53 cm which is filled with air and open at one end. The location and sharpness of this peak are predicted closely by our model which represents the respiratory tract as a single effective tube of length 38.5 cm, which is non-rigid, open at one end, and increased to 56.5 cm by the 18 cm length of rigid tube leading to the sound source. This agreement indicates the importance of the airway geometry in the determination of the fundamental resonance in this experimental model. The fundamental resonance of a rigid tube which is 56.5 cm in length, filled with air, and open at one end is roughly 155 Hz. The location of the model resonance frequency at 168 Hz indicates that the model airway walls are primarily massive in this frequency range and cause an increase in the fundamental resonance frequency.

The location of the second resonance peak in the spectra obtained from measurements performed at the tracheal site is underestimated by approximately 100 Hz by this single tube approximation of the respiratory tract. The model represents the subglottal airways as a tube with a uniform cross-sectional area equal to the total area of the branching network, which is

filled with air and open at one end. The average mechanical properties of the walls of the first five bronchial generations are incorporated into the model. This procedure results in model wall properties which are not a function of the distance of the airway below the carina. The discrepancy between the locations of the predicted and observed higher frequency resonance peaks suggest that the acoustical characteristics of the intact subglottal airways deviate at higher frequencies from those of a single tube with odd-harmonic resonances. Further investigation is required to determine if an increase in the complexity of the model, for example, to include the effects of branching or non-uniformity of airway wall properties as a function of the distance below the carina, is required in order to account for these differences at higher frequencies.

A shift in the location of the second resonance peak in the model spectrum to higher frequencies could account for the difference between the predicted and observed quality factors of 4.9 and 6.8 \pm 1.7, respectively. It may also explain, at least in part, the overestimation of the measured acceleration by the model at frequencies between 300 and 600 Hz since a shift in the peak location would cause a deeper valley in the spectrum of transmission between the two resonance peaks. This factor does not exclude the possibility that the predicted magnitude of the thermal loss may underestimate the actual absorp-

tive characteristics of the parenchyma and result in model predictions which exceed the measured acceleration of the chest wall at higher frequencies.

The magnitude of the difference between the measured acceleration over the trachea and the chest wall is approximately 20 dB at lower frequencies. Our theoretical approach predicts this difference well and suggests that it stems primarily from two factors that are roughly equal in magnitude (in dB); the radial dependence of cylindrical wave propagation through the parenchyma due to the motion of the large airway walls and the more massive chest wall as compared to the mass of the tissue overlying the trachea.

The decreased transmission of sound to the chest wall with increasing frequency is consistent with the measurements of Kraman (1983a), who observed poor transmission at frequencies greater than approximately 400 Hz. In pulmonary medicine, the lung has long been thought of as a low-pass acoustical filter. In our model, the lung parenchyma is represented as a homogeneous mixture of gas and tissue in the form of air bubbles and water. The thermal losses associated with the polytropic expansions and compressions of these bubbles are included. To represent resting lung volume, the volumetric proportion of tissue in the mixture is 0.25 (see Armstrong et al.,

1982) and the alveolar radii are 0.015 cm. The predicted decrease in sound pressure due to wave propagation through 10 cm of parenchyma is a strong function of frequency; it is negligible at 100 Hz and increases to more than 30 dB at 600 Hz. As depicted in figures 38 and 39, it accounts for the majority of the observed decrease in acceleration of the chest wall at higher frequencies. Since the predicted attenuation is a sensitive function of the volumetric proportion of tissue and the alveolar radii, altering these values slightly may result in a more favorable agreement between the predictions and the experimental observations. It is also possible that other dissipative mechanisms may play a role in the determination of the absorption of the parenchyma.

4.7 Summary

The characteristics of sound transmission from the mouth to the chest wall at low frequencies were measured in healthy adult subjects. An effort was made to employ a sound source and measurement transducers in our experimental model which could be well-characterized from a theoretical perspective. The resulting spectra of acceleration over the extrathoracic trachea and of the chest wall depicted similar patterns in all of the subjects. However, there was a large intersubject

variability in the magnitude of the acceleration which was measured. The overall spectral characteristics agreed favorably with the predictions of a theoretical model of the acoustical properties of the system which we had developed. This agreement suggests that the frequency regions where the amplitude of transmission is the largest are determined by the geometry and the wall properties of the respiratory tract, while the decreased transmission to the chest wall at higher frequencies can be largely attributed to thermal losses in the surrounding lung parenchyma.

5. CONCLUSIONS

5.1 Theoretical

5.1.1 Strengths and weaknesses of the approach

The model of sound transmission in the intact respiratory system was developed in order to understand the relationship between the structure and the acoustical properties of the system. This model provides a theoretical framework not only to begin to comprehend many of the pathological signs which physicians have observed for centuries, but to develop novel diagnostic and monitoring technologies which are non-invasive and inexpensive.

During the construction of the model, an attempt was made to limit the complexity of the approach, while still incorporating the effects of the key respiratory structures. This proved to be a difficult task primarily due to the heterogeneous anatomy of the system. The task was simplified somewhat by the limited frequency range of interest, which was chosen based upon previous observations of poor sound transmission to the chest wall at higher frequencies.

The representation of the subglottal airways as a single effective tube greatly simplified the theoretical approach, both computationally and intuitively. It allowed the thorax to be modeled as a large cylinder which is filled with lung parenchyma with a smaller cylindrical sound source at the center. Although this is an oversimplification of the true anatomy, the model respiratory tract predicted the locations and the quality factors of the resonance peaks reasonably well, especially at low frequencies. The deviations of the experimental observations from the model predictions at higher frequencies suggests that the branching bronchi, with their non-uniform airway wall properties with respect to the distance from the trachea, are not represented as accurately in this frequency range by a single uniform tube.

The lung parenchyma is a heterogeneous structure. In our model, it is represented as a homogeneous mixture of gas and tissue in the form of air bubbles in water. This representation allowed the mechanical and absorptive characteristics of the parenchyma to be estimated and incorporated into the relationships which describe the cylindrical wave propagation to the chest wall. At low frequencies, where the magnitude of the absorption is predicted to be small, the predicted properties of this wave propagation quantitatively account for the observed decrease in acceleration of the chest wall with respect to the tissue overlying the trachea.

The effect of the absorptive characteristics of the parenchyma on the cylindrical wave propagation were approximated by the effect on a plane wave traveling the same distance. This procedure was employed in order to simplify the approach from a computational perspective. The magnitude of the predicted absorption accounts for the majority of the observed decrease in the acceleration of the chest wall relative to the tissue overlying the trachea at higher frequencies. However, the predictions overestimate the observed acceleration between roughly 300 and 500 Hz, which suggests that the absorptive properties should be investigated in greater detail.

The consideration of only the outgoing wave ignores the possible effects of reflections at the parenchymal-chest wall interface. These reflections may be most important at low frequencies, where the predicted absorption is small, and result in an increase in the magnitude of the observed acceleration in this range due to thoracic resonance effects.

In summary, the theoretical approach described in this thesis employs a number of approximations concerning the acoustical properties of the sound transmission from within the large airways to the chest wall. These include the representation of the branching airways below the glottis as a single ef-

fective tube and the heterogeneous parenchyma as a mixture of air bubbles in water. The predicted frequency characteristics of transmission agree reasonably well with our experimental observations. This agreement suggests that this particular model provides a firm foundation in which to begin to understand the acoustical properties of this complex physiological system.

5.1.2 Recommendations for future research

In the evaluation of the strengths and weaknesses of this first theoretical approach to modeling the transmission of sound in the respiratory system, a number of possible model revisions and extensions become evident. These range from minor changes in some of the parameter values which were employed to major alterations in the approach which was taken. The current version of the model is relatively simple from an acoustical perspective in light of the complex anatomy of the system. Thus, any increase in the complexity of the model should be weighed against the resulting increase in accuracy or predictive capability. One would hope to eventually obtain a model which is accurate enough to be employed successfully in a predictive manner, yet simple enough to elucidate the key relationships between the structure and the acoustical properties.

As previously mentioned, there are a number of additional theoretical considerations which could be incorporated into the model. For the respiratory tract, these include the effects of bronchial branching and the changing wall properties with distance from the trachea. This incorporation could also include the spatial mechanical effects of the mediastinal structures, such as the heart, and result in model predictions of acceleration at any location on the chest wall.

Some of the effects of the local heterogeneity of parenchymal structure could be added to the model. For example, the gravitational dependence of the size of the alveoli could be included. Modeling the parenchyma as a more complicated geometrical mixture than spherical air bubbles in water would increase the complexity of the approach significantly. It may be more productive to attempt to measure the deviation of the parenchymal characteristics from that of this model geometry and include these differences directly in the theoretical representation.

The magnitude of the possible interactions between the waves generated by adjacent airway segments should be evaluated. For example, the waves generated by the tracheal segment could be assumed to have a spherical component, and the effect over bronchial regions estimated. Also, the predicted

absorption due to the wave propagation in the parenchyma should be estimated in cylindrical coordinates and quantitatively compared to the results of the plane wave approximation which was employed.

The model can be employed to predict the changes in lung structure which occur in various diseases. The effects of the changes in parenchymal structure in pulmonary edema and emphysema have been qualitatively assessed in this thesis research. The resulting model predictions of the frequency characteristics of acceleration, as compared to those of the healthy respiratory system, are in agreement with clinical observations. With some modifications, the effects of other alterations could be modeled in an attempt to better understand the changes in the acoustical properties that occur and to elicit any important parameters to measure as a function of disease.

Lastly, this general theoretical approach could be applied to the transmission of sound in the infant respiratory system. Through this application, the ability of the model to accurately describe the acoustical properties of a much smaller physical system would be assessed. Also, the use of non-invasive acoustical techniques to diagnose or monitor different types of pediatric respiratory diseases could begin to be evaluated.

5.2 Experimental

5.2.1 Thoughts on the experimental model

In the development of our experimental model, care was taken to employ sound production and measurement devices which could be characterized well from an acoustical perspective. These characteristics were then incorporated directly into our theoretical model.

The chest wall and the tissue overlying the extrathoracic trachea were assumed to be primarily massive over the frequency range of interest. This approximation is consistent with previous measurements of the impedance of the chest wall, and greatly simplifies the relationship between the pressure at the model parenchymal-chest wall interface and the acceleration of the chest wall. However, it does not include any resistive properties of the chest wall and therefore may overestimate the magnitude of the acceleration. Also, the locations of the transducers on the chest wall during the protocol are determined approximately using anatomical landmarks.

The large inter-subject variability of the measurements are reflected in the 95% confidence intervals for the group of

roughly ± 4 dB at the tracheal site and ± 6 dB on the chest wall. Qualitatively, some of this variability is due to the differences in the anatomy of the respiratory systems of the subjects. The model suggests that the acceleration of the chest wall is a sensitive function of a number of structural parameters. However, part of the variability is due to the spectral estimation procedures which were employed and the exact configurations of the vocal tracts of the subjects during the procedure.

5.2.2 Recommendations for future research

The current experimental protocol could be extended in order to obtain new information concerning the properties of sound transmission in the respiratory system. The number of measurement sites on the chest wall could be increased to provide more spatial information. The effects of the sound source and the transducers could be reduced by estimating parameters such as the transfer function of acceleration between a chest wall and a tracheal site. The effects of changing the resident gas composition could be assessed. All of these measurements could be directly compared to model predictions after some modifications have been performed.

An attempt can be made to reduce the effects of the exact configuration of the vocal tract by either assessing the configuration through another measurement technique or altering the sound induction system. It would be invaluable to develop a measurement system which is not a function of the ability of the subject to adopt the appropriate vocal tract configuration. Such a system would allow accurate sound transmission studies to be performed on individuals such as infants or critically-ill patients. The details of such a device will have to be investigated further.

The adaptation of the sound transmission studies to an animal model may prove helpful in the assessment of the accuracy and the predictive capabilities of the approach. A sound source can be placed at different locations within the large airways, measurements can be performed on the chest wall and on the underlying lung surface, and interventions reflecting pathological changes can be performed. However, prior to direct comparison with the model predictions, the model would have to be adapted in scale to represent the particular animal being studied.

The application of these experimental techniques in the study of human pathologies is underway. We are currently identifying possible patient populations to study which have

structural changes that are well-characterized. Measurements of sound transmission in such populations will allow qualitative comparisons to be performed with theoretical predictions. In this manner, the predictive capabilities of the model can be assessed, model revisions performed, and the development of new technologies guided.

| | # | length (cm) | diameter (cm) | L_w (g/cm ⁴) | R_w (dyne-s/cm ⁵) | C_w (cm ⁵ /dyne) |
|---------|---|----------------|------------------|-------------------------------|------------------------------------|----------------------------------|
| ----- | | | | | | |
| Vocal | | | | | | |
| Tract | 3 | 5.5 | 2.8 | 0.032 | 30 | 0.00093 |
| Trachea | 2 | 6.0 | 1.8 | 0.0086 | 8.5 | 0.00049 |
| Bronchi | 2 | 5.0 | 1.8 | 0.00032 | 0.7 | 0.0017 |

Table I: Dimensions of the airway segments represented by T equivalent networks and the values of the elements representing the airway walls.

| G_2 | κ | B | f |
|-------|----------|--------|-------|
| ----- | ----- | ----- | ----- |
| 0.5 | 1.001 | 0.0095 | 90 |
| 1.0 | 1.003 | 0.019 | 180 |
| 2.0 | 1.011 | 0.036 | 360 |
| 5.0 | 1.053 | 0.074 | 900 |

Table II: Numerical values of the polytropic constant, κ , and the dimensionless thermal damping constant, B , as a function of G_2 for $10^{-7} < G_1 < 10^{-6}$. Adapted from Prosperetti (1977).

| SUBJECT | F_1 | Q_1 | F_2 | Q_2 |
|---------|----------------|-------------|----------------|-------------|
| 1 | 169.3 +/- 4.6 | 5.1 +/- 1.6 | 588.0 +/- 0.0 | 8.3 +/- 0.5 |
| 2 | 168.0 +/- 10.2 | 2.8 +/- 0.7 | 627.2 +/- 24.2 | 6.5 +/- 1.4 |
| 3 | 173.6 +/- 4.6 | 4.9 +/- 1.1 | 649.6 +/- 23.4 | 7.5 +/- 2.3 |
| 4 | 180.8 +/- 12.5 | 3.1 +/- 0.4 | 645.6 +/- 31.9 | 6.9 +/- 1.4 |
| 5 | 135.0 +/- 13.6 | 3.1 +/- 1.1 | 552.0 +/- 28.3 | 5.4 +/- 0.9 |
| 6 | 146.4 +/- 10.8 | 3.2 +/- 1.3 | 592.8 +/- 7.7 | 6.1 +/- 1.6 |
| 7 | 170.7 +/- 6.1 | 4.0 +/- 0.4 | 620.0 +/- 25.0 | 8.8 +/- 2.0 |
| 8 | 157.3 +/- 6.1 | 3.6 +/- 0.3 | 580.0 +/- 6.9 | 5.6 +/- 0.4 |
| GROUP | 162.9 +/- 17.2 | 3.7 +/- 1.2 | 610.5 +/- 38.6 | 6.8 +/- 1.7 |

Table III: Frequencies (F_1 , F_2) and quality factors (Q_1 , Q_2) of the two resonance peaks for the eight subjects. Values are mean +/- sd in units of Hz for F and dimensionless for Q.

| Parameter ----- | Value ----- |
|---|----------------|
| Amplifier Output Resitance (R_g) | 0.20 Ω |
| Electrical Resistance (R_e) | 3.9 Ω |
| Magnetic Induction x Wire Length (Bl) | 1.9 Tesla-m |
| Mechanical Resistance (R_m) | 0.52 Kg/s |
| Mechanical Mass (M_m) | 0.00075 Kg |
| Mechanical Compliance (C_m) | 0.000090 m/N |

Table IV: Electro-mechanical specifications for the Peavey model 22A compression driver as provided by the manufacturer, in mks units.

| Frequency | dB |
|-----------|-------|
| ----- | ----- |
| 100 | 18 |
| 150 | 17 |
| 200 | 15 |
| 250 | 9 |
| 300 | 5 |
| 350 | 2 |
| 400 | -1 |
| 450 | -3 |
| 500 | -5 |
| 550 | -7 |
| 600 | -7 |

Table V: Amplitude of the voltage adjustment, in dB, performed by the equalizer as a function of frequency.

| Length | Diameter |
|--------|----------|
| ----- | ----- |
| 5.0 | 0.95 |
| 7.5 | 1.30 |
| 5.5 | 1.50 |

Table VI: Dimensions of the rigid tube segments represented as T equivalent networks in the circuit model.

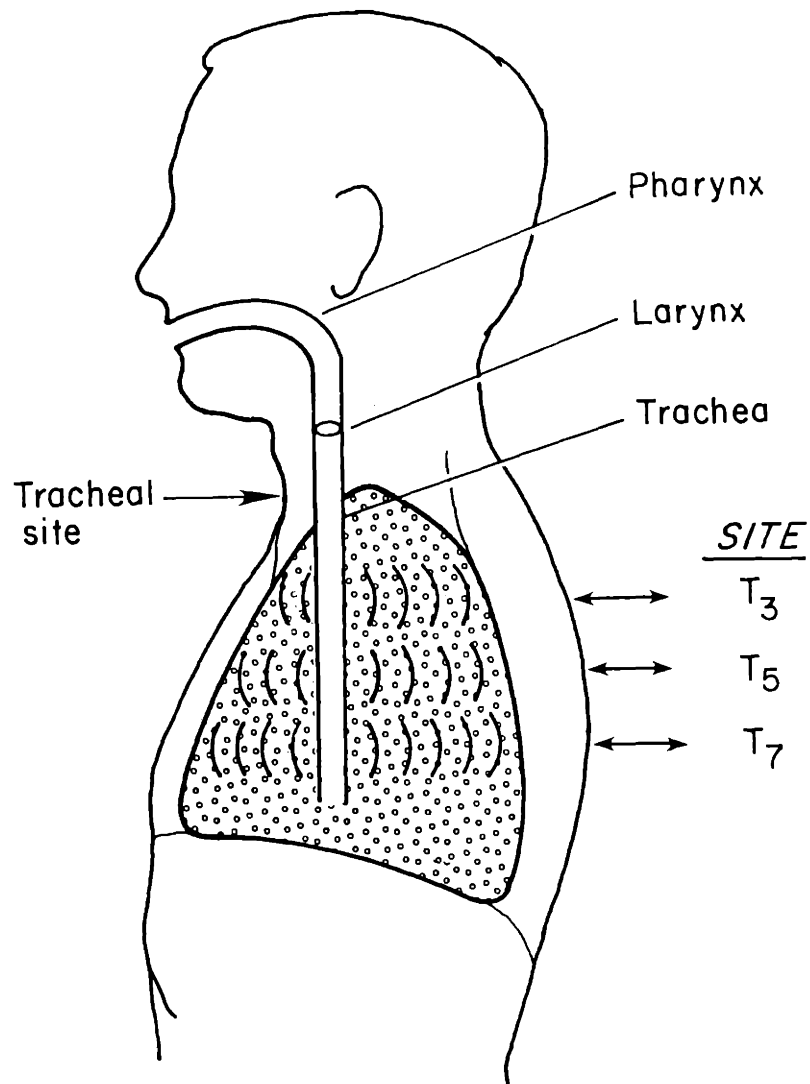


Figure 1: Diagram of the model respiratory system. The respiratory tract is represented as a single effective tube which acts as a cylindrical sound source. The surrounding lung parenchyma is represented as a homogeneous mixture of air bubbles in water with thermal losses. The magnitude of acceleration is estimated over the extrathoracic trachea and three locations (T_3 , T_5 , T_7) on the posterior chest wall.

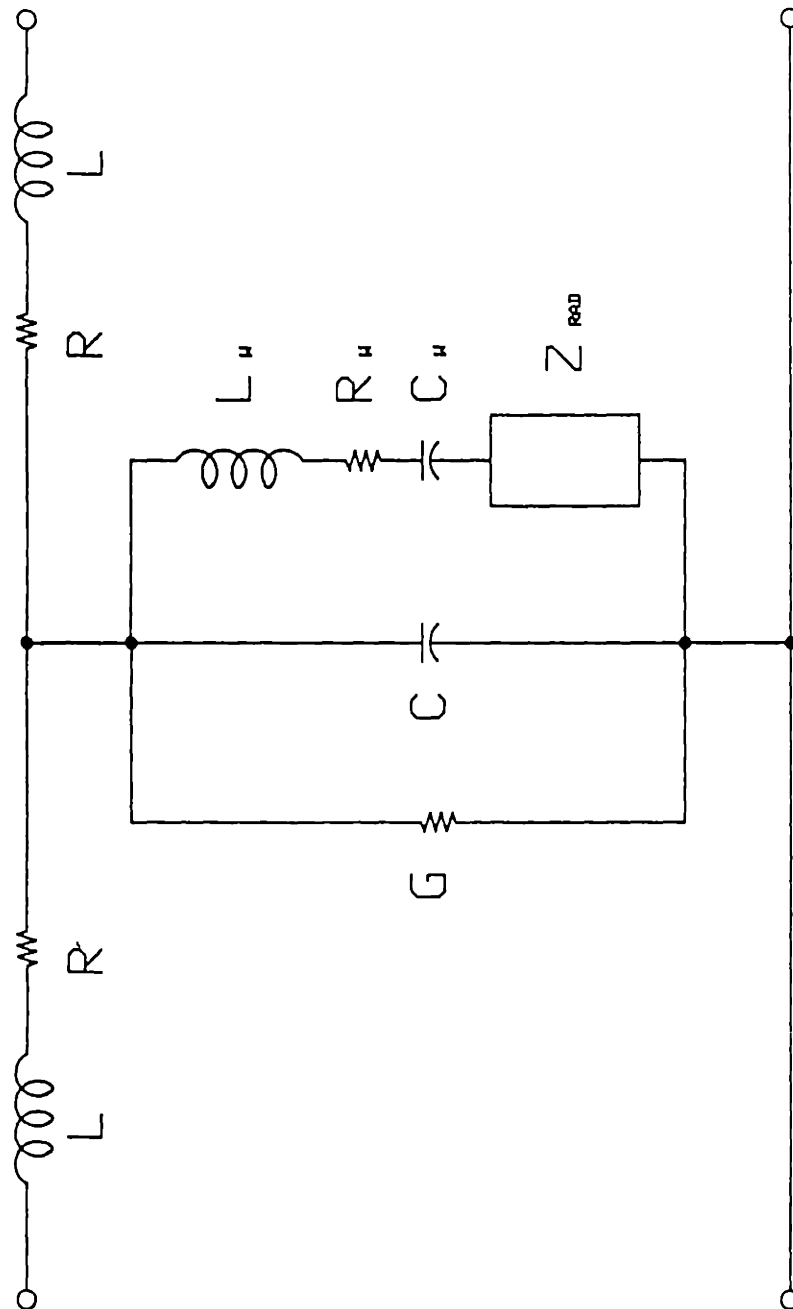


Figure 2: T equivalent circuit of an airway segment which relates intra-airway pressure to volume velocity.

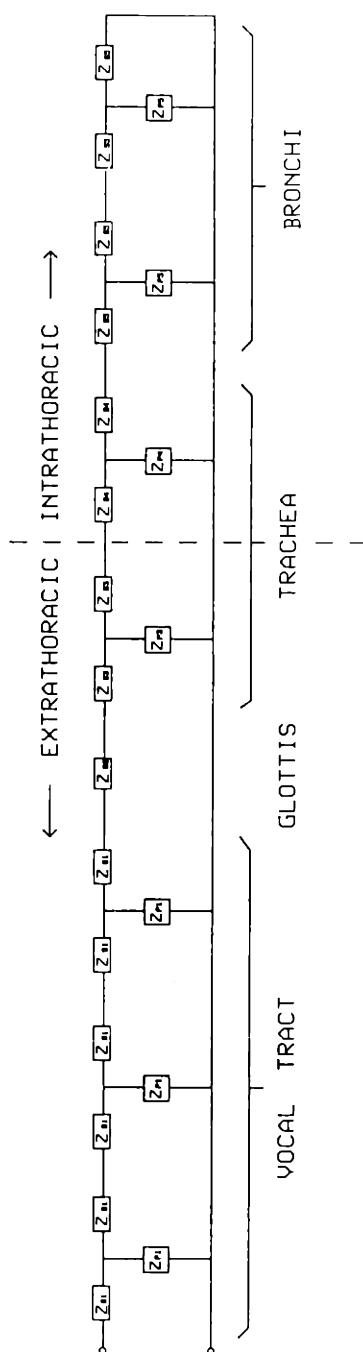


Figure 3: Block diagram of the equivalent acoustic circuit which represents the respiratory tract.

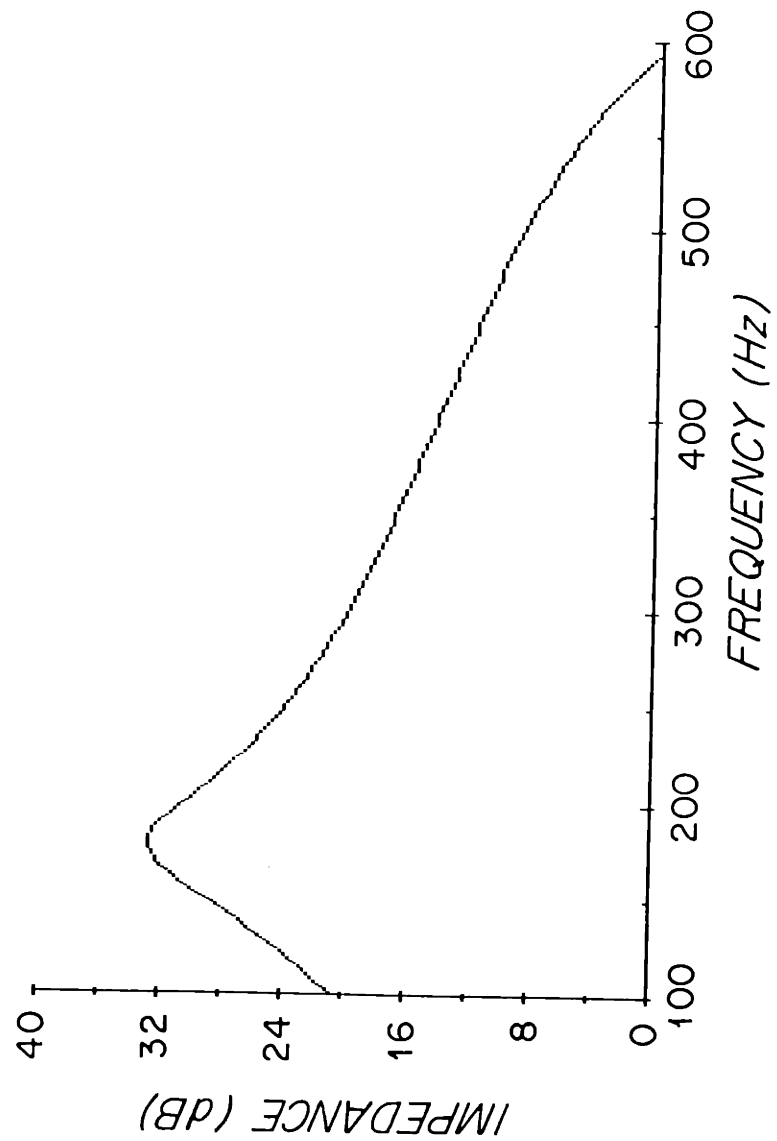


Figure 4: Magnitude of the input acoustic impedance of the model vocal tract with the glottis closed. The units are decibels referenced to 1 cgs acoustic ohm.

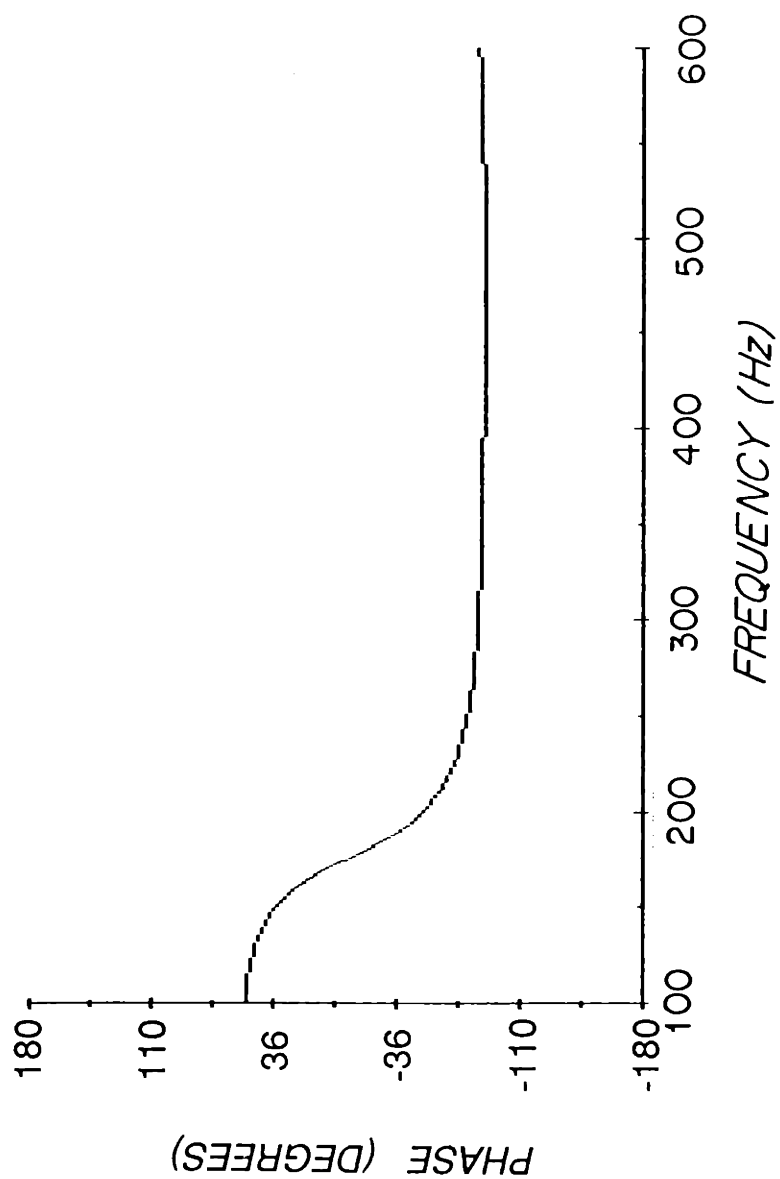


Figure 5: Phase angle of the input acoustic impedance of the model vocal tract with the glottis closed. The unit are degrees.

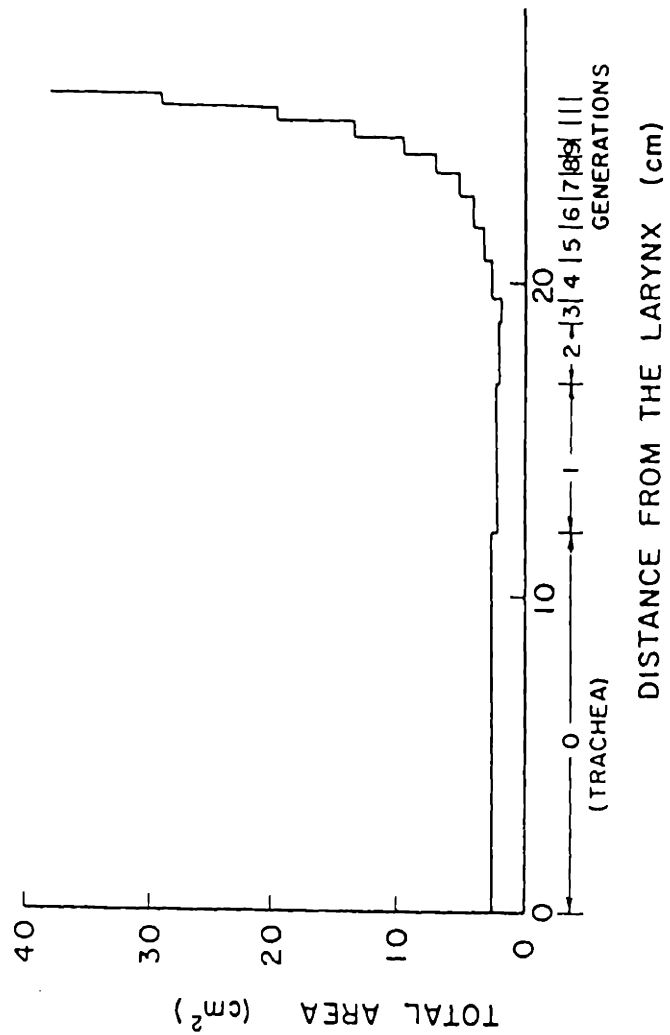


Figure 6: Total cross-sectional area of the branching airways as a function of the distance below the glottis (from Gupta, Wilson and Beavers, 1973).

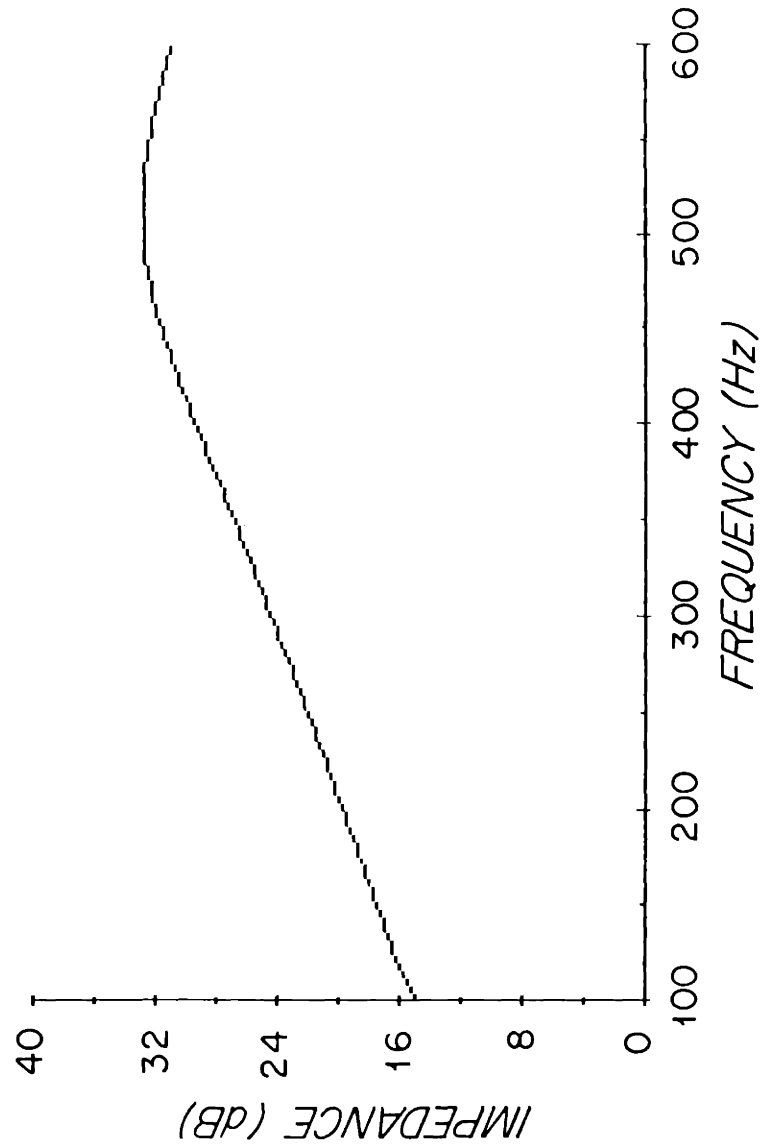


Figure 7: Magnitude of the input acoustic impedance of the model subglottal system. The units are decibels referenced to 1 cgs acoustic ohm.

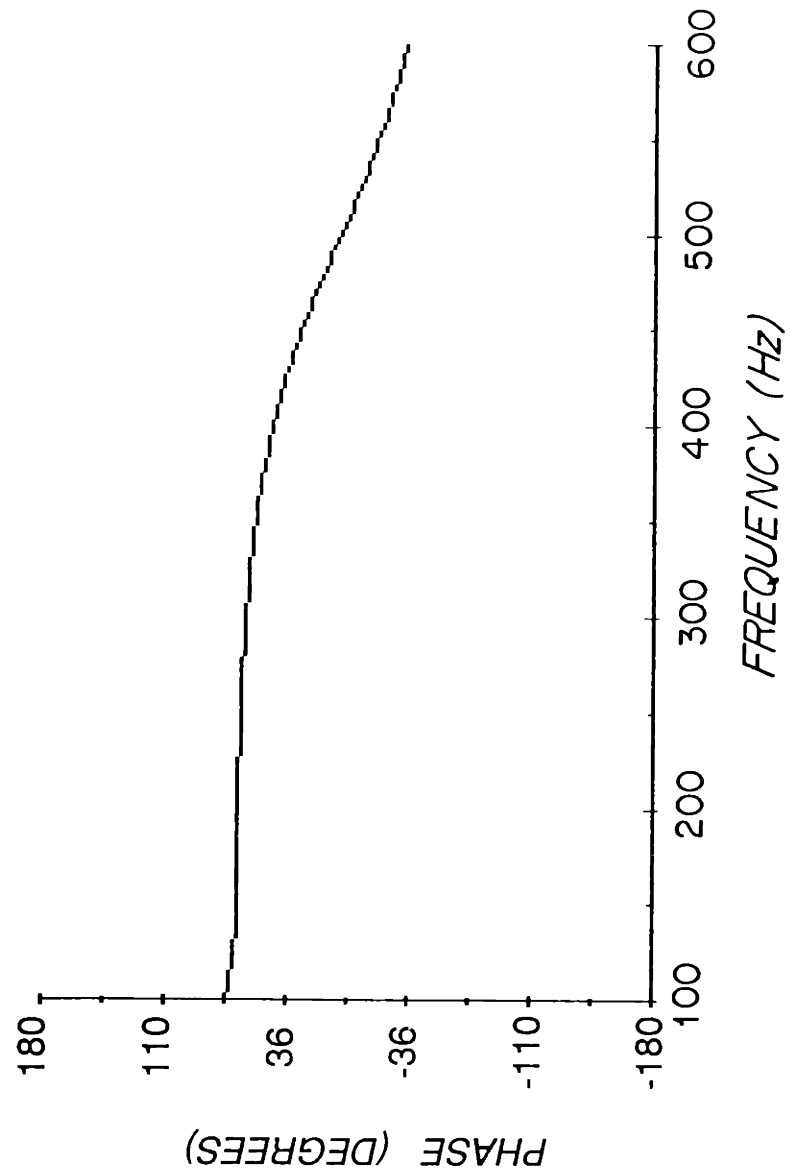


Figure 8: Phase angle of the input acoustic impedance of the model subglottal system. The units are degrees.

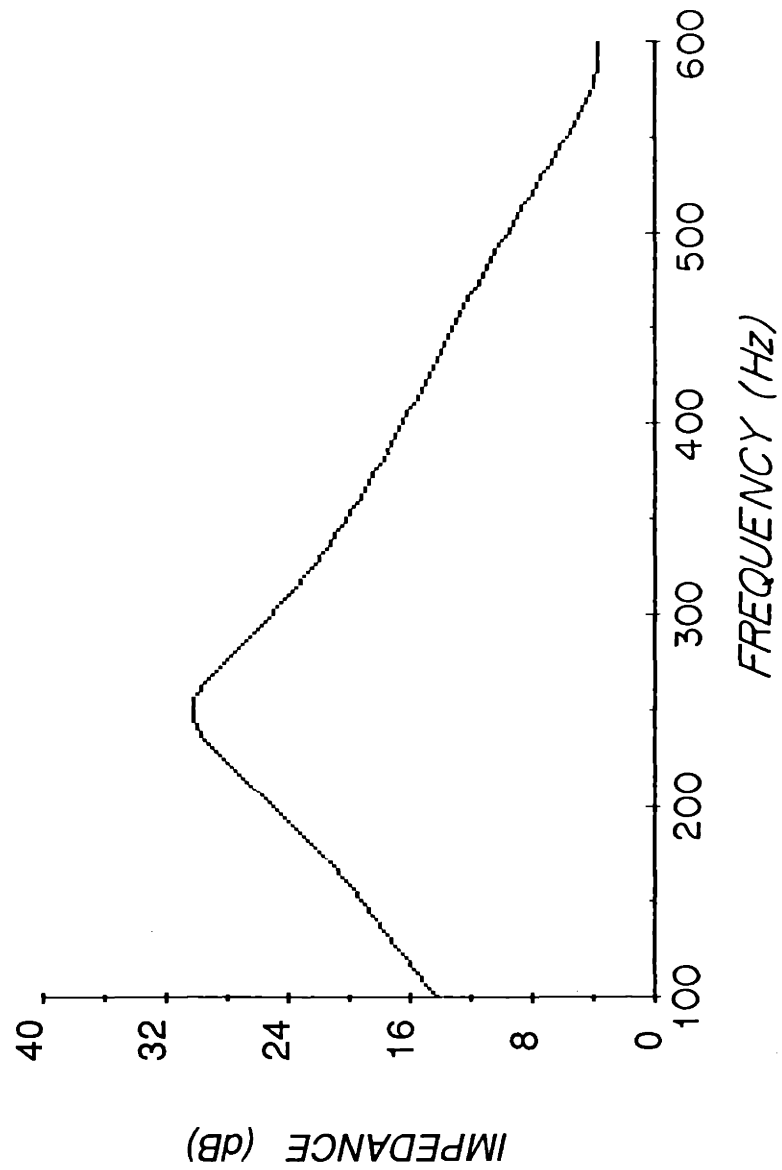


Figure 9: Magnitude of the input acoustic impedance of the model respiratory tract. The units are cgs acoustic ohms.

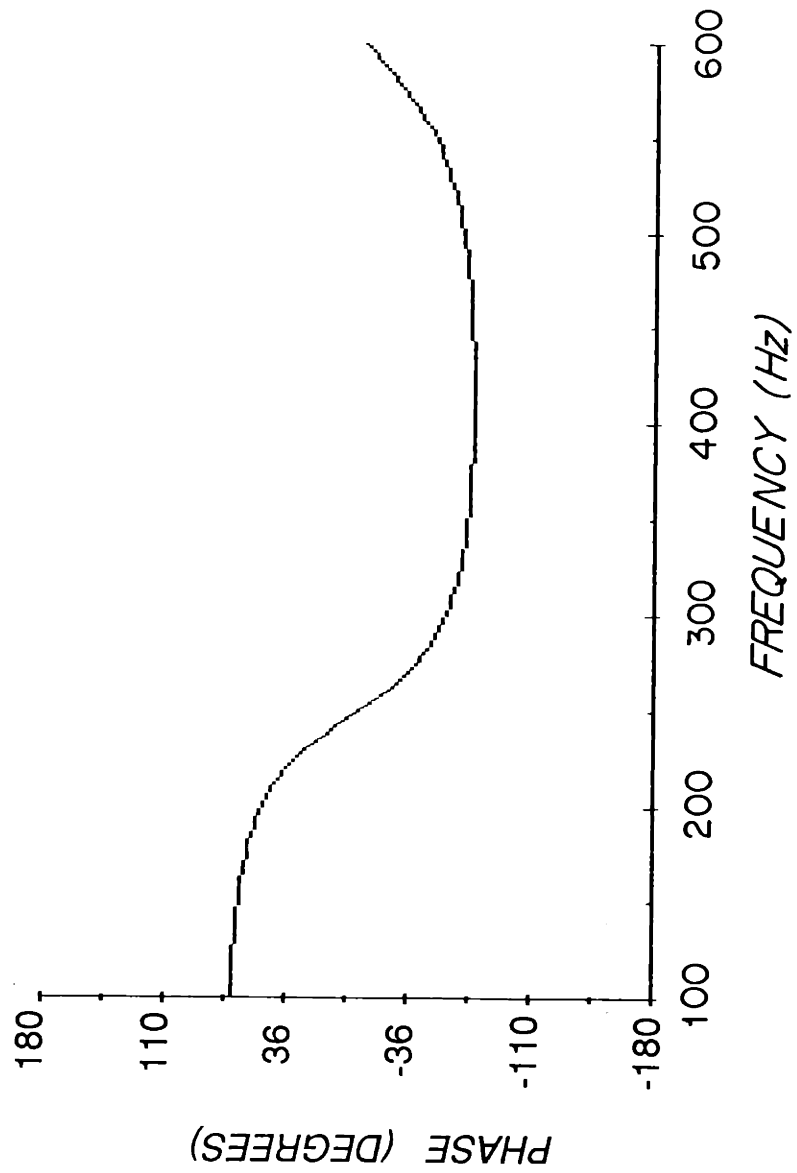


Figure 10: Phase angle of the input acoustic impedance of the model respiratory tract. The units are degrees.

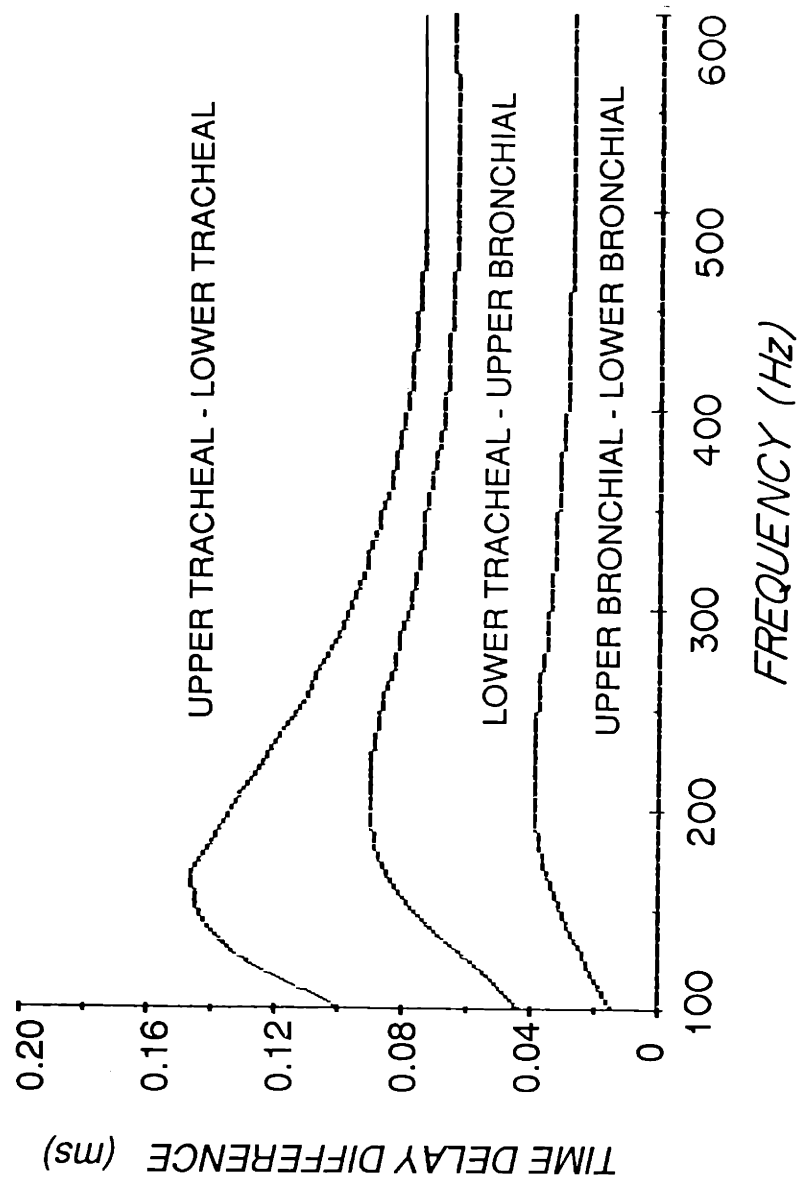


Figure 11: Time delay difference between the oscillations of adjacent model subglottal airway wall segments. The units of time are ms.

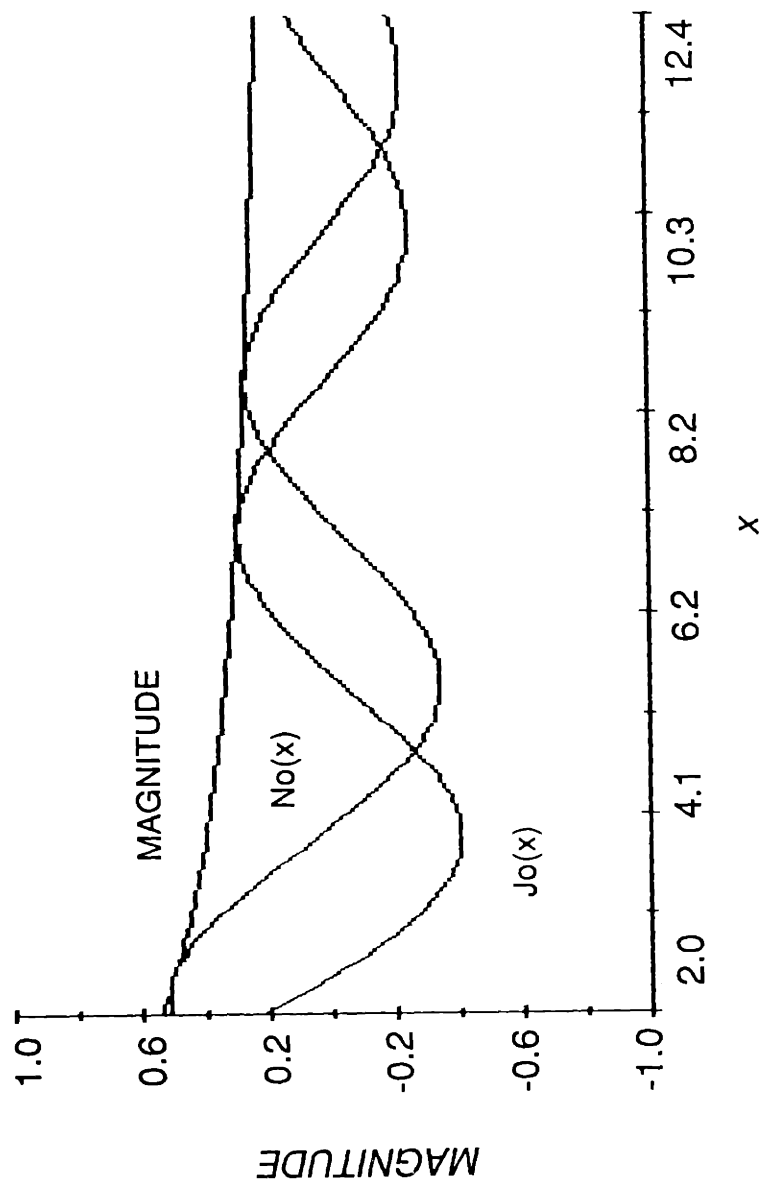


Figure 12: Amplitude of Bessel ($J_0(x)$) and Neumann ($N_0(x)$) functions and the magnitude of their sum as it appears in the solution of the cylindrical wave equation. The functions are evaluated at a distance of 10 cm from the model airway wall, which represents the posterior chest wall-parenchyma interface.

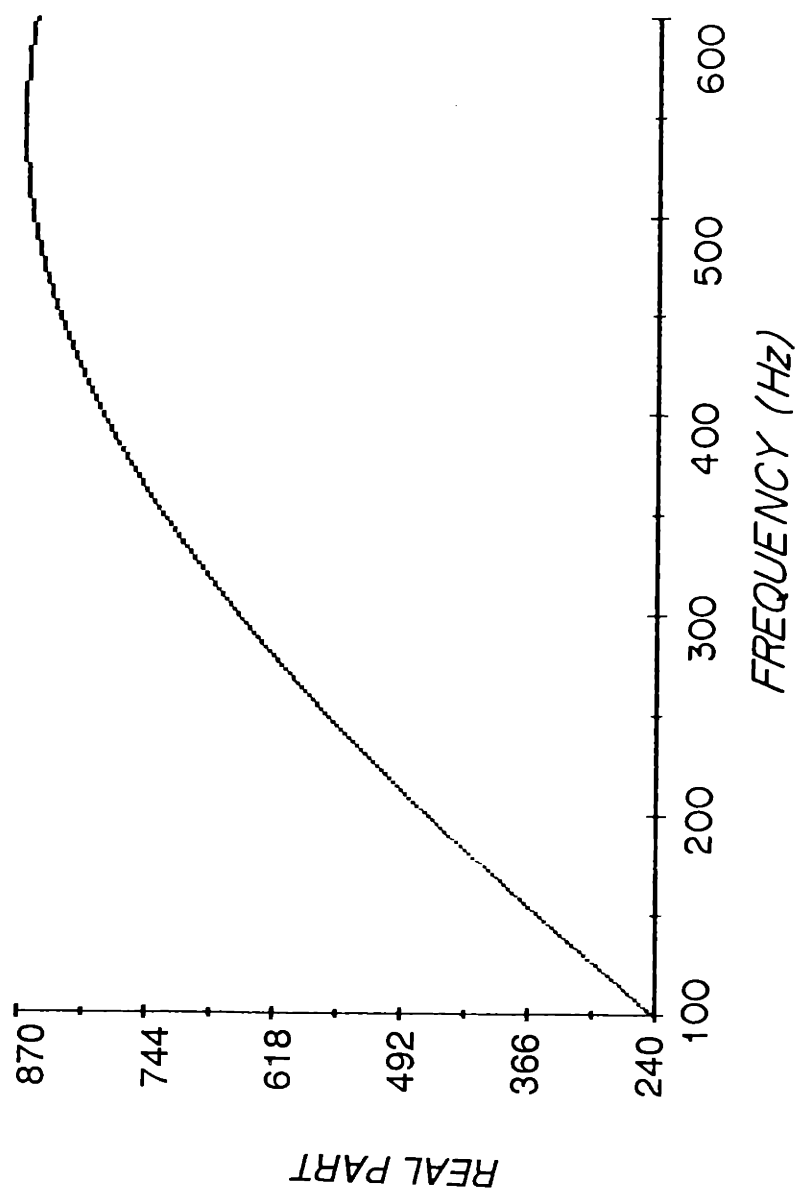


Figure 13: Real part of the estimated radiation mechanical impedance imposed by the parenchyma upon the subglottal airway walls. The unit are cgs ohms.

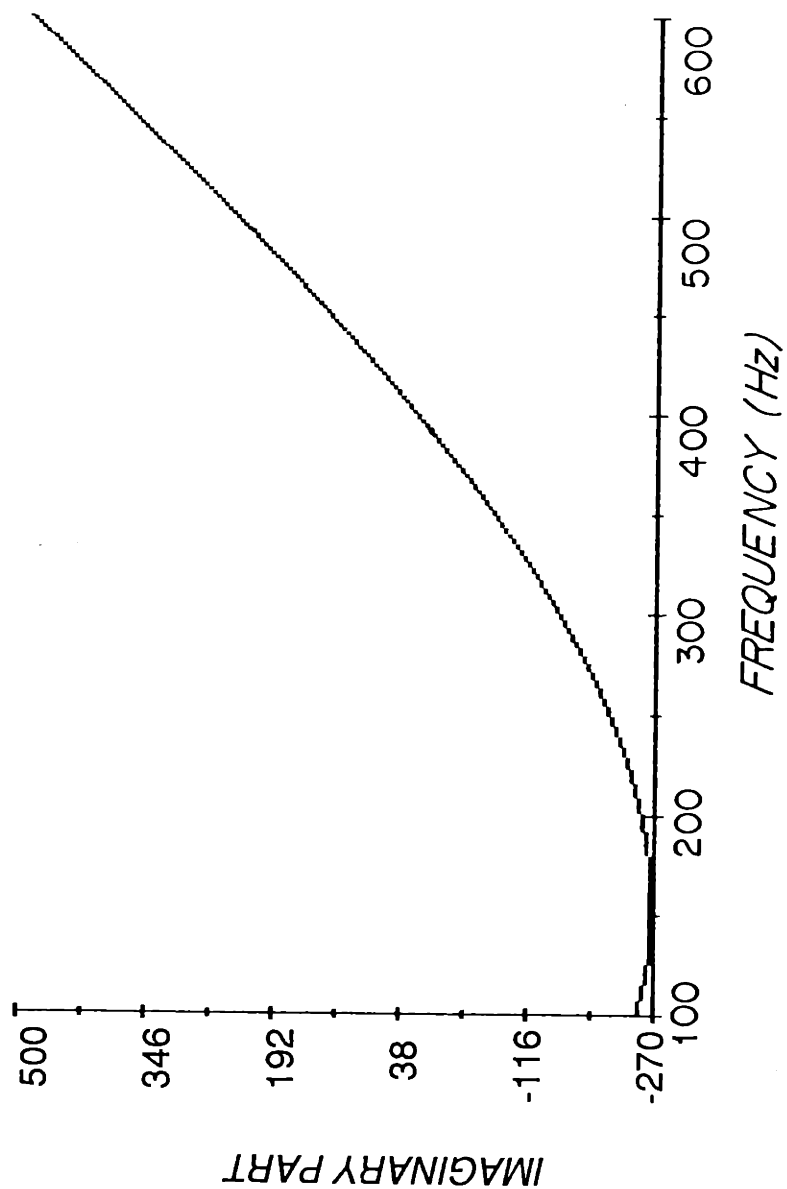


Figure 14: Imaginary part of the estimated radiation mechanical impedance imposed by the parenchyma upon the subglottal airway walls. The units are cgs ohms.

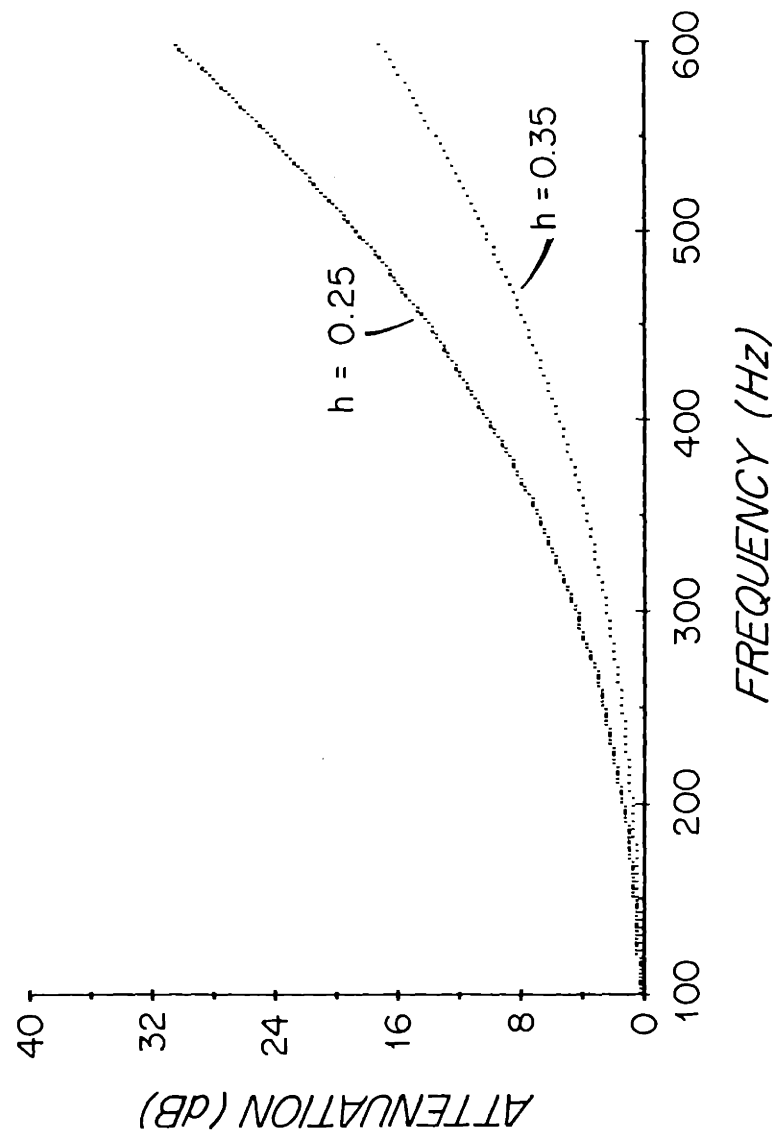


Figure 15: Attenuation of the pressure wave after propagation through 10 cm of model parenchyma. The units of decibels are arbitrary.

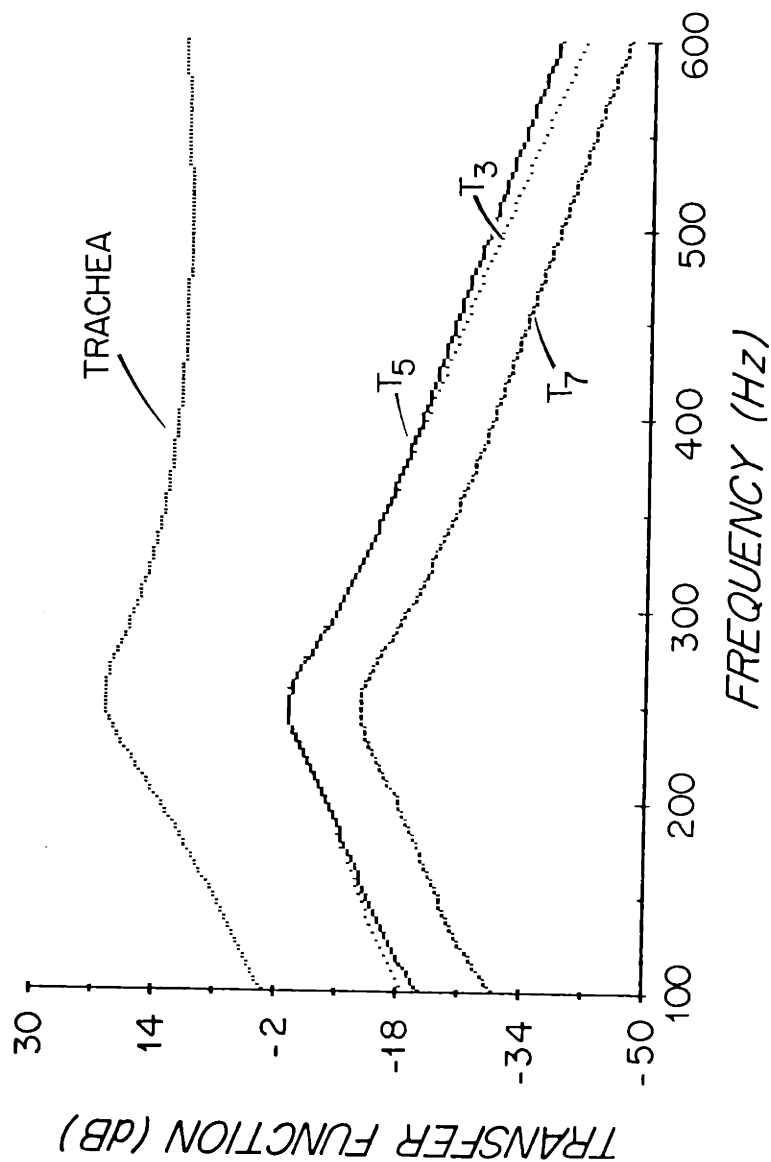


Figure 16: Transfer function of the model acceleration at the tracheal and three chest wall locations (T₃, T₅, T₇) to volume velocity at the mouth. The units are decibels, with acceleration in cm/s^2 and volume velocity in cm^3/s .

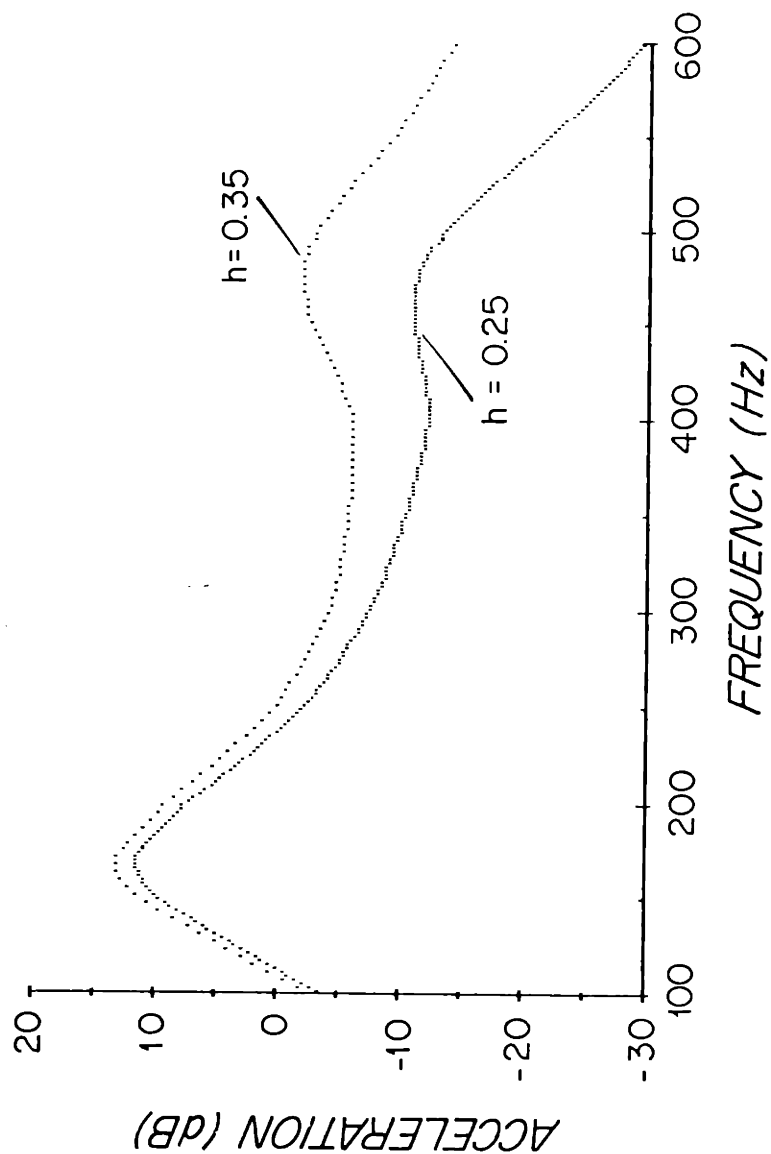


Figure 17: The effect of changing the volumetric proportion of tissue, h , from 0.25 (solid line) to 0.35 (dotted line) on the magnitude of acceleration at the T_5 chest wall site in the model. The units are decibels referenced to 1 cm/s^2 .

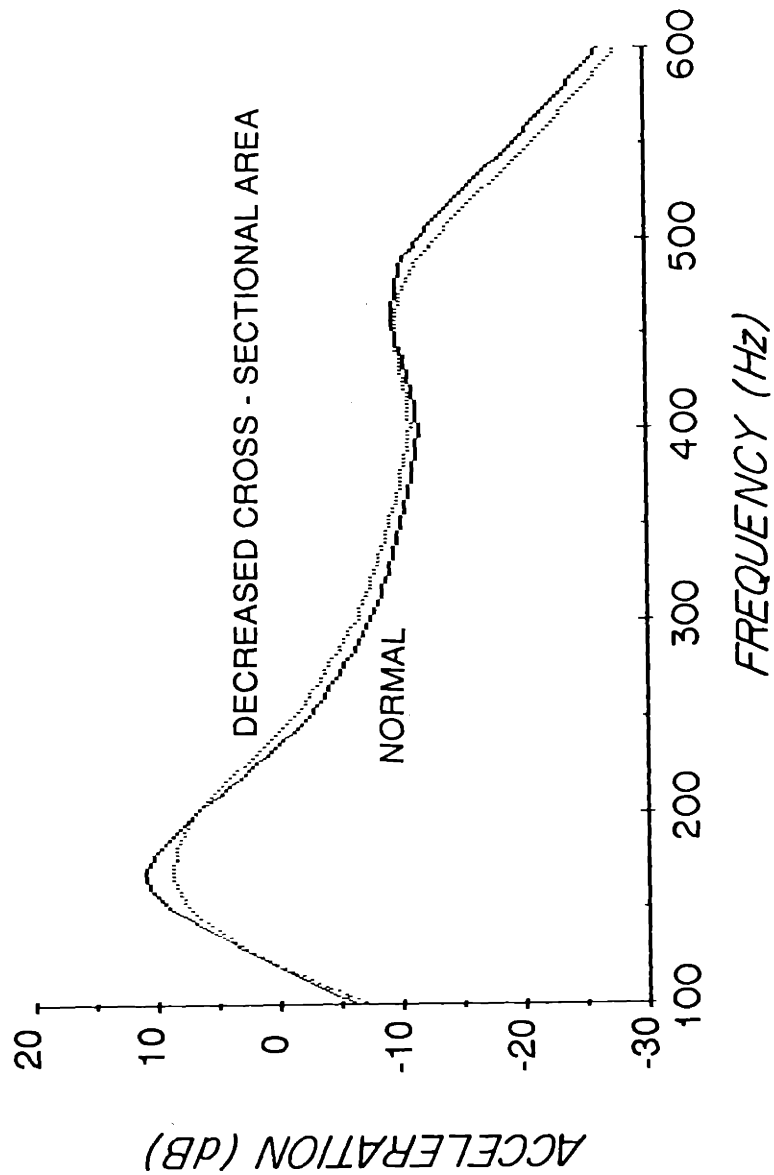


Figure 18: The effect of altering the effective bronchial cross-sectional area from a nominal value of 2.54 cm^2 to a decreased value of 1.52 cm^2 on the magnitude of acceleration at the T_5 chest wall site. The units are decibels referenced to 1 cgs acoustic ohms.

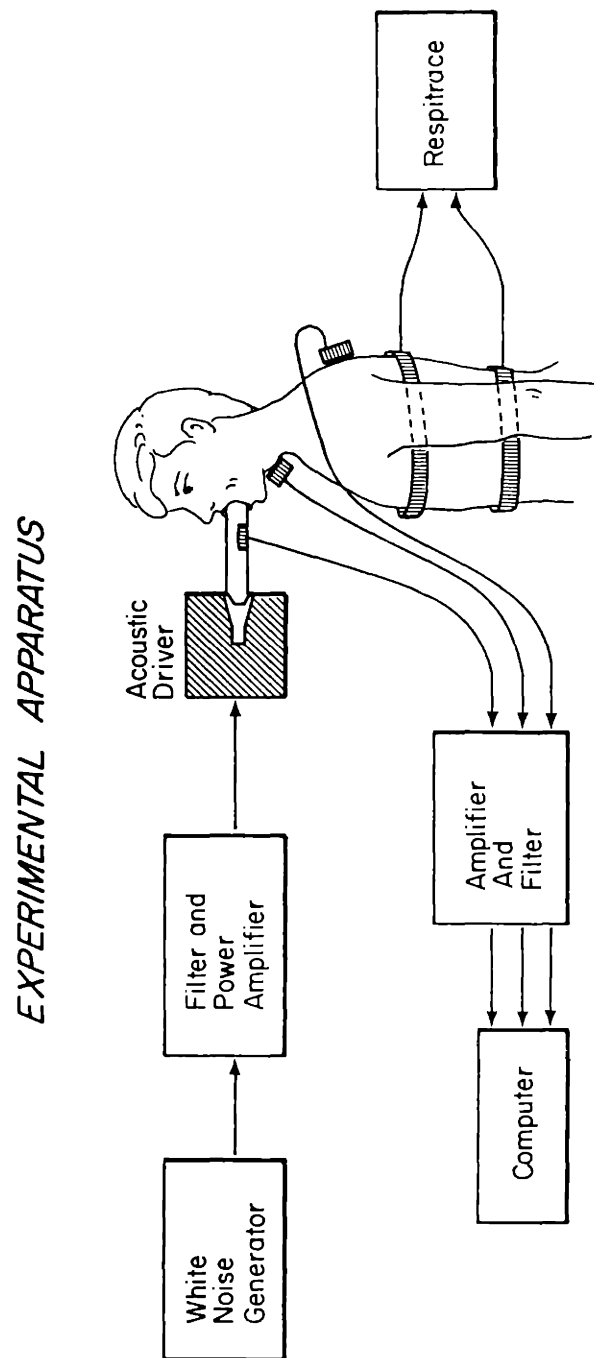


Figure 19: Experimental apparatus employed to perform the acoustic transmission measurements on healthy adult subjects.

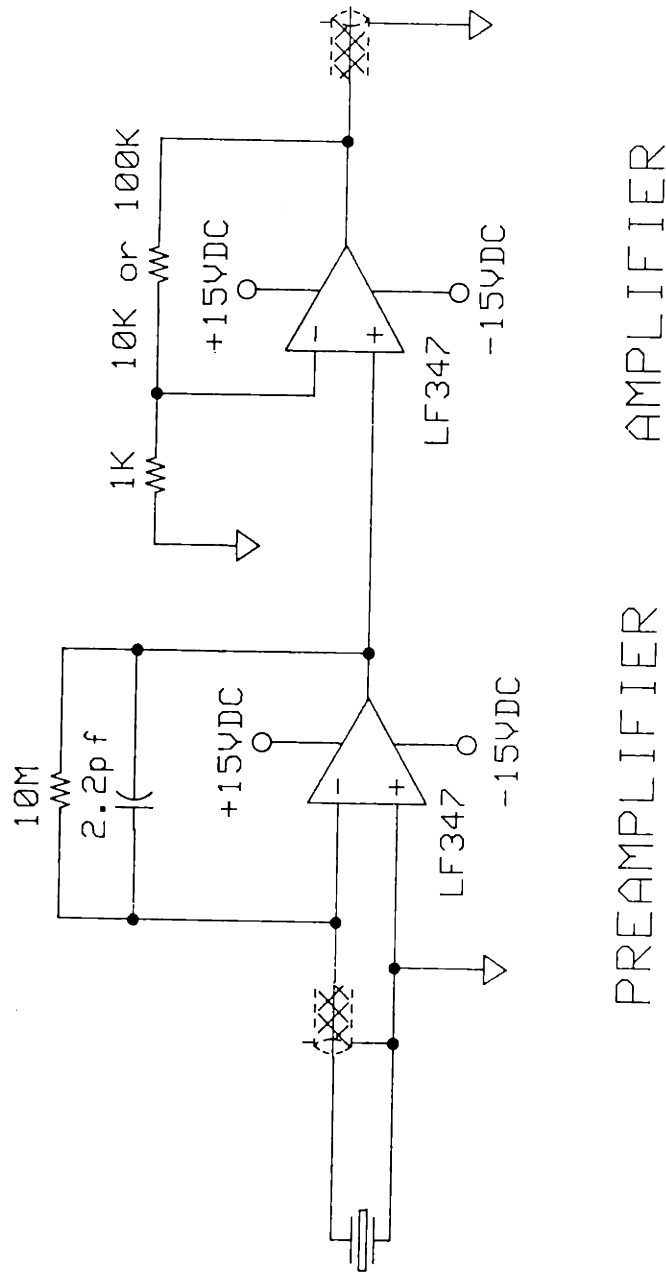


Figure 20: Diagram of one channel of the amplification scheme employed for the acceleration signals. A gain of 10 was used in the amplifier stage for the signal obtained from measurements at the tracheal site, and a gain of 100 for the signals obtained from the chest wall measurement sites.

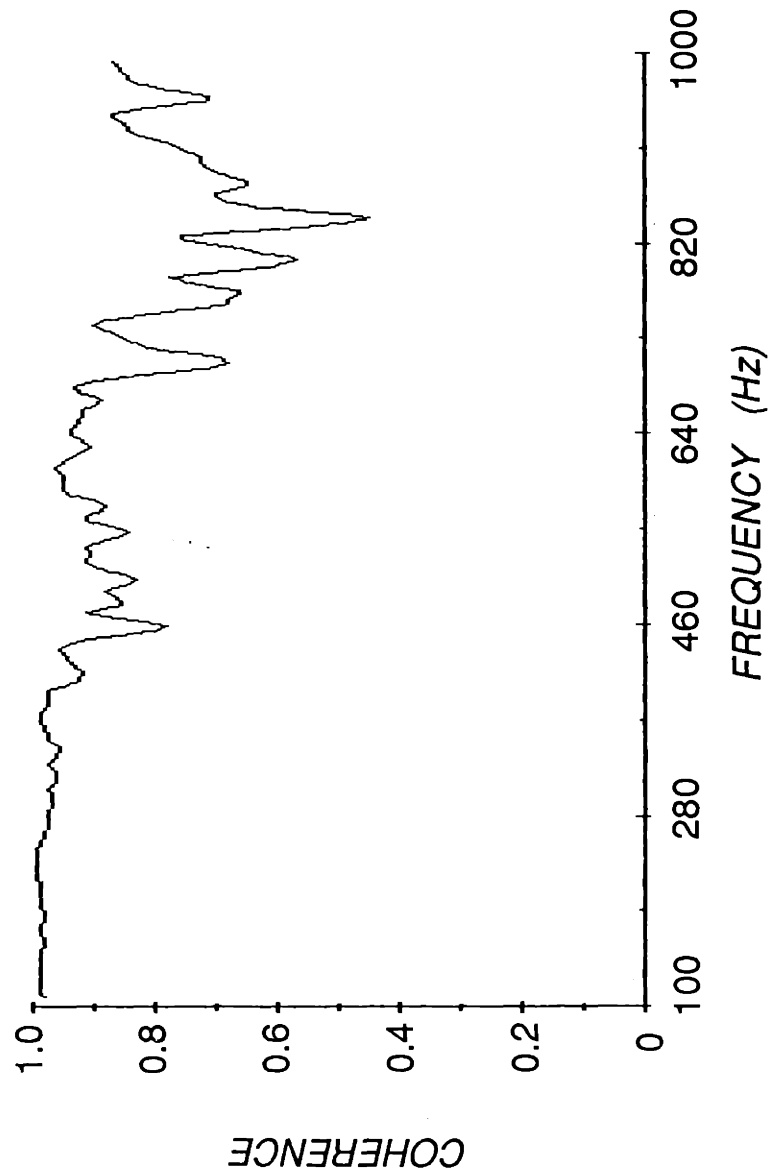


Figure 21: A representative coherence spectrum estimated from measurements of acceleration at a chest wall site at the level of the sixth thoracic vertebra (T_6) and a site overlying the extrathoracic trachea.

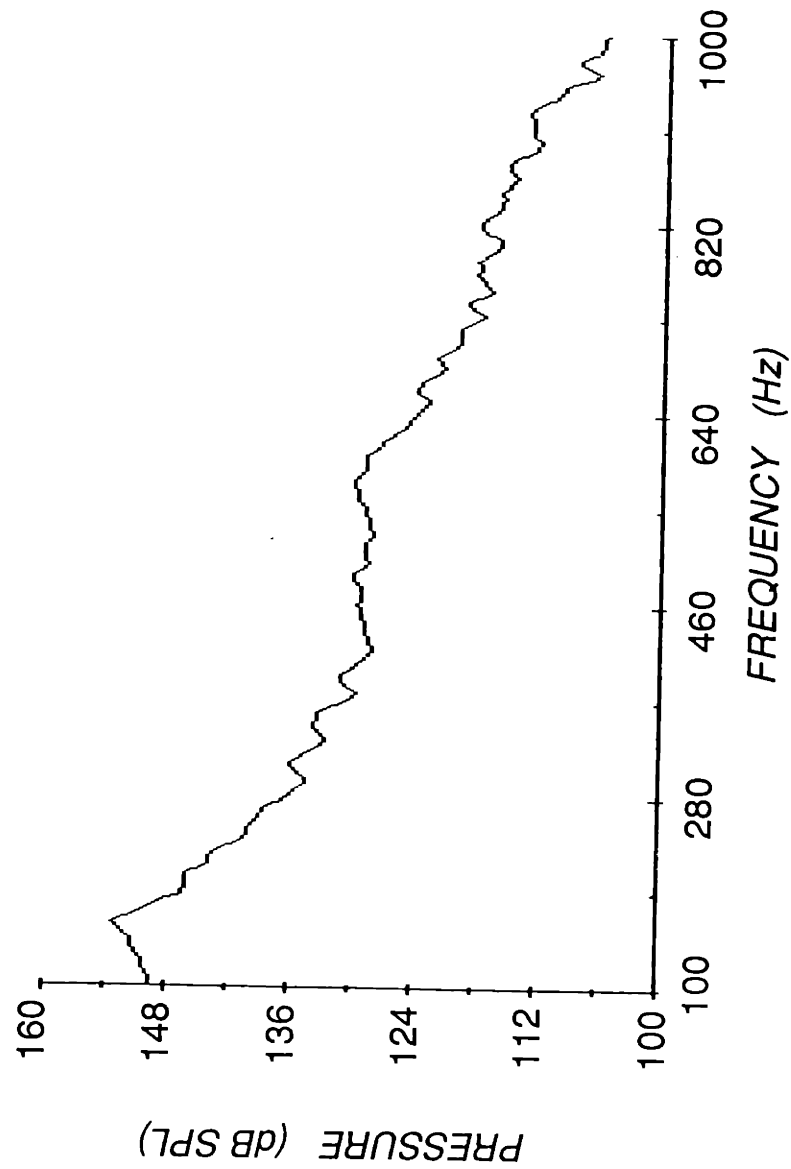


Figure 22: A representative power spectrum of the sound pressure measured by a microphone in the tube through which sound is introduced into a subject's mouth. The subject vocal tract is in a closed-velum, open-glottis position. The units are decibels SPL.

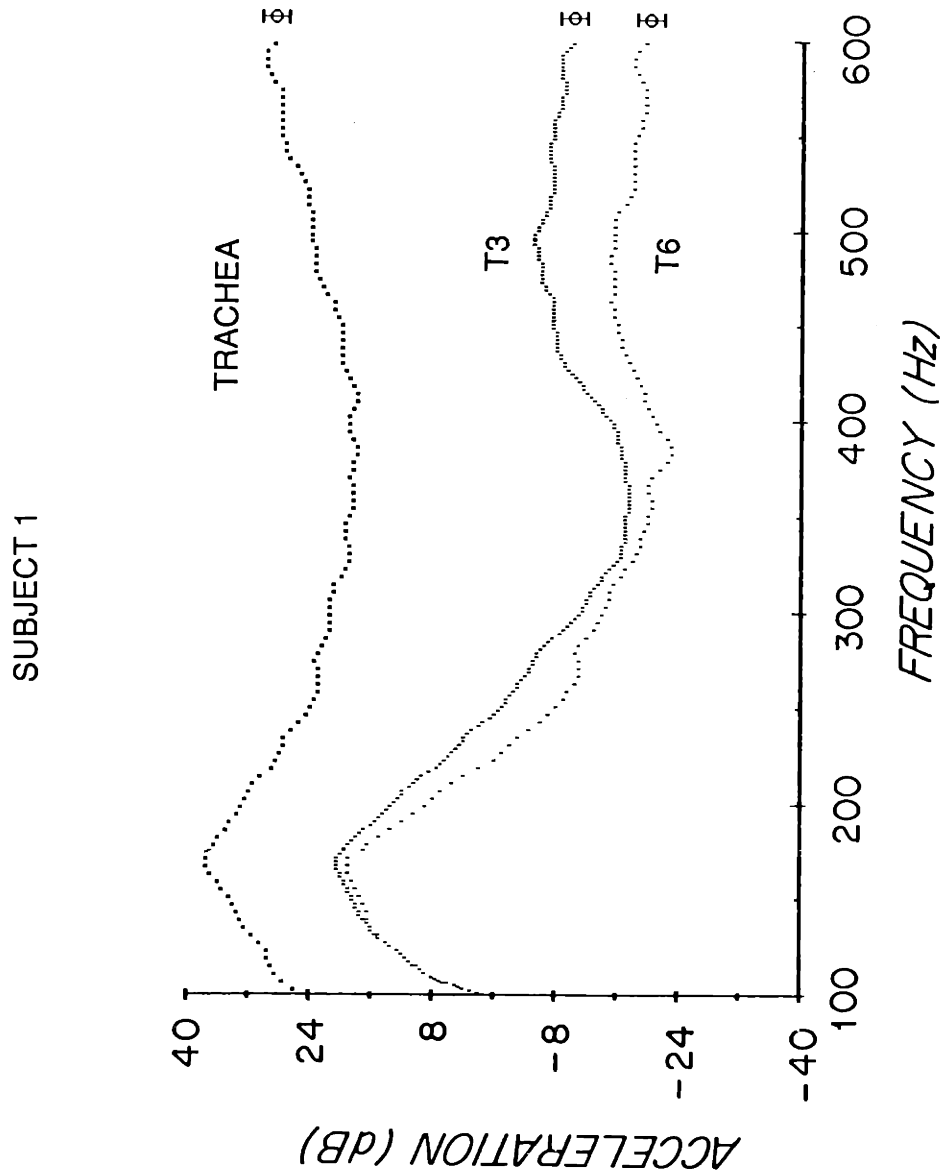


Figure 23: Average power spectra of acceleration estimated for subject 1 at the tracheal and the two chest wall measurement sites (T_3 and T_6). The error bars represent the average 95% confidence intervals of the estimates over the entire frequency range at a particular site. The units are decibels referenced to 1 cm/s^2 .

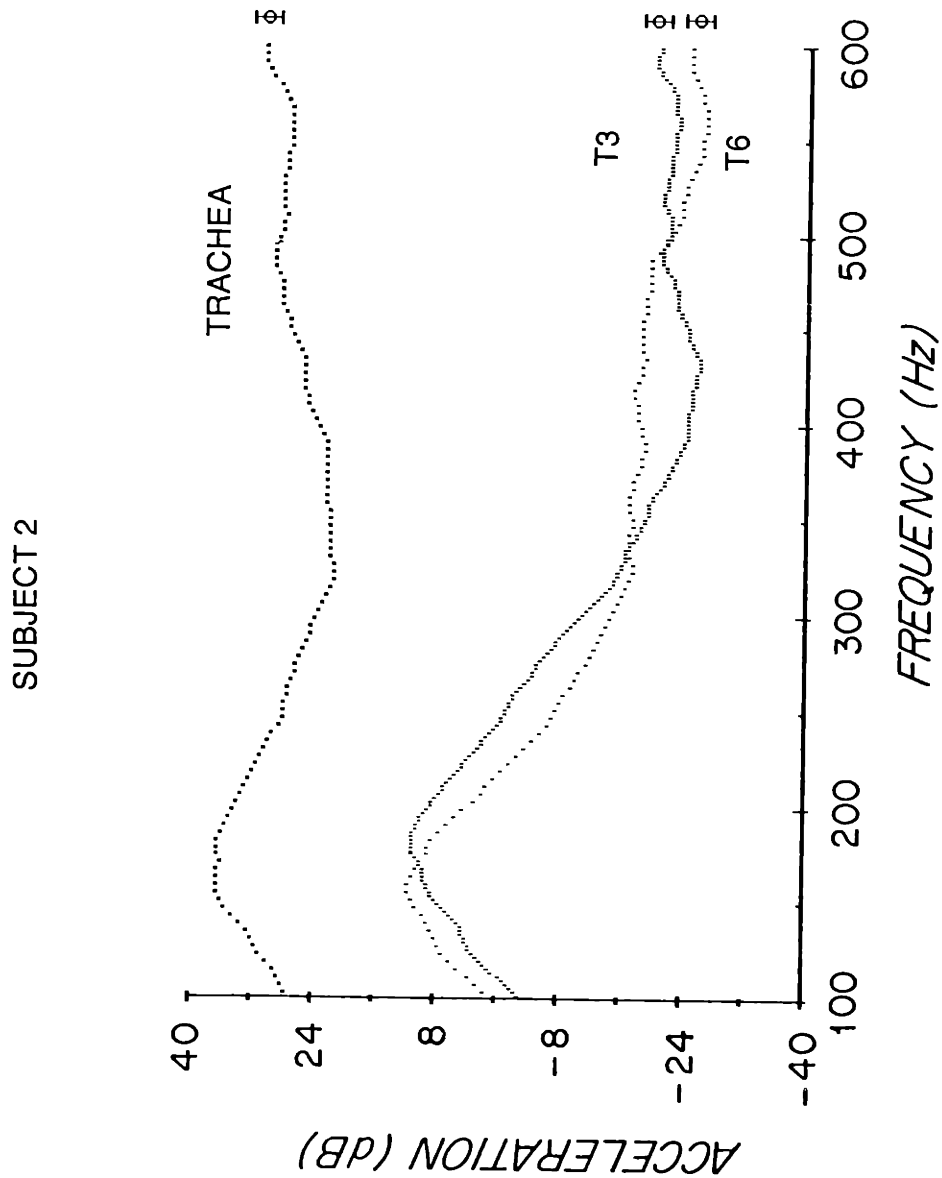


Figure 24: Average power spectra of acceleration estimated for subject 2 at the tracheal and the two chest wall measurement sites (T_3 and T_6). The error bars represent the average 95% confidence intervals of the estimates over the entire frequency range at a particular site. The units are decibels referenced to 1 cm/s^2 .

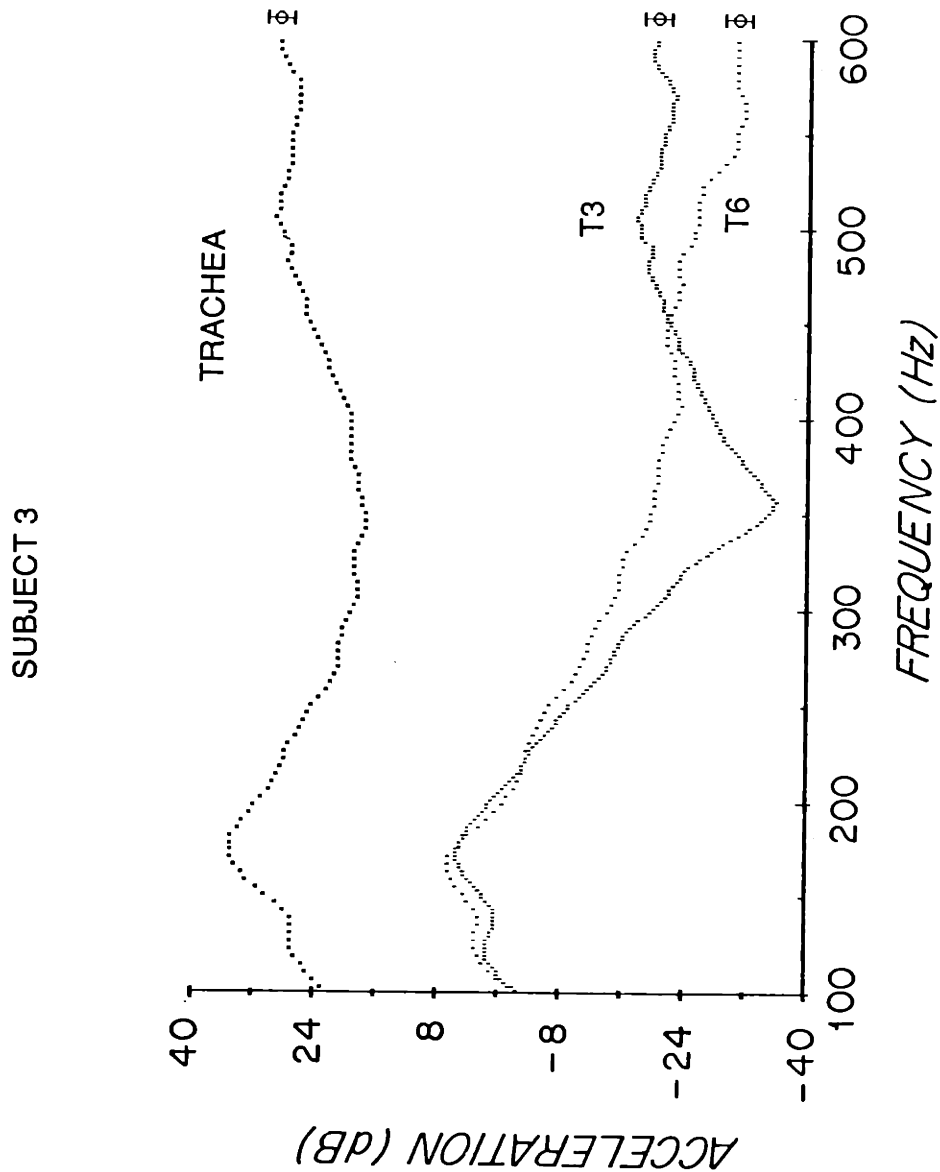


Figure 25: Average power spectra of acceleration estimated for subject 3 at the tracheal and the two chest wall measurement sites (T_3 and T_6). The error bars represent the average 95% confidence intervals of the estimates over the entire frequency range at a particular site. The units are decibels referenced to 1 cm/s^2 .

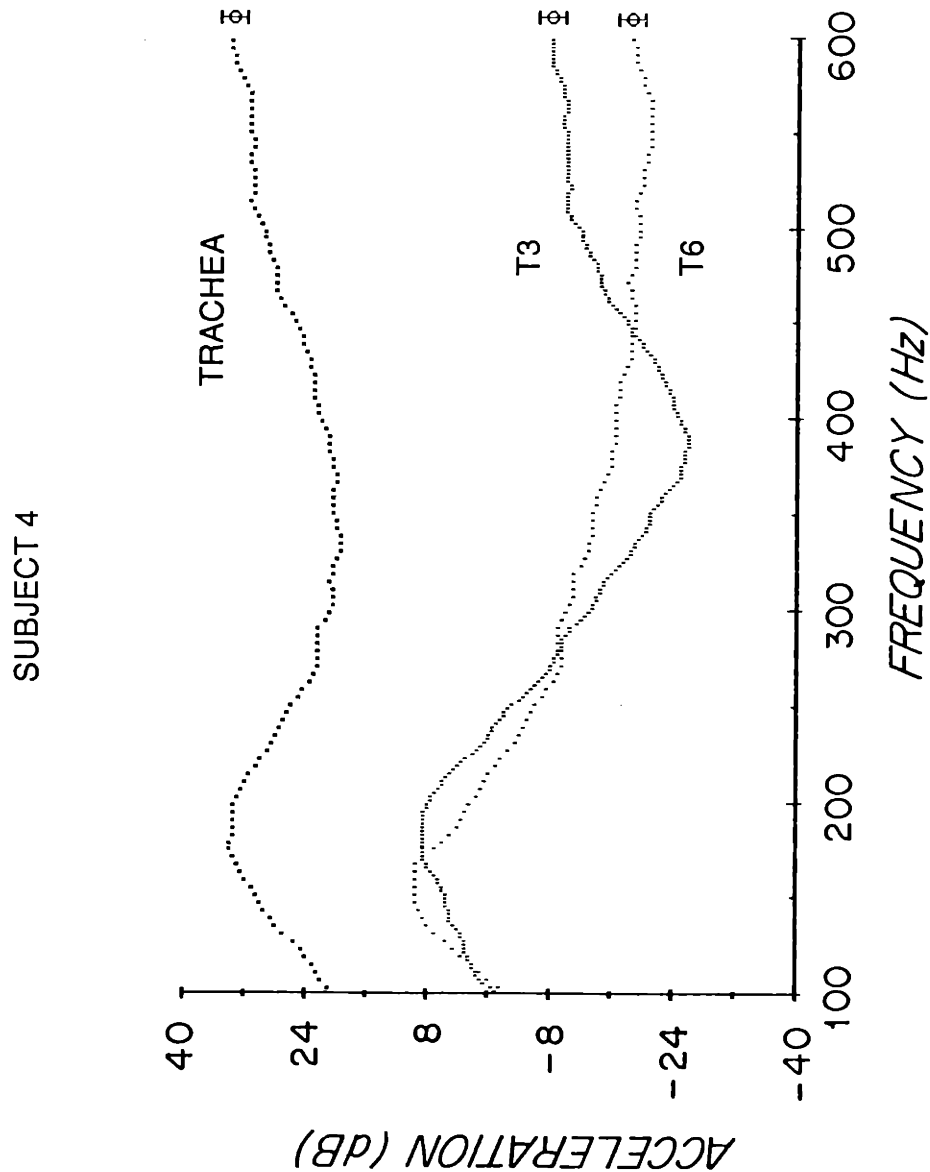


Figure 26: Average power spectra of acceleration estimated for subject 4 at the tracheal and the two chest wall measurement sites (T_3 and T_6). The error bars represent the average 95% confidence intervals of the estimates over the entire frequency range at a particular site. The units are decibels referenced to 1 cm/s^2 .

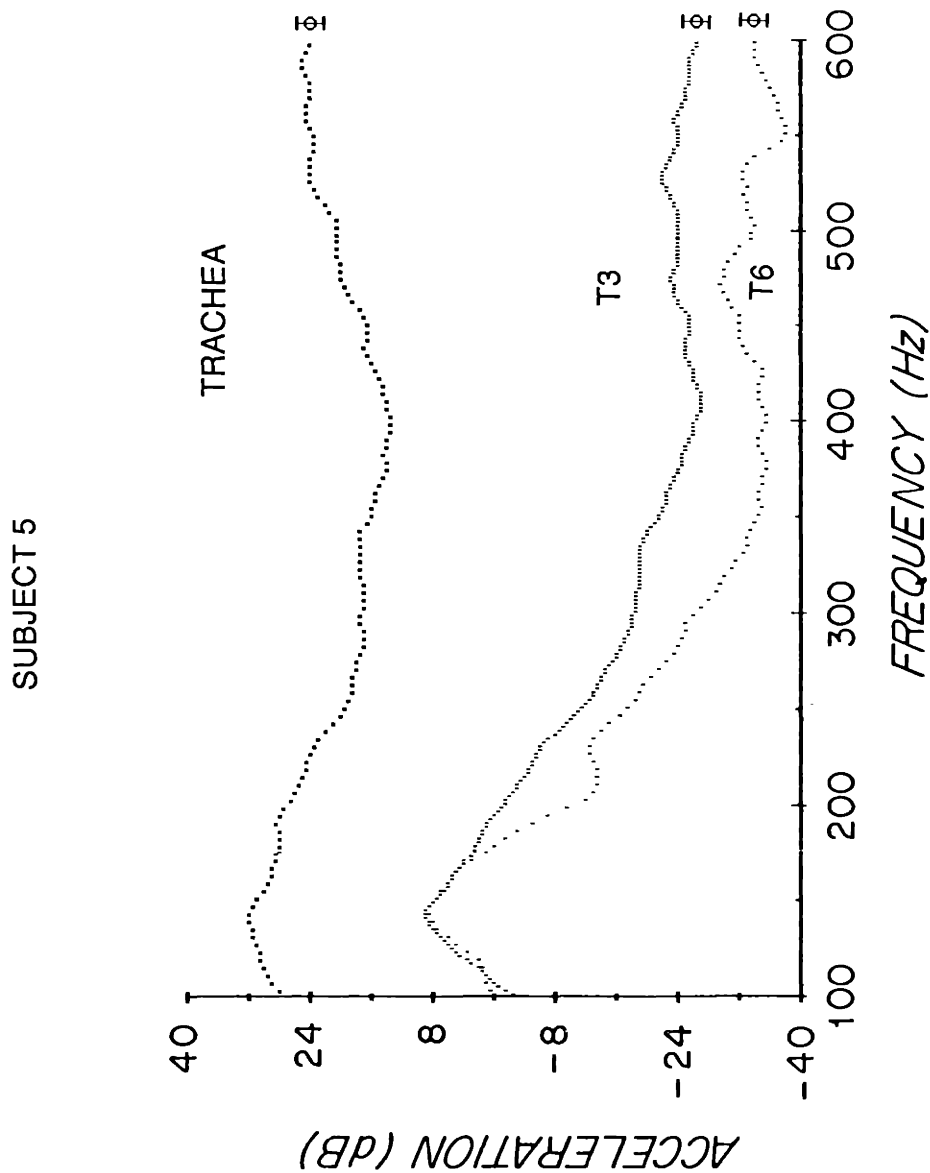


Figure 27: Average power spectra of acceleration estimated for subject 5 at the tracheal and the two chest wall measurement sites (T_3 and T_6). The error bars represent the average 95% confidence intervals of the estimates over the entire frequency range at a particular site. The units are decibels referenced to 1 cm/s^2 .

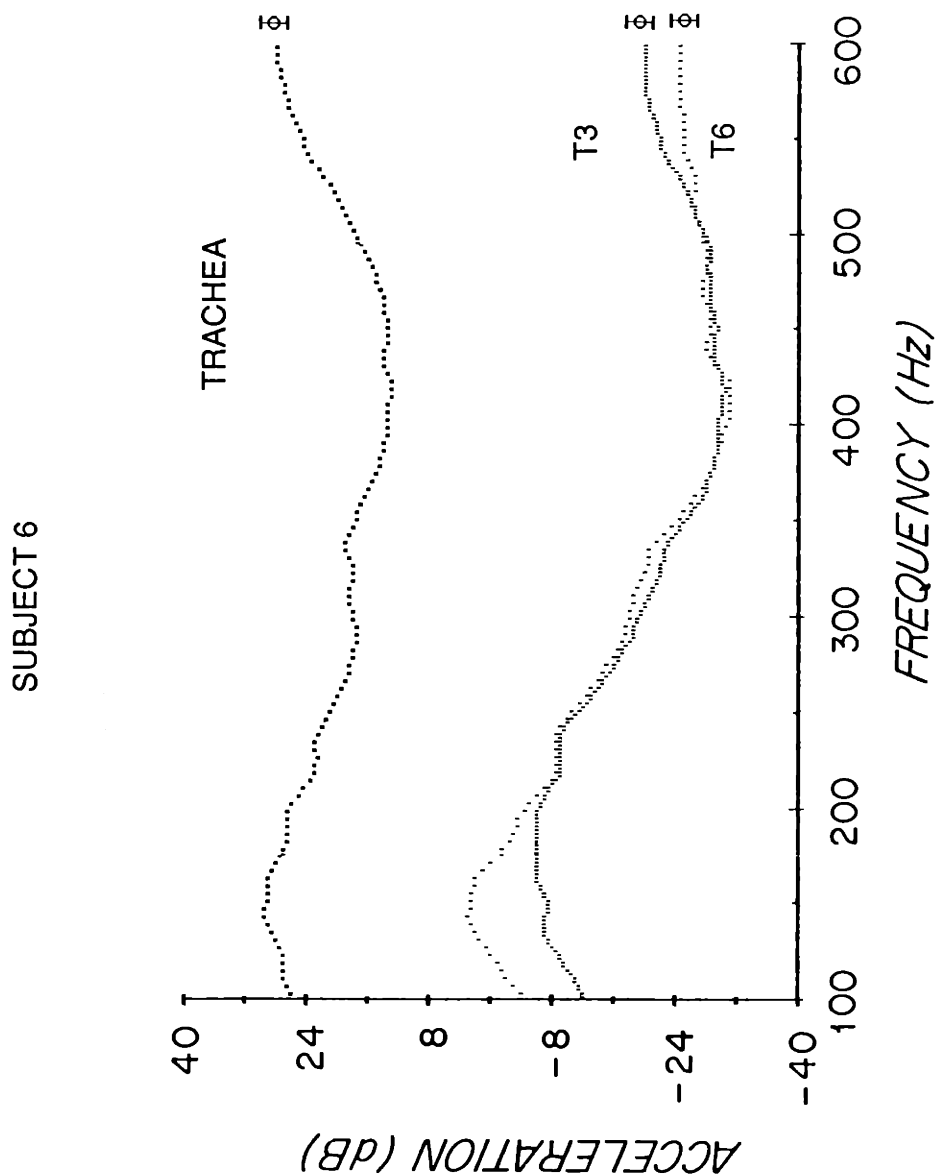


Figure 28: Average power spectra of acceleration estimated for subject 6 at the tracheal and the two chest wall measurement sites (T_3 and T_6). The error bars represent the average 95% confidence intervals of the estimates over the entire frequency range at a particular site. The units are decibels referenced to 1 cm/s^2 .

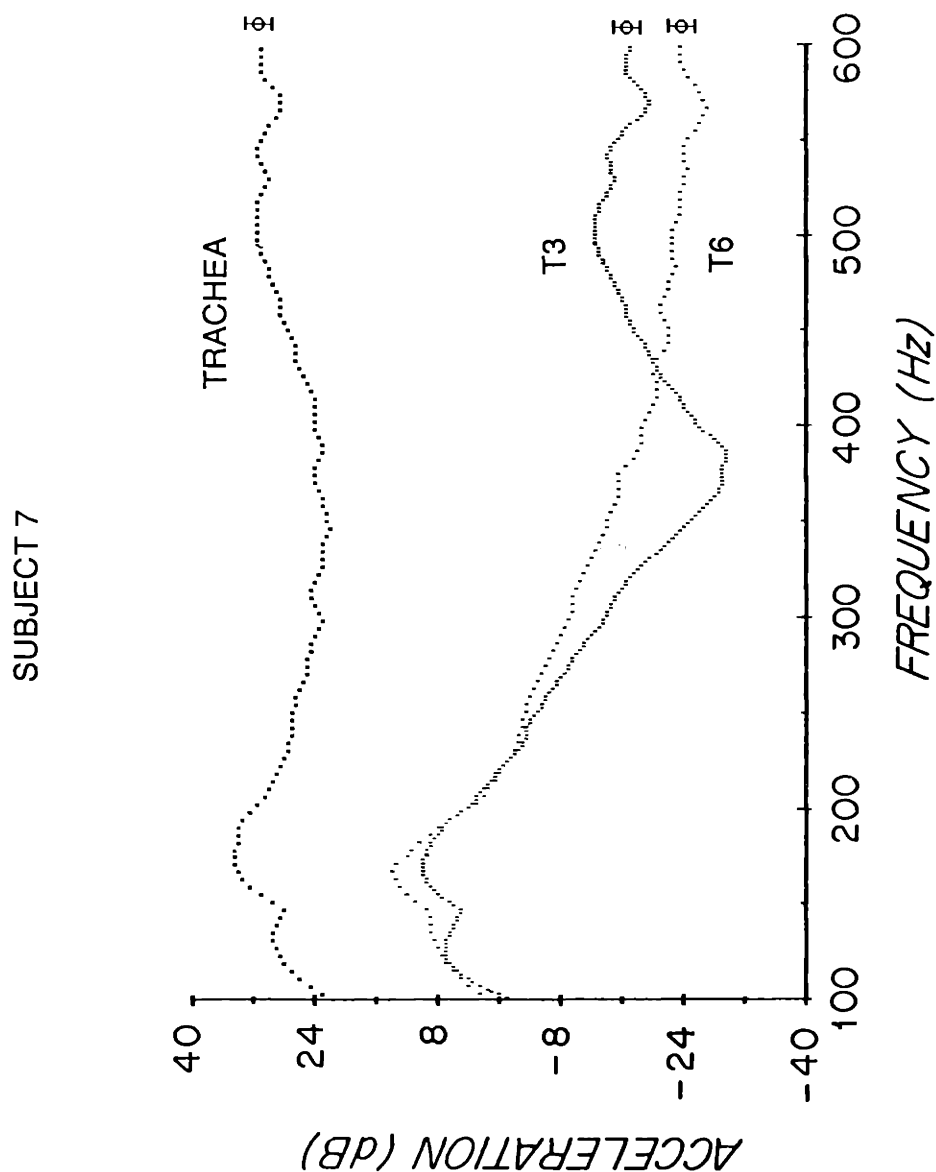


Figure 29: Average power spectra of acceleration estimated for subject 7 at the tracheal and the two chest wall measurement sites (T_3 and T_6). The error bars represent the average 95% confidence intervals of the estimates over the entire frequency range at a particular site. The units are decibels referenced to 1 cm/s^2 .

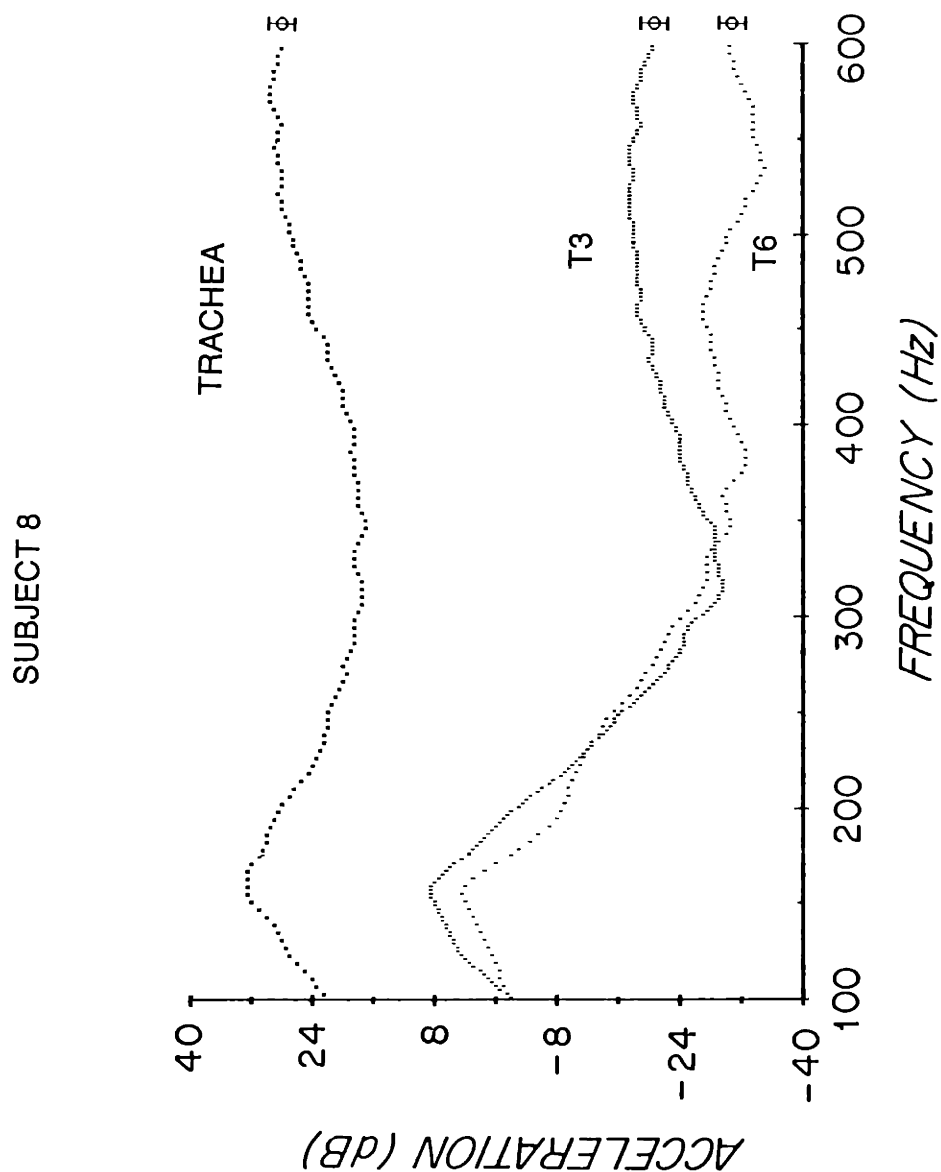


Figure 30: Average power spectra of acceleration estimated for subject 8 at the tracheal and the two chest wall measurement sites (T_3 and T_6). The error bars represent the average 95% confidence intervals of the estimates over the entire frequency range at a particular site. The units are decibels referenced to 1 cm/s^2 .

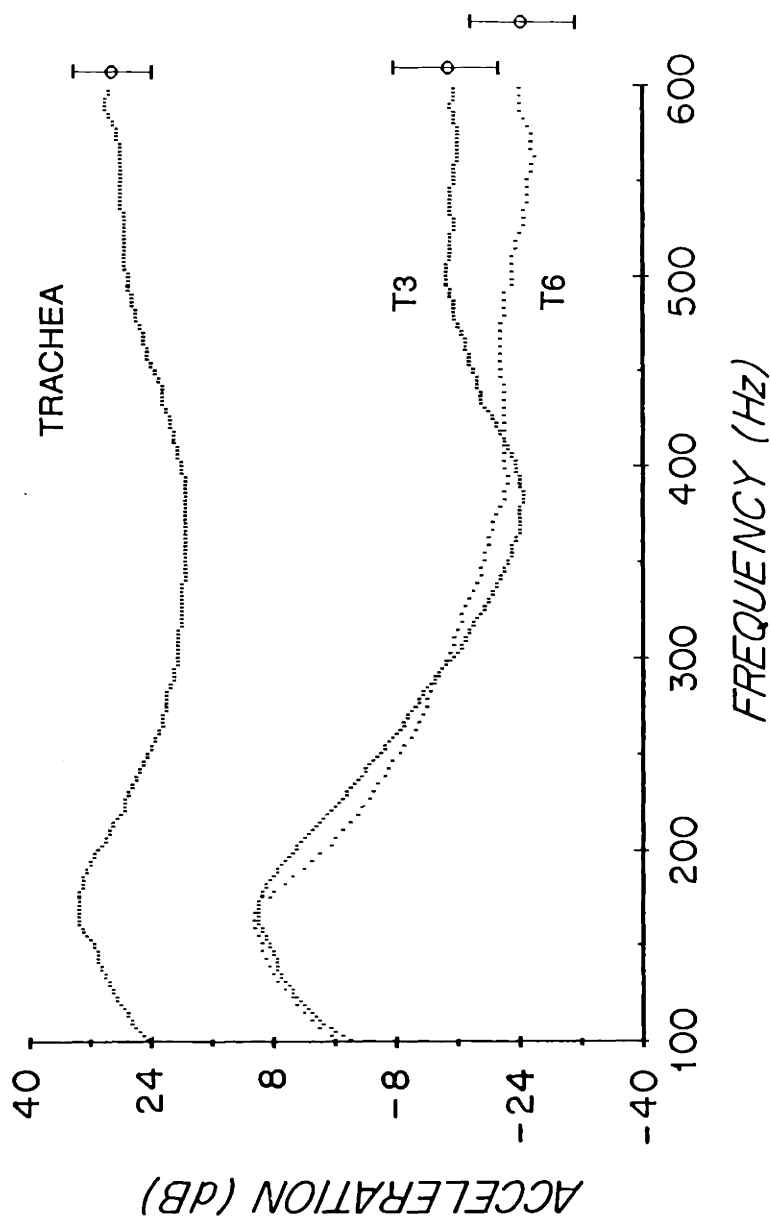


Figure 31: Average power spectra of acceleration estimated for the entire study group at the tracheal and the two chest wall measurement sites (T_3 and T_6). The error bars represent the average 95% confidence intervals of the estimates for the group over the entire frequency range at a particular site. The units are decibels referenced to 1 cm/s^2 .

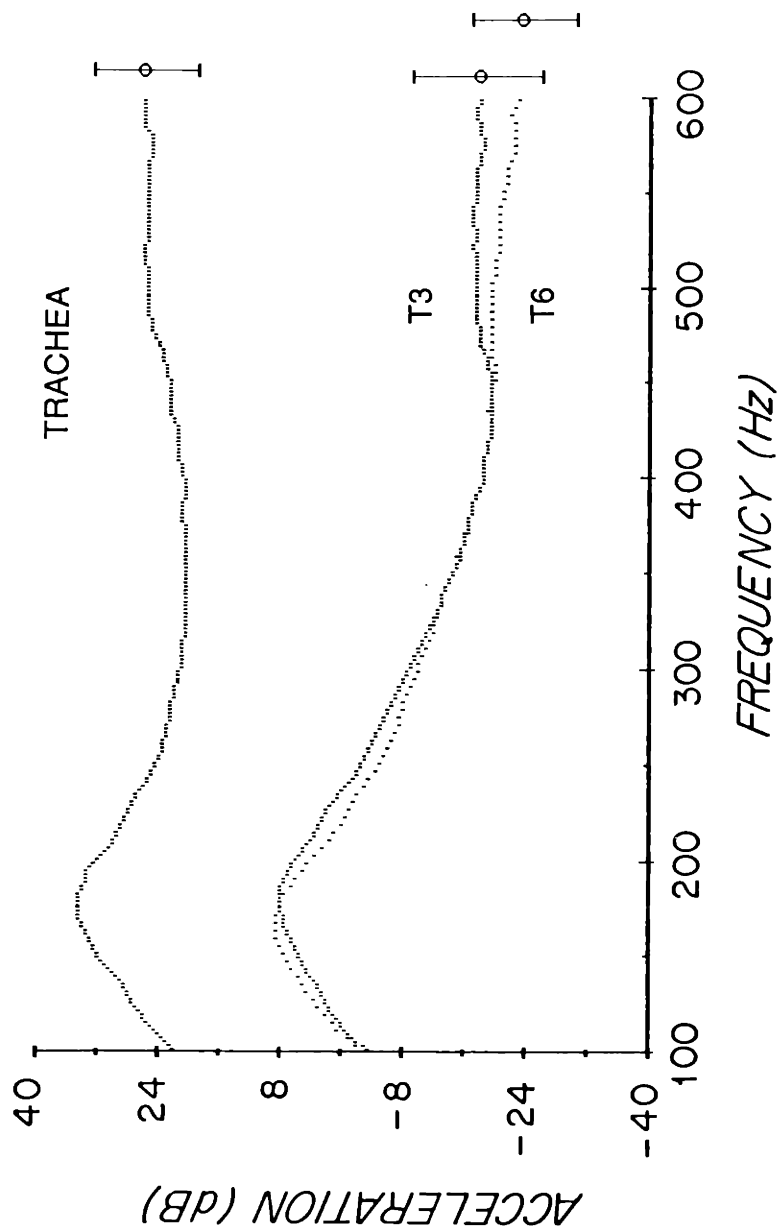


Figure 32: Average power spectra of acceleration estimated for the entire study group at the tracheal and the two chest wall measurement sites (T_3 and T_6), at total lung capacity. The error bars represent the average 95% confidence intervals of the estimates for the group over the entire frequency range at a particular site. The units are decibels referenced to 1 cm/s^2 .

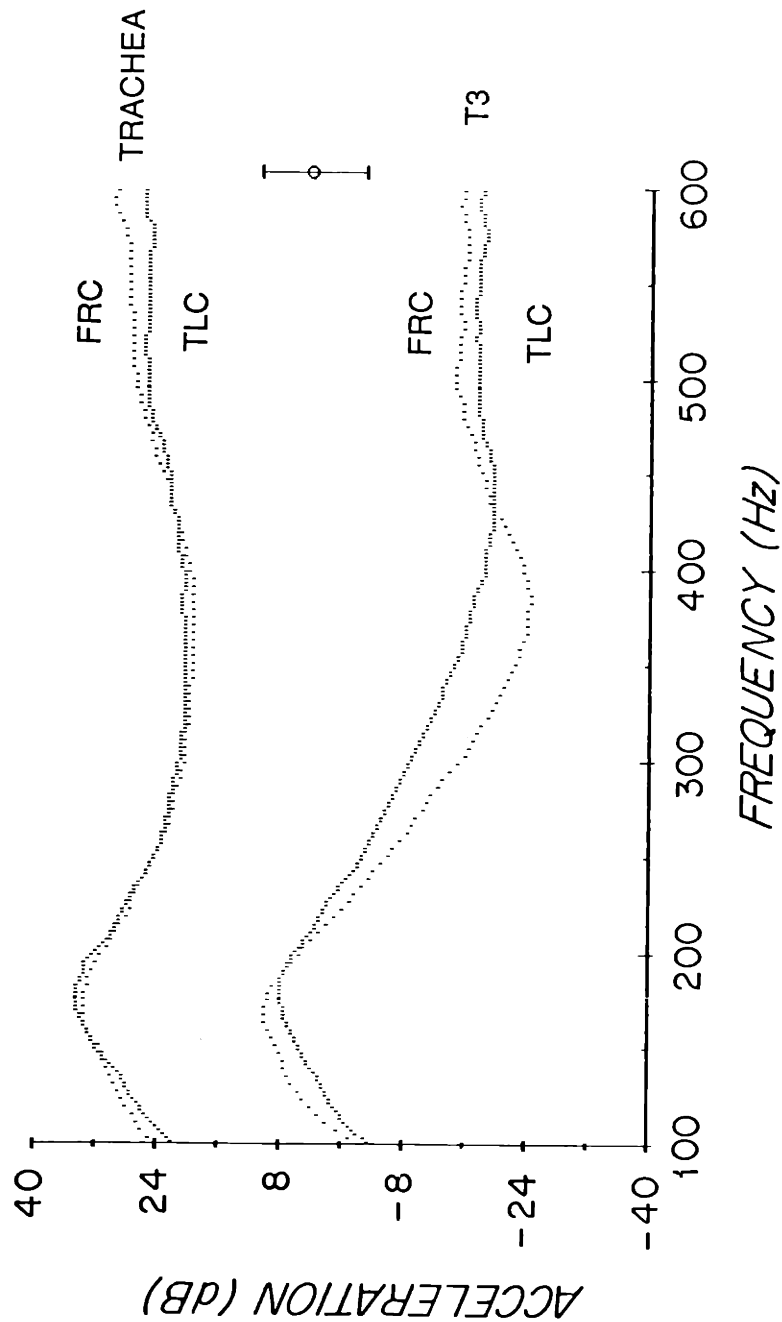


Figure 33: A direct comparison between the spectra estimates of acceleration at resting lung volume (functional residual capacity, FRC) and total lung capacity (TLC) for the tracheal and the T₃ measurement sites. The error bars represent the 95% confidence intervals of the estimates over the entire frequency range at a particular site and lung volume. The units are decibels referenced to 1 cm/s².

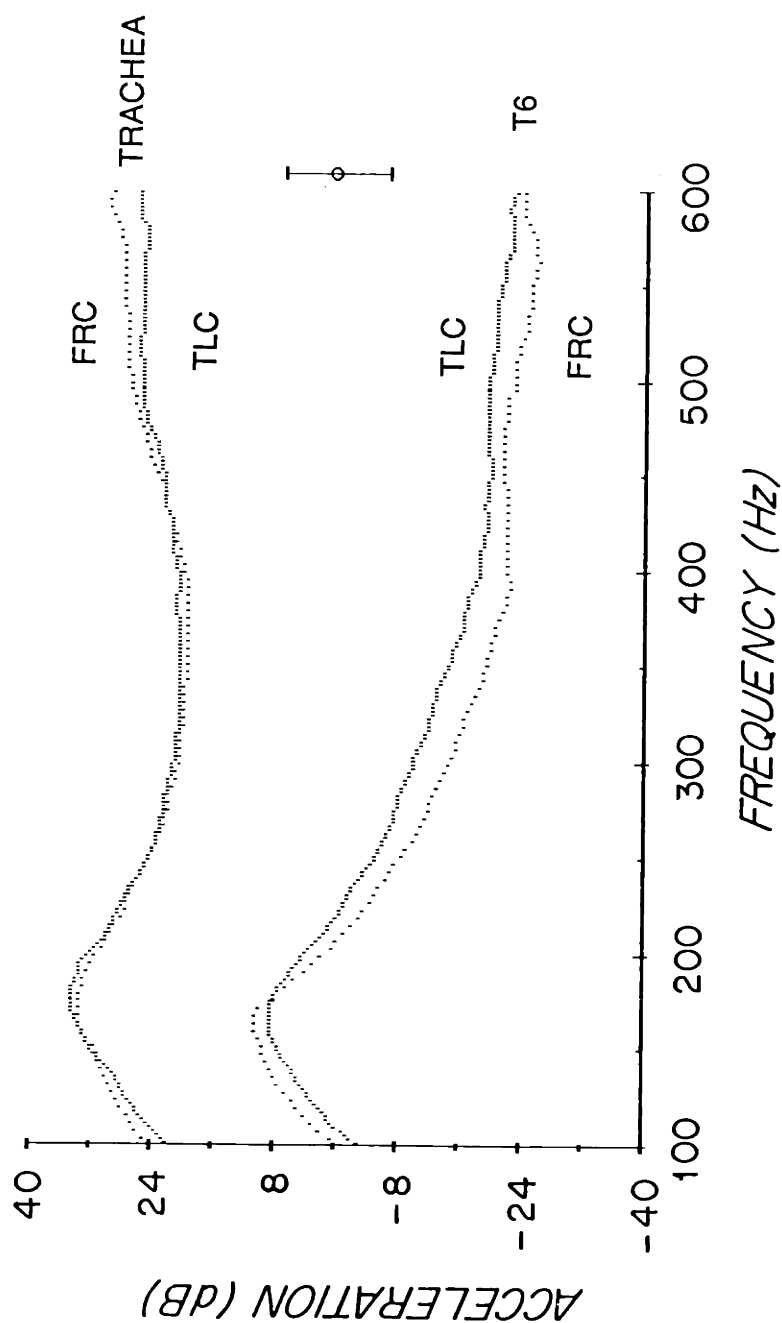


Figure 34: A direct comparison between the spectra estimates of acceleration at resting lung volume (functional residual capacity, FRC) and total lung capacity (TLC) for the tracheal and the T₆ measurement sites. The error bars represent the 95% confidence intervals of the estimates over the entire frequency range at a particular site and lung volume. The units are decibels referenced to 1 cm/s².

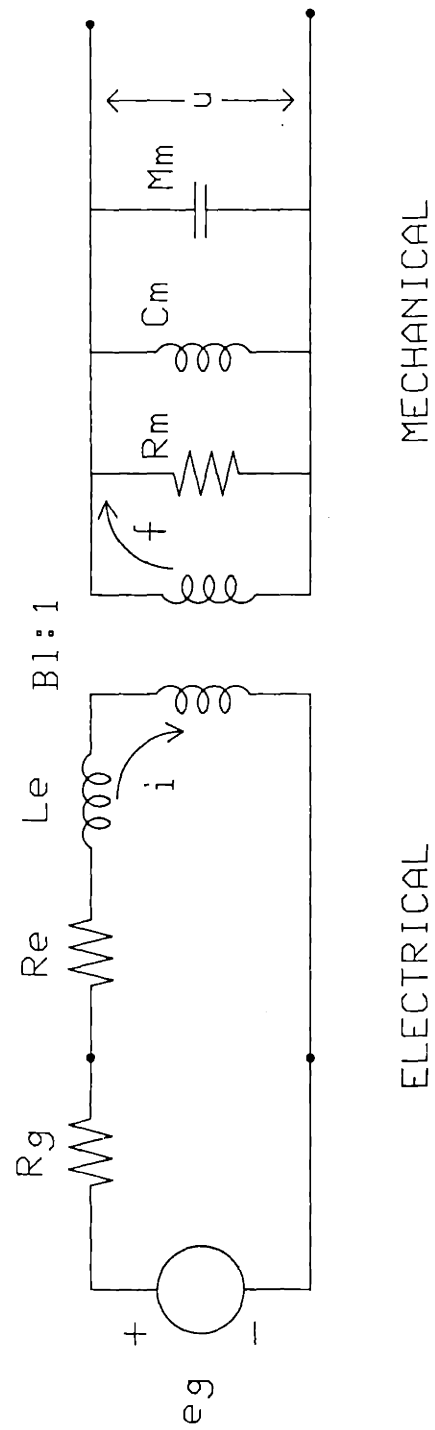
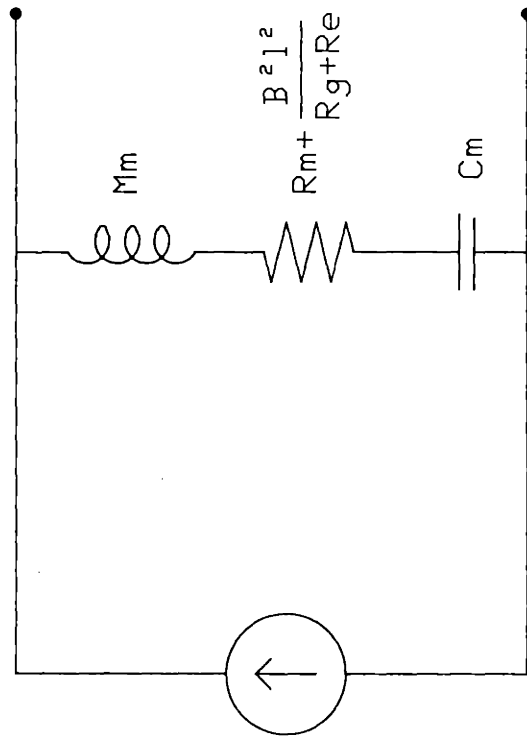


Figure 35: Equivalent electro-mechanical circuit of the sound source.



$$u = \frac{e_g B l}{R_g + R_e} \frac{1}{Z}$$

Figure 36: Norton equivalent acoustic circuit of the sound source at low frequencies.

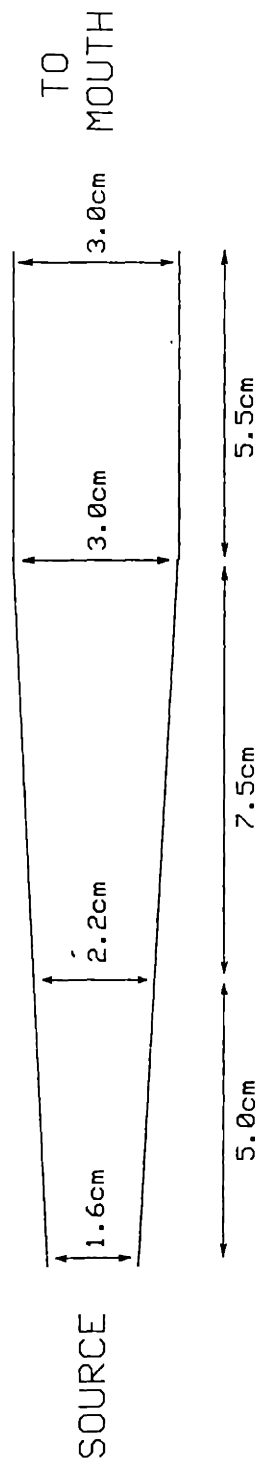


Figure 37: Diagram of the rigid tube which is employed to introduce sound into the mouths of the subjects.

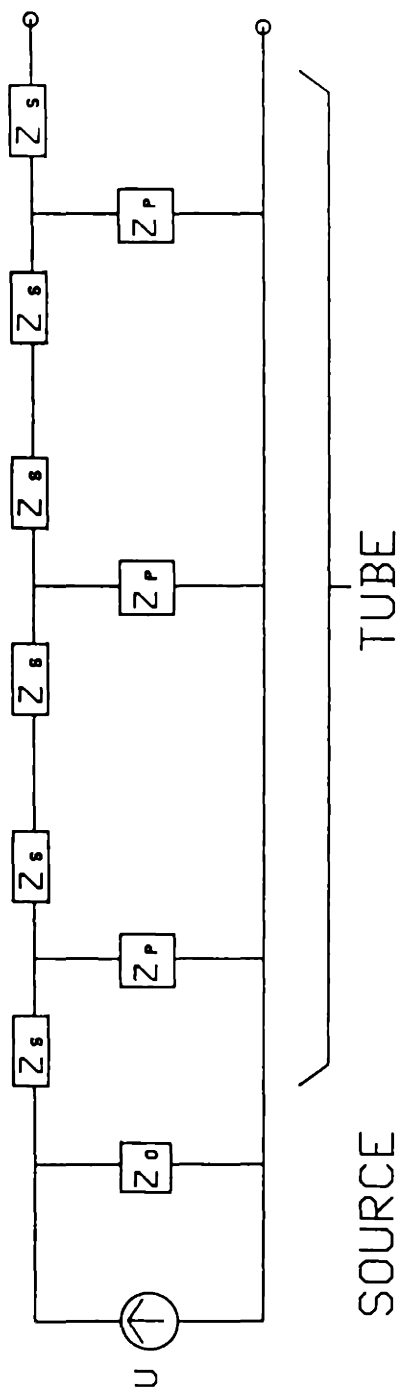


Figure 38: Block diagram of the equivalent acoustic circuit which represents the sound source, and the tube through which sound is introduced into the mouth. The sound source is represented as a Norton equivalent acoustic circuit with volume velocity U and internal impedance Z_0 , and the tube of length 18 cm and diameter 3 cm is represented as three T networks.

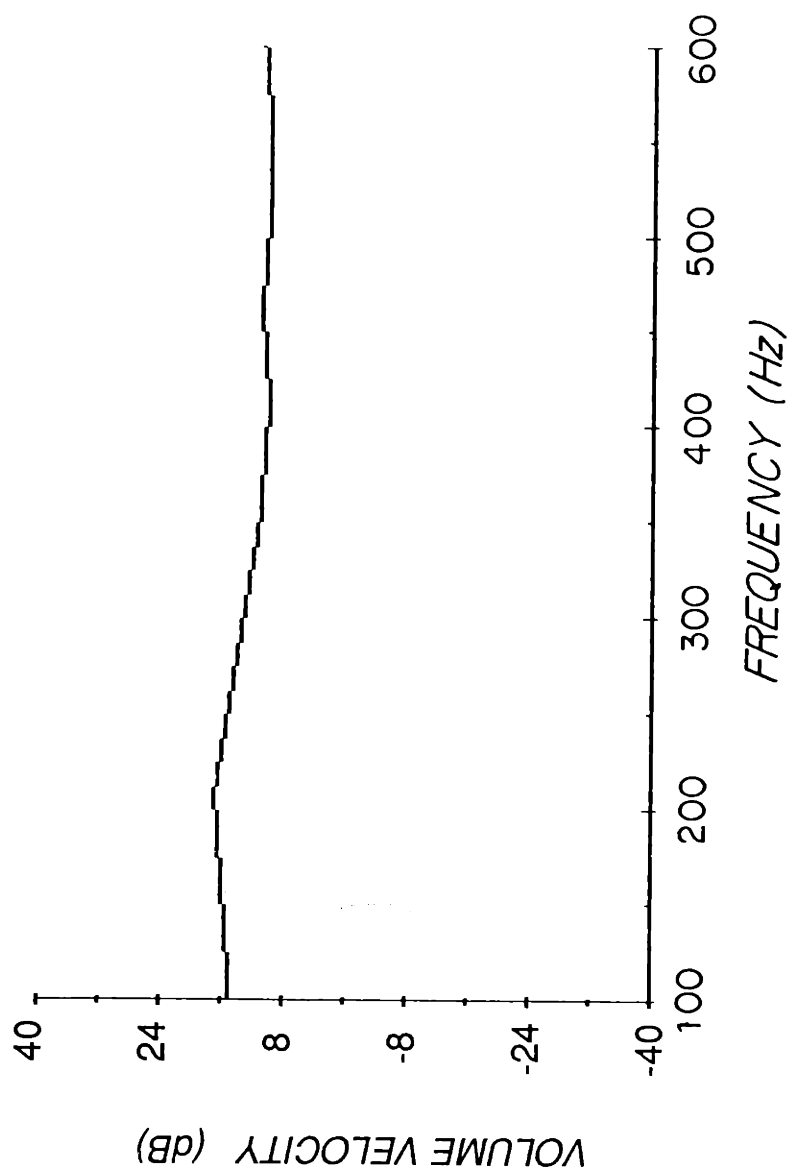


Figure 39: Estimated volume velocity, U , of the Norton equivalent acoustic circuit which represents the sound source used in this study. The units are dB referenced to $1 \text{ cm}^3/\text{s}$ and the ordinate range of 80 dB was employed to facilitate comparison with the other figures.

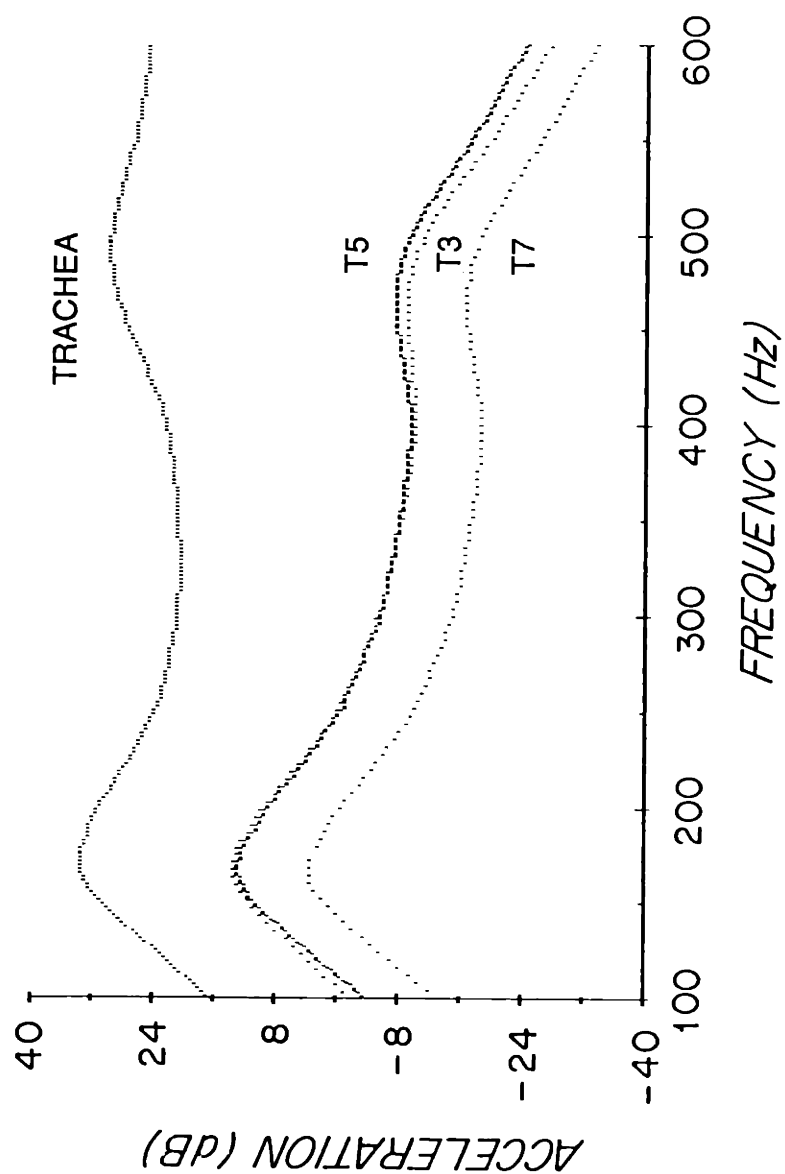


Figure 40: Model power spectra of acceleration at the tracheal and three chest wall locations (T_3 , T_5 , T_7), including the effects of the sound source, tube, and accelerometers. The units are decibels referenced to 1 cm/s^2 .

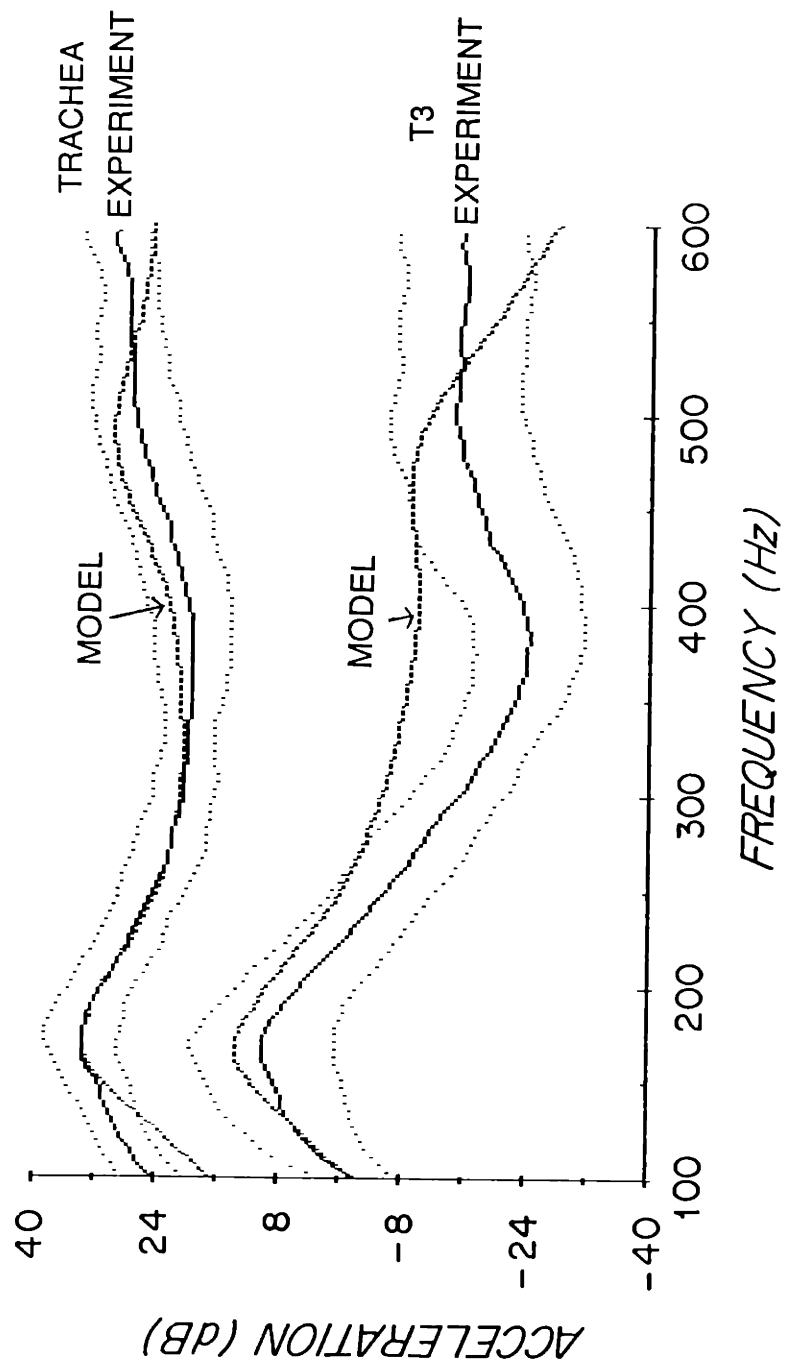


Figure 41: Direct comparison between the model power spectra of acceleration and the average spectral estimates obtained for the entire study group at the tracheal and T_3 measurement sites. The dotted lines demarcate the 95% confidence intervals of the estimates for the group at a particular site. The units are decibels referenced to 1 cm/s^2 .

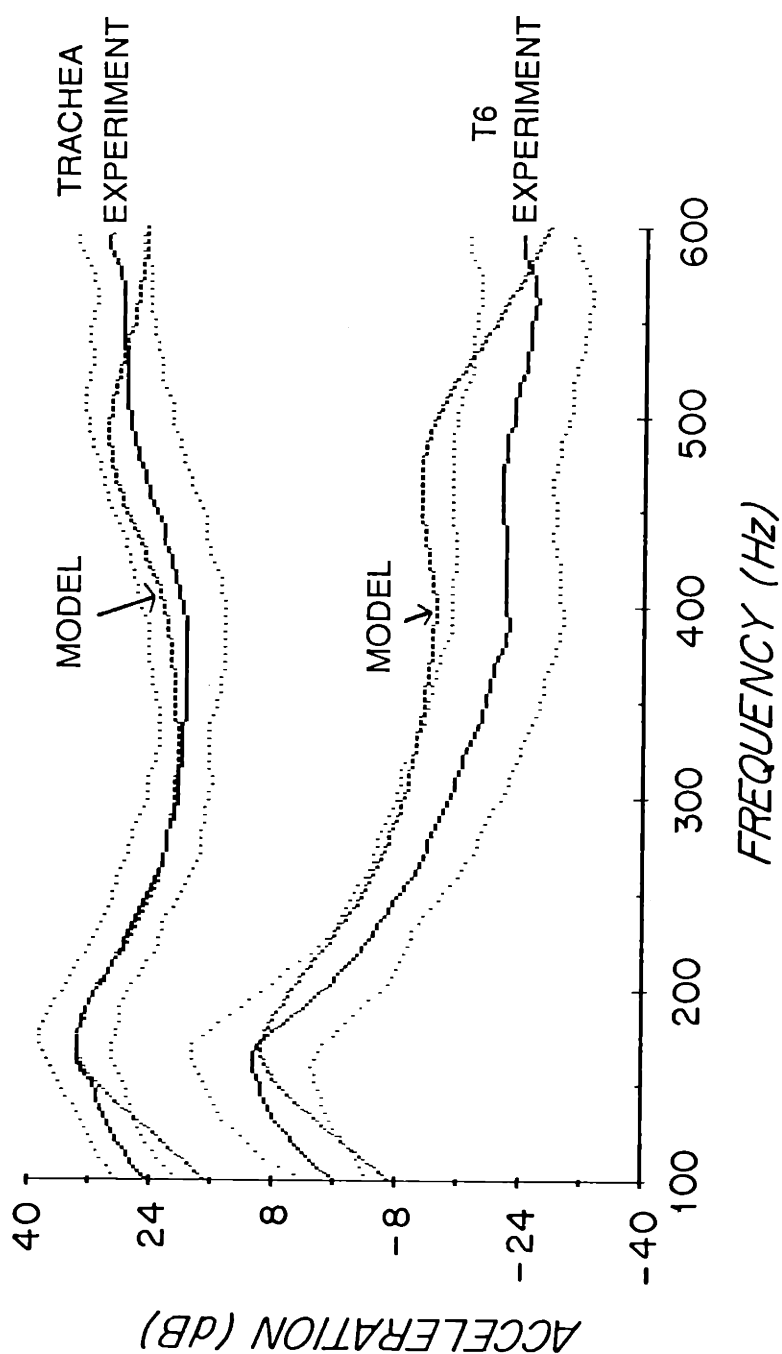


Figure 42: Direct comparison between the model power spectra of acceleration and the average spectral estimates obtained for the entire study group at the tracheal and T_6 measurement sites. The dotted lines demarcate the 95% confidence intervals of the estimates for the group at a particular site. The units are decibels referenced to 1 cm/s^2 .

REFERENCES

- Armstrong, J. D., E. H. Gluck, R. O. Crapo, H. A. Jones, and J. M. B. Hughes, "Lung Tissue Volume Estimation by Simultaneous Radiographic and Helium Dilution Methods", *Thorax*, vol. 37, pp. 676-679, 1982.
- Bates, B., *A Guide to Physical Examination*, Philadelphia: J. B. Lippincott, 1979.
- Beranek, L. L., *Acoustics*, New York: American Institute of Physics, 1986.
- Butler, J. P., J. L. Lehr and J. M. Drazen, "Longitudinal elastic wave propagation in pulmonary parenchyma", *J. Appl. Physiol.*, vol. 62, pp. 1349-1355, 1987.
- Cranen, B., and L. Boves, "On the Measurement of Glottal Flow", *J. Acoust. Soc. Am.*, vol. 84, pp. 888-900, 1988.
- Devin, C., "Survey of Thermal, Radiation, and Viscous Damping of Pulsating Air Bubbles in Water", *J. Acoust. Soc. Am.*, vol. 31, pp. 1654-1667, 1959.
- Donnerberg, R. L., C. K. Druzgalski, R. L. Hamlin, G. L. Davis, R. M. Campbell and D. A. Rice, "Sound Transfer Function of the Congested Canine Lung", *Br. J. Dis. Chest*, vol. 74, pp. 23-31, 1980.
- Flanagan, J. L., *Speech Analysis, Synthesis and Perception*, New York: Springer Verlag, 1972.
- Fredberg, J. J. and A. Hoenig, "Mechanical Response of the Lungs at High Frequencies", *J. Biomech. Eng.*, vol. 100, pp. 57-66, 1978.
- Fredberg, J. J., "Spatial Considerations in Oscillation Mechanics of the Lung", *Fed. Proc.*, vol. 39, pp. 2747-2754, 1980.
- Gupta, V., T. A. Wilson, and G. S. Beavers,, "A Model for Vocal Cord Excitation", *J. Acoust. Soc. Am.*, vol. 54, pp. 1607-1617, 1973.
- Ishizaka, K., J. C. French, and J. L. Flanagan, "Direct Determination of Vocal Tract Wall Impedance", *IEEE Trans. Acoustics, Speech, and Signal Processing*, vol. 23, pp. 370-373, 1975.

- Ishizaka, K., M. Matsudaira, and T. Kaneko, "Input acoustic-impedance measurement of the subglottal system", J. Acoust. Soc. Am., vol. 60, pp. 190-197, 1976.
- Jacobs, J. E., "Wideband Acoustic Energy Studies of Pulmonary Airways", Bioelectromagnetics, vol. 3, pp. 167-177, 1982.
- Judson, L. S., and A. T. Weaver, Voice Science, New York: F. S. Crofts & Co., 1942.
- Kinsler, L. E., A. R. Frey, A. B. Coppens and J. V. Sanders, Fundamentals of Acoustics, New York: John Wiley & Sons, 1982.
- Kraman, S. S., "Speed of Low-Frequency Sound Through the Lungs of Normal Men", J. Appl. Physiol., vol. 55, pp. 1862-1867, 1983.
- Kraman, S. S., "Comparison of Lung Sound and Transmitted Sound Amplitude in Normal Men", Am. Rev. Respir. Dis., vol. 128, pp. 451-454, 1983.
- Kraman, S. S., "The Determination of the Resonant Frequency of the Respiratory System Above 50 Hz", Clin. Res. (abstract), p. 145, 1986.
- Lara, M. E., Comparison of Lung Sounds Measurement Techniques, Harvard University, M.D. Thesis, 1988.
- Laennec, R. T. H., De L'Auscultation Mediate, Paris: Brosson and Chande, 1819.
- Morse, P. M. and K. U. Ingard, Theoretical Acoustics, Princeton: Princeton University Press, 1986.
- Plesset, M. S. and A. Prosperetti, "Bubble Dynamics and Cavitation", Ann. Rev. Fluid. Mech., vol. 9, pp. 145-185, 1977.
- Ploysongsang, Y., J. A. P. Pare, and P. T. Macklem, "Lung Sounds in Patients with Emphysema", Am. Rev. Resp. Dis., vol. 124, pp. 45-49, 1982.
- Prosperetti, A., "Thermal Effects and Damping Mechanisms in the Forced Radial Oscillations of Gas Bubbles in Liquids", J. Acoust. Soc. Am., vol. 61, pp. 17-27, 1977.
- Rice, D. A., "Sound Speed in the Upper Airways", J. Appl. Physiol., vol. 49, pp. 326-336, 1980.
- Rice, D. A., "Sound Speed in Pulmonary Parenchyma", J. Appl. Physiol., vol. 54, pp. 304-308, 1983.

Rice, D. A., "Transmission of Lung Sounds", Sem. Resp. Med., vol. 6, pp. 166-170, 1985.

Rice, D. A., "The Effect of Ambient Pressure and Gas on Sound Speed in the Lung", Clin. Res. (abstract), p. 145, 1986.

Rice, D. A. and J. C. Rice, "Central to Peripheral Sound Propagation in Excised Lung", J. Acoust. Soc. Am., vol. 82, pp. 1139-1144, 1987.

Stevens, K. N., Acoustic Phonetics, in preparation.

Takagi, S., "Trial and Success in the Technical Realization of Requirements for Phonocardiographic Microphones", Med. Elec. Biol. Eng., vol. 2, pp. 123-124, 1964.

Van Den Berg, Jw., "An Electrical Analogue of the Trachea, Lungs and Tissues, Acta Physiol. Pharmacol. Neerlandica, vol. 9, pp. 361-385, 1960.

Vermarian, H. and E. van Vollenhoven, "The Recording of Heart Vibrations: A Problem of Vibration Measurement on Soft Tissue", Med. Biol. Eng. Comput., vol. 22, pp. 168-178, 1984.

Weibel, E. R., Morphometry of the Human Lung, Berlin: Springer Verlag, 1963.

Winter, D. C., "Wave Speed in the Dog Trachea", Fed. Proc. (abstract), vol. 37, p. 554, 1978.

Wodicka, G. R., K. N. Stevens, H. L. Golub, E. G. Cravalho, and D. C. Shannon, "A Model of Acoustic Transmission in the Respiratory System", IEEE Trans. Biomed. Eng., 1989, in press.